Macrophage mechanosensing during their pro-inflammatory response

Dissertation

zur Erlangung des akademischen Grades
Doctor rerum naturalium
(Dr. rer. nat.)

Vorgelegt
der Fakultät Mathematik und Naturwissenschaften
der Technischen Universität Dresden

von

Joan Carles Escolano Caselles

geboren am 04.06.1991 in Mollerussa, Spanien.

Eingereicht im August 2021

Thesis Betreuer: Prof. Dr. Jochen Guck

1. Gutachter: Prof. Dr. Michael Schlierf

2. Gutachter: Prof. Dr. Clare Bryant

“Si vols que surti el sol, abans s’haurà de fer de nit”

Mishima

Dedicated to all the past, present and future scientists;
for keeping up their hard work despite all the failures.

Summary

Macrophages are innate immune cells responsible for engulfing microbes and cell debris through phagocytosis and orchestrating immune responses to maintain homeostasis. While conducting immune surveillance over all types of organs and tissues, macrophages face inherently heterogeneous microenvironments with unique biophysical features. For instance, microglia residing in the brain, Kupffer cells living in the skin and bone osteoclasts are exposed to very distinct tissue stiffnesses. Despite the research done in the last decade clearly indicates that macrophages are sensitive to physical factors, how mechanical cues modulate their inflammatory response remains poorly understood.

The present study aims at investigating how microenvironment stiffness influences the pro-inflammatory behaviour of macrophages. Besides characterising the regulatory effect on pro-inflammatory gene expression and cytokine production, this work examines the impact of stiffness on the inflammasome, one of the main macrophage signalling platforms.

For this, an *in vitro* system based in 2D polyacrylamide hydrogels whose stiffness can be independently tuned was established. Using substrates with an elastic moduli between 0.2 and 33.1 kPa, bone marrow-derived macrophages adopted a less spread and rounder morphology on compliant compared to stiff polyacrylamide. Upon priming with lipopolysaccharide, the expression levels of the gene encoding for TNF-α were higher on more compliant hydrogels, yet there were no significant differences in the expression of other major pro-inflammatory genes. Additionally stimulating macrophages with the ionophore nigericin revealed higher secreted protein levels of IL-1β and IL-6 on compliant substrates. Interestingly, macrophages challenged on compliant polyacrylamide also displayed an enhanced formation of the NLRP3 inflammasome as well as increased levels of pyroptotic cell death. The upregulation of inflammasome assembly on compliant hydrogels was not primarily attributed to the reduced cell spreading, since spatially confining cells on micropatterns led to a decrease of inflammasome-positive cells compared to well-spread cells. Finally, interfering with actomyosin contractility diminished the differences in inflammasome formation between compliant and stiff substrates.

In summary, these results show that substrate stiffness affects the pro-inflammatory response of macrophages and for the first time describe that the NLRP3 inflammasome is one of the signalling components affected by stiffness mechanosensing. The work presented here expands our understanding of how microenvironment stiffness affects macrophage behaviour and which elements of their machinery might contribute to integrate mechanical cues into the regulation of their inflammatory functions. The onset of pathological processes or the implant of foreign bodies represent immune challenges in which macrophages can face a mechanically changing environment. Therefore, a better insight on how macrophages detect and process biophysical signals could potentially provide a basis for new strategies to modulate inflammatory responses.

Kurzfassung

Als Teil des angeborenen Immunsystems sind Makrophagen dafür verantwortlich Pathogene und Zellrückstände durch Phagozytose zu beseitigen. Sie orchestrieren Immunantworten um homöostatische Bedingungen von Organen und Geweben aufrechtzuerhalten. Dabei sind sie extrem heterogenen Mikroumgebungen ausgesetzt, welche sich jeweils durch eine einzigartige Kombination von (bio)chemischen und mechanischen Eigenschaften, vor allem Gewebesteifigkeiten, auszeichnen. Dies veranschaulichen beispielsweise im Gehirn residierende Mikroglia, Kupffer-Zellen in der Haut und Osteoklasten in Knochen. Obwohl diverse Studien aus dem letzten Jahrzehnt eindeutig zeigen, dass Makrophagen auf mechanische Signale reagieren, ist der zugrunde liegende Mechanismus, wie diese Signale eine Entzündungsreaktion modulieren, noch immer unzureichend verstanden.

Die vorliegende Studie beinhaltet die systematische Untersuchung, wie die Steifigkeit der Mikroumgebung das proinflammatorische Verhalten von Makrophagen beeinflusst. Neben der Charakterisierung der regulatorischen Wirkung auf die proinflammatorische Genexpression und Zytokinproduktion untersucht diese Arbeit auch den Einfluss der Steifigkeit auf das Inflammasom; eine der wichtigsten Signalplattformen für Makrophagen.

Zu diesem Zweck wurde zunächst ein Zellkultursystem mit 2D-Polyacrylamid-Hydrogelen als Zellsubstrat entwickelt, bei dem das Elastizitätsmodul der Gelsubstrate gezielt eingestellt werden kann. Unter Verwendung von Substraten mit einem Elastizitätsmodul zwischen 0,2 kPa und 33,1 kPa zeigt die mikroskopische Analyse, dass aus Knochenmark stammende Makrophagen im Vergleich zu steifem Polyacrylamid eine weniger ausgebreitete und rundere Morphologie annehmen. Nach dem Primen mit Lipopolysaccharid waren die Expressionsniveaus des Gens, das für TNF-α kodiert, auf deformierbareren Hydrogelen höher, jedoch gab es keine signifikanten Unterschiede in der Expression anderer wichtiger pro-inflammatorischer Gene. Eine zusätzliche Stimulierung von Makrophagen mit dem Ionophor Nigericin bewirkte höhere sekretierte Proteinspiegel von IL-1β und IL-6 auf deformierbaren Substraten. Makrophagen, die deformierbarem Polyacrylamid ausgesetzt waren, zeigten auch eine verstärkte Bildung des NLRP3-Inflammasoms sowie ein erhöhtes Ausmaß an pyroptotischem Zelltod. Die Hochregulierung der Inflammasom-Assemblierung auf deformierbaren Hydrogelen wurde nicht primär auf die reduzierte Zellausbreitung zurückgeführt, da räumlich begrenzte Zellen auf Mikromustern zu einer Abnahme von Inflammasom-positiven Zellen im Vergleich zu stark ausgebreiteten Zellen führten. Schließlich verringerte eine Störung der Aktomyosin-Kontraktilität die Unterschiede in der Inflammasombildung zwischen deformierbaren und steifen Substraten.

Zusammenfassend zeigen diese Ergebnisse, dass die Substratsteifigkeit die proinflammatorische Reaktion von Makrophagen beeinflusst und beschreiben erstmalig, dass das NLRP3-Inflammasom eine der Signalkomponenten ist, die von der zellulären Steifheitswahrnehmung beeinflusst werden. Die hier vorgestellte Arbeit erweitert unser Verständnis davon, wie die Steifigkeit der Mikroumgebung das Verhalten von Makrophagen beeinflusst und welche Elemente ihrer Maschinerie dazu beitragen könnten mechanische Signale in die Regulierung ihrer Entzündungsfunktionen zu integrieren. Das Einsetzen pathologischer Prozesse oder die Implantation von Fremdkörpern stellen Immunherausforderungen dar, bei denen Makrophagen einer sich mechanisch verändernden Umgebung ausgesetzt sein können. Daher könnte ein besserer Einblick in die Art und Weise, wie Makrophagen biophysikalische Signale erkennen und verarbeiten, möglicherweise eine Grundlage für neue Strategien zur Modulation von Entzündungsreaktionen bieten.

Contents

INTRODUCTION 1

1.1 Macrophage cell biology..**1**

1.1.1 The origin of macrophages 1

1.1.2 The macrophage: a swiss army knife 3

1.1.3 The macrophage pro-inflammatory response 4

1.2 Immunobiophysics: the force of the immune system...**10**

1.2.1 Exertion of immune cell forces 10

1.2.2 Immune cell mechanosensing...13

1.3 Cellular mechanosensing and mechanotransduction...**15**

1.3.1 Cell adhesions to the extracellular matrix...15

1.3.2 Nuclear mechanotransduction 19

1.3.3 Membrane mechanosensing elements..22

1.4 Macrophage mechanosensing..**25**

AIMS AND SCOPE OF THE THESIS 27

RESULTS.. 29

3.1 Morphol. characterisation of macrophages cultured on substrates of varying stiffness....29

3.1.1 BMDMs adhere and can be cultured on polyacrylamide hydrogels..............................29

3.1.2 Macrophage morphology is influenced by substrate stiffness 32

3.1.3 PEG-Hep hydrogels induce similar morphological differences as PAA substrates but do not constitute a suitable macrophage culture platform 34

3.1.4 Substrate stiffness affects membrane architecture...36

3.2 Impact of substrate stiffness on the pro-inflammatory response of macrophages............38

3.2.1 The morphol. differences induced by different stiffness persist after macrophage priming...38

3.2.2 Tuning substrate stiffness does not cause major changes in the expression of pro-inflammatory genes 39

3.2.3 Lower substrate stiffness upregulates the secretion of the cytokines IL-6 and IL-1β.40

3.2.4 Stiffer substrates diminish macrophage pyroptotic cell death 42

3.2.5 Compliant substrates enhance NLRP3 inflammasome formation 43

3.3 Investigation of macrophage mechanotransducing elements 46

3.3.1 Limiting cell spreading alone does not recapitulate the effects induced by stiffness on inflammasome formation 46

3.3.2 Actomyosin contractility may play a role in transducing the mechanical cues given by substrate stiffness 48

DISCUSSION AND CONCLUSIONS 51

4.1 Compliant substrates enhance the macrophage pro-inflammatory response 51

4.2 Substrate stiffness influences the formation of the NLRP3 inflammasome.........................54

4.3 Exclusively altering cell spreading does not explain the differences induced by substrate stiffness 55

4.4 Actomyosin contractility as a potential macrophage mechanotransducer element.............56

4.5 Potential impact of the study in the context of cancer...59

4.6 Potential impact of the study in the context of implant design 60

4.7 Conclusions of the study...62

MATERIALS AND METHODS 63

5.1 Production of polyacrylamide (PAA) hydrogels...63

5.2 Production of polyethylenglycol-heparin (PEG-Hep) hydrogels...64

5.3 Mechanical characterisation of hydrogels and macrophages 66

5.4 Isolation and culture of bone marrow-derived macrophages (BMDMs)...............................67

5.5 Fluorescence confocal microscopy 70

5.6 Scanning electron microscopy (SEM)...73

5.7 Gene expression analysis using quantitative real-time PCR (qRT-PCR)...............................73

5.8 Cytokine quantification assays..74

5.9 Cell viability assay 75

5.10 Culture of BMDMs on micropatterns 75

5.11 Optical diffraction tomography (ODT) 76

5.12 Statistical analysis and data visualisation 77

APPENDIX.. 79

LIST OF ACRONYMS AND ABBREVIATIONS 84

LIST OF FIGURES.. 87

BIBLIOGRAPHY.. 89

ACKNOWLEDGEMENTS 115

INTRODUCTION

1.1 Macrophage cell biology

1.1.1 The origin of macrophages

On Christmas 1882, in a family house located in the Sicilian city of Messina, a 37-year-old zoologist plucked some thorns from a tangerine tree and introduced them under the skin of starfish larvae. The next day, looking at the transparent specimen through his microscope, he observed that a bunch of motile cells had surrounded the foreign material. This landmark experiment, together with previous observations on nutrient uptake by the same cells, enabled Élie Metchnikoff to establish the concept of "phagocytosis", a term derived from the Greek *phago* (to devour) and *cytos* (cell) (Metschnikoff, 1878, 1884d, 1884b, 1884a). During the following years he documented the presence of phagocytes in vertebrates, differentiated between macrophages and microphages (polymorphonuclear leukocytes), and studied their function in several infectious diseases (Metschnikoff, 1883, 1884c, 1887, 1888), further developing the idea of phagocytosis as a defence mechanism of the organism against external pathogens and dead cells. These discoveries granted Metchnikoff a visit to Stockholm in 1908 to receive the Nobel Prize together with Paul Ehrlich, who are considered the "fathers of cellular and humoral immunity", respectively (Kaufmann, 2008).

By now it is well established that macrophages are heterogeneous cells widely distributed across all kinds of organs, taking specific names in some of the tissues where they reside. This is the case of microglia (central nervous system, CNS), alveolar macrophages (lung), Kupffer cells (liver), osteoclasts (bone), Langerhans cells (skin) and histiocytes (spleen and connective tissue) (Gordon et al., 2014; Ruytinx et al., 2018). Besides the different stimuli they might receive during their lifetime, it is important to note that the specific anatomical site macrophages reside in also conditions their gene expression and functional profiles (Gautier et al., 2012; Lavin et al., 2014).

Being cells that conduct immune surveillance and that are constantly exposed to perturbations from their microenvironment, macrophages need to be frequently replaced. Research done in the last years has provided a more complete view of their origin and maintenance (see Fig. 1.1). For decades, the prevailing dogma was that tissue-resident macrophages were only repopulated from monocytes circulating in peripheral blood (van Furth et al., 1972; Yona and Gordon, 2015). Monocytes originate from progenitors in the bone marrow, where haematopoietic stem cells (HSCs) go through a series of intermediate differentiation steps of myeloid cells and generate promonocytes that fully maturate once released into the bloodstream. Circulating monocytes can then either migrate into tissues and finally differentiate into resident macrophages or enter apoptosis 1-2 days after their production if unused (Ginhoux and Jung, 2014). This generation process is especially relevant to replenish the pools of tissue-resident macrophages under inflammatory settings. Nevertheless, during homeostatic conditions, monocyte-derived macrophages only contribute to populate certain locations, such as the intestine and the dermis, suggesting the existence of additional sources of macrophages. As proved by recent advances, in many other sites resident macrophages are developed before birth and initially originate from embryonic progenitors, mostly from early yolk sac progenitors and in some cases from foetal liver HSCs. This is for example the case of microglia and alveolar macrophages (Ginhoux et al., 2010; Hashimoto et al., 2013; Jakubzick et al., 2013; Yona et al., 2013). Moreover, during adulthood, these local macrophages keep some self-renewal capacity, enabling to maintain their numbers during steady-state conditions and also contributing to cell expansion during situations of infection and inflammation (Sieweke and Allen, 2013; Gordon and Martinez-Pomares, 2017).

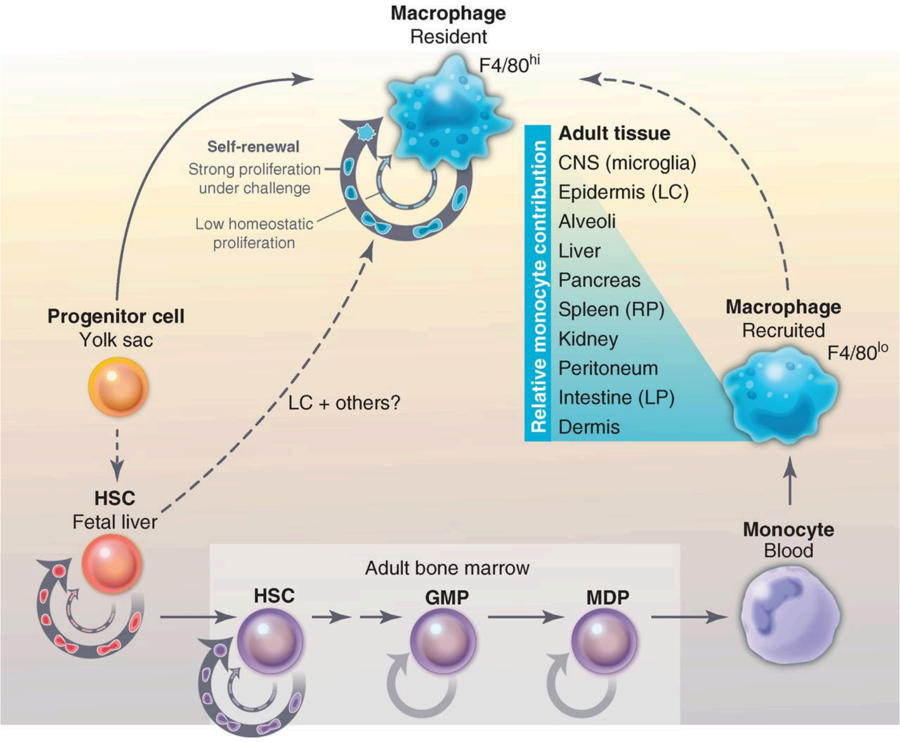
Macrophage
Resident
F4/80hi
Self-renewal
Strong proliferation under challenge
Low homeostatic proliferation
Adult tissue
CNS (microglia)
Epidermis (LC)
Alveoli
Liver
Pancreas
Spleen (RP)
Kidney
Peritoneum
Intestine (LP)
Dermis
Relative monocyte contribution
Macrophage
Recruited
F4/80lo
Progenitor cell
Yolk sac
LC + others?
HSC
Fetal liver
Monocyte
Blood
Adult bone marrow
HSC
GMP
MDP

Figure 1.1 | Macrophage origin and self-renewal.
Tissue-resident macrophages can arise from early embryonic progenitors in the yolk sac or sometimes even from HSCs of foetal liver origin. Once the organism is developed, haematopoiesis shifts to the bone marrow, where HSCs can differentiate into blood-circulating monocytes. Upon certain stimuli, monocytes migrate into tissues and maturate into macrophages. Whether resident macrophages originate from monocytes or not is highly dependent on the type of tissue (their relative contribution to the resident cell pool is indicated in the figure in increasing order from top to bottom). Moreover, resident macrophages also have self-renewal capacities, which are lower during homeostasis and higher during development, depletion or stimulatory challenges. GMP, granulocyte-macrophage progenitor; MDP, macrophage-dendritic progenitor; LC, Langerhans cells; RP, red pulp; LP, lamina propria. Figure adapted from Sieweke and Allen (2013).

1.1.2 The macrophage: a Swiss army knife

The innate immune system represents the first line of defence of our organism against invading pathogens and internal threats. Upon activation of the innate immune system, its different cellular components identify infected and damaged host cells to destroy them, initiate adaptive immune responses tailored to the specific threat and trigger the onset of tissue repair to recover homeostasis. Being a key component of this defensive system, macrophages are versatile cells involved in a broad spectrum of functions.

First, macrophages are professional phagocytes: they are capable of phagocyting particles larger than 0.5 μm with high efficiency (Rabinovitch, 1995). Phagocytosis is a process comprised of multiple stages, which begins with the detection of the target particle. This is done via pattern recognition receptors (PRRs), which recognise either pathogen-associated molecular patterns (PAMPs) in the case of microbes, or damage-associated molecular patterns (DAMPs) in the case of damaged or mutated host cells. The recognition of PAMPs or DAMPs present on the surface of the target activate signalling pathways that promote its phagocytosis. This triggers the changes in the membrane lipids and the reorganisation of the actin cortex, leading to an extension of the membrane that enables the cell to start covering the particle (Freeman and Grinstein, 2014). When this phagocytic cup fully surrounds it, the membrane protrusions fuse and the particle is internalised, forming a specialised structure called phagosome. This so-called "early phagosome" undergoes the fusion and fission with vesicles of the endocytic compartment that modify the composition of the membrane, transitioning into a "late phagosome". This organelle then fuses with lysosomes to become a phagolysosome, a microbicidal vacuole that becomes increasingly acidic due to the protons pumped inwards, that accumulates multiple hydrolytic enzymes such as proteases, lipases and lysozymes, and that contains enzymes capable of producing reactive oxygen species (ROS) and hypochlorous acid (Levin et al., 2016). Altogether, these different mechanisms catalyse the degradation of the engulfed particle and help eliminating the infectious threat or cell debris (Gordon, 2016; Uribe-Querol and Rosales, 2020).

Second, the digestion of foreign pathogens and damaged host cells done by macrophages also confers these cells the ability to function as antigen-presenting cells (APCs). Upon destruction of the target, macrophages can present antigens to T lymphocytes, which recognise them and activate an adaptive immune response. Macrophages can do this presentation via their major histocompatibility complexes (MHCs) of class I or class II, activating different T cells (Burgdorf and Kurts, 2008). If the antigen is presented via MHC I, cytotoxic T cells ($CD8^+$ T_c) are activated, whose function is to directly contact and eliminate infected and cancerous cells. If it is done via MHC II, the receptors of T helper cells ($CD4^+$ T_h) engage, leading to the release of different cytokines that will promote the activation of other immune cells (Burgdorf et al., 2007; Gaudino and Kumar, 2019).

The third role played by macrophages is being one of the main coordinators of the inflammatory response. They participate in all phases of inflammation, from its initiation to its peak as well as during its resolution to recover tissue homeostasis. Depending on the input signals given by the microenvironment of the injured tissue, macrophages can polarise towards pro- or anti-inflammatory phenotypes, with distinct surface markers and gene expression profiles (Mantovani et al., 2002; Murray et al., 2014; Ruytinx et al., 2018). On the one side, certain antigens and cytokines cause naïve (M0) macrophages to differentiate into the "classically activated" or M1 phenotype, which promote an inflammatory response that leads to the destruction of microorganisms or cancerous cells. These macrophages secrete chemokines that recruit additional immune cells as well as release other pro-inflammatory cytokines and factors such as IL-6, IL-1β, TNF-α or inducible nitrogen oxide synthase (iNOS) (Mosser and Edwards, 2008). On the other side, different signals trigger the adoption of an immunosuppressive state called "alternatively activated" or M2 phenotype. These macrophages produce anti-inflammatory proteins like arginase-1, IL-4, IL-10 or IL-13, which promote tissue repair and drive the re-establishment of tissue homeostasis (Mantovani et al., 2002; Sica and Mantovani, 2012).

Although the M1/M2 classification has been traditionally used by immunologists due to its convenience, it is important to note that this is oversimplified since the macrophage phenotype is not binary but actually a continuous spectrum. Furthermore, macrophages are remarkably plastic cells and can undergo a "phenotype switch", i.e., they can transition from one phenotype to an other depending on the stimuli received from their microenvironment. Therefore, the M1/M2 phenotypes only represent the extremes of the possible states macrophages can adopt depending on the specific tissue and stimulatory conditions they are exposed to (Murray and Wynn, 2011; Sica and Mantovani, 2012).

Among the different macrophage functions introduced above, the research done in this thesis focuses on understanding the influence of substrate stiffness on their pro-inflammatory behaviour. The next paragraphs describe in more depth some of the most relevant signalling events involved in this response.

1.1.3 The macrophage pro-inflammatory response

For the initial detection of their targets, macrophages take advantage of pattern-recognition receptors (PRRs) located both within their plasma membrane and intracellularly. As mentioned above, these receptors recognise specific molecular signatures presented by the particles that may pose a threat to the organism. In the case of foreign pathogens, PRRs identify their PAMPs, which are evolutionarily conserved components of microbes usually not present in mammalian cells. To detect host cells that have been damaged, macrophages and other innate immune cells bind to DAMPs, endogenous molecules that are released upon cell infection as well as a consequence of other events, such as traumas, burns or the effect of chemical toxins. Upon detection of these PAMPs and DAMPs, macrophages activate different signalling cascades that lead to phagocytosis onset and the regulation of gene expression programmes to promote the synthesis of inflammatory cytokines (Newton and Dixit, 2012).

The inflammasome is one of the most relevant macrophage pro-inflammatory signalling platforms. It is a cytoplasmic macromolecular complex whose ultimate function is to activate inflammatory caspases like caspase-1, an enzyme responsible of catalysing the maturation of the cytokines IL-1β and IL-18 and promoting a form of cell death called pyroptosis. Inflammasomes are composed of three different types of proteins: a stimuli sensor, an adaptor protein – usually the protein ASC (apoptosis-associated speck-like protein containing a caspase-recruitment domain) – and an effector caspase. In order to recognise different stress-indicating molecules, innate immune cells contain a diverse repertoire of sensor proteins that give name to the multiple existing inflammasome types, such as NLRP1, NLRP3, NLRC4, pyrin or AIM2 (Bateman et al., 2021).

Extensively studied in the last 20 years, the NLRP3 (NOD-, LRR- and pyrin domain-containing protein 3) is one of the best characterised inflammasomes, and multiple publications have highlighted the potential role it may play in different pathologies. As mentioned above, the NLRP3 inflammasome mediates the response against viruses (Shrivastava et al., 2016; Zhao and Zhao, 2020) and bacteria (Anand et al., 2011; Vladimer et al., 2013). One of the latest examples is the participation of this inflammasome in the pathogenesis caused by SARS-CoV-2. It has been shown that the viral infection of human primary monocytes *in vitro* causes the activation of the inflammasome (Rodrigues et al., 2020; Toldo et al., 2021). Moreover, assembled inflammasomes have been detected in lung tissue of patients with acute respiratory distress syndrome who died from COVID-19 (Rodrigues et al., 2020). Together with the fact that inflammasome-derived proteins such as IL-1β and IL-18 are increased in severe cases of the disease, these findings support the idea that NLRP3 inflammasome activation may be contributing to the cytokine storm and hyper-inflammation state linked to severe COVID-19 cases (Huang et al., 2020; Lucas et al., 2020; Brodin, 2021).

Besides participating in the response against microbes, NRLP3 has been linked to a range of non-infectious diseases associated with chronic inflammation (Mangan et al., 2018). Gain-of-function mutations in NLRP3 are the cause of systemic cryopyrin-associated autoinflammaotry diseases (CAPS), where an overproduction of proteins such as IL-1β causes several inflammatory syndromes (see review by Alehashemi and Goldbach-Mansky (2020) for further details). Moreover, the activity of the NLRP3 inflammasome helps maintaining a low-grade chronic inflammation state in the white adipose tissue, promoting the development of metabolic disorders such as insulin resistance and diabetes (Vandanmagsar et al., 2011; Esser et al., 2013; Lee et al., 2013; Wani et al., 2021). And NLRP3 also becomes activated by crystals and protein aggregates. Usually these are formed endogenously, such as monosodium urate (MSU) crystals, which cause gout flares (Martinon et al., 2006); or beta-amyloid plaques, formed in Alzheimer disease (Heneka et al., 2013). Nevertheless, inflammasome activation can also occur upon assimilation of particles from the environment, such as asbestos and silica crystals entering the lungs and inducing asbestosis and silicosis, respectively (Dostert et al., 2008). Given its association with so many pathological processes, it is of particular interest to identify which mechanisms regulate the formation and activation of the NLRP3 inflammasome.

The main constituting elements of the NLRP3 inflammasome (Swanson et al., 2019) are the following:

i. The sensor – NLRP3: contains an N-terminal PYD domain that binds to the adaptor protein, a central NACHT domain which upon activation allows the self-oligomerisation of the protein, and C-terminal LRRs (leucine-rich repeats) that mediate the recognition of the stimulus.

ii. The adaptor – ASC: comprises an N-terminal PYD to interact with NLRP3 and a C-terminal CARD domain to interact with the effector caspase.

iii. The effector – Caspase-1: present in the canonical inflammasome, its inactive form pro-caspase-1 contains an N-terminal CARD that enables the interaction with ASC, and a central (p20) and C-terminal (p10) catalytic domains. Upon inflammasome formation, caspase-1 self-cleaves and activates its catalytic domains, which can then start processing their target substrates.

The inflammasome represents a key element of the pro-inflammatory signalling network and in order to ensure a timely and adequate response its activation is tightly controlled. For the successful formation of the canonical NLRP3 inflammasome, two steps are usually required: 1) priming, which induces the synthesis of some of its components; and 2) activation, where the different proteins assemble and the effectors are activated. This 2-step model is illustrated in Fig. 1.2 and described in the following lines.

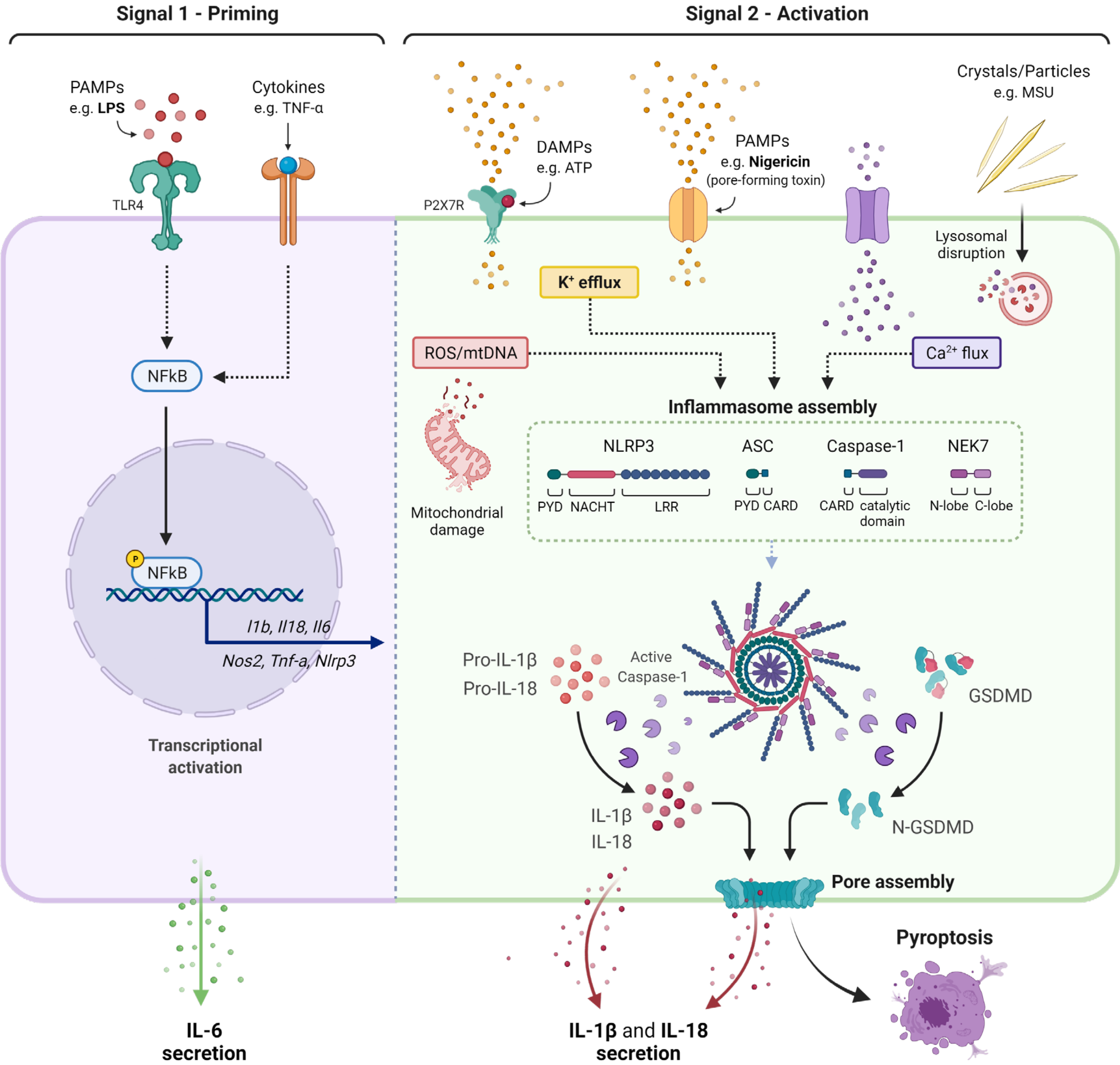
Signal 1 - Priming
Signal 2 - Activation
PAMPs
e.g. LPS
Cytokines
e.g. TNF-α
TLR4
NFkB
P
NFkB
I1b, Il18, Il6
Nos2, Tnf-a, Nlrp3
Transcriptional activation
IL-6 secretion
DAMPs
e.g. ATP
P2X7R
PAMPs
e.g. Nigericin
(pore-forming toxin)
Crystals/Particles
e.g. MSU
Lysosomal disruption
K⁺ efflux
ROS/mtDNA
Ca²⁺ flux
Mitochondrial damage
Inflammasome assembly
NLRP3
PYD
NACHT
LRR
ASC
PYD
CARD
Caspase-1
CARD
catalytic domain
NEK7
N-lobe
C-lobe
Pro-IL-1β
Pro-IL-18
Active Caspase-1
GSDMD
IL-1β
IL-18
N-GSDMD
Pore assembly
Pyroptosis
IL-1β and IL-18 secretion

Figure 1.2 | Control of NLRP3 inflammasome formation.
For the activation of this inflammasome, two steps are required. The signal 1 (left) is provided by PAMPs or cytokines, which bind their corresponding PRRs, leading to the nuclear translocation of NFκB and the transcriptional upregulation of different pro-inflammatory genes. Signal 2 is provided by different PAMPs and DAMPs that trigger different signalling events, including K^+ efflux, Ca^{2+} flux or the release of mitochondrial ROS and DNA. Together, priming and activation stimuli induce the oligomerisation of the different inflammasome components into a large multi-protein complex. This causes the activation of caspase-1, enzyme that can then catalyse the cleavage and maturation of the cytokines IL-1β and IL-18, which are then secreted out of the cell. Caspase-1 also cleaves gasdermin D (GSDMD), which then forms pores in the plasma membrane, facilitating cytokine release and inducing pyroptotic cell death.

1.1.3.1 Priming of the NLRP3 inflammasome

The main purpose of this step (signal 1) is to enhance the production of the inflammasome component NLRP3 as well as the expression of some of the main inflammasome substrates: the cytokine immature forms pro-IL-1β and pro-IL18.

Various PAMPs (e.g. LPS, CpG oligonucleotides) and certain cytokines (TNF-α, type I IFN, IL-1β) represent stimuli that, upon recognition by their respective membrane receptors, can trigger the priming of NLRP3 (Bauernfeind et al., 2009; Franchi et al., 2009; Moretti and Blander, 2021; Paik et al., 2021). Among them, lipopolysaccharide (LPS) remains one of the most commonly used ligands to license this inflammasome and promote pro-IL-1β production, and it has been the priming molecule used along all the experiments performed in this dissertation.

LPS is a cell wall component of gram-negative bacteria that can be recognised by the toll-like receptor 4 (TLR4) present on the surface of macrophages. Preceded by the assistance of the proteins LBP and CD14, the complex formed by TLR4 and its partner MD-2 detects the presence of LPS (Park et al., 2009; Ryu et al., 2017). This event promotes the homodimerisation of TLR4 molecules, triggering conformational changes in the intracellular side of the receptor that activate two important signalling pathways. On the one hand, the TLR4/TRIF/IRF3 pathway, which is responsible of inducing the transcription of type I interferon genes (Honda et al., 2006). And on the other hand, the TLR4/MyDD88/NF-ϰB pathway, which ultimately leads to the activation and translocation of NF-ϰB into the nucleus (Akira and Takeda, 2004; Kawai and Akira, 2010). There, this transcription factor upregulates the expression of genes encoding for several major pro-inflammatory proteins, including the cytokines IL-6, TNF-α, pro-IL-1β and pro-IL-18 and the inflammasome component NLRP3 (Bauernfeind et al., 2009; Kuzmich et al., 2017; Zamyatina and Heine, 2020). Therefore, LPS priming promotes the synthesis of some of the most important inflammasome substrates and contributes to license the macrophage for the subsequent assembly and activation of the complex.

Besides the increase in the transcription of pro-inflammatory genes, it is important to note that during the priming step the sensor protein NLRP3 can also undergo through several post-translational modifications (PTMs) that facilitate its rapid regulation. So far, ubiquitylation, phosphorylation, sumoylation, acetylation and nitrosylation of NRLP3 residues have been recently described (McKee and Coll, 2020). These events can affect the structure, activity, localisation, degradation and interactions of NLRP3 and, in consequence, influence the inflammasome formation dynamics in both positive and negative manners (Moretti and Blander, 2021; Paik et al., 2021).

1.1.3.2 Activation of the NLRP3 inflammasome

After the priming step, an NLRP3 inducer (signal 2) initiates a second set of signalling events that lead to the final assembly and activation of the inflammasome.

A variety of PAMPs and DAMPs can trigger NLRP3 activation through different mechanisms (see Swanson et al. (2019) for an extended review). The best documented one is potassium (K^+) efflux. Events that cause a substantial efflux of K^+ ions from the cytosol to the extracellular space trigger the assembly of the inflammasome. This is for example the case for extracellular ATP, detected by the membrane purinergic receptor P2X7R (Franchi et al., 2007; Piccini et al., 2008). Or the K^+/H^+ ionophore nigericin, a toxin derived from the gram-positive bacteria Streptomyces hygroscopicus and the substance employed in this study to trigger inflammasome activation (Pétrilli et al., 2007; Muñoz-Planillo et al., 2013). Despite not being yet completely understood, changes in the flux of other ions such as Calcium (Ca^{2+}) (Lee et al., 2012; Murakami et al., 2012; Katsnelson et al., 2015) and chlorine (Cl^-) (Tang et al., 2017; Green et al., 2018) have also been associated with inflammasome formation. Other events causing impairment or destabilisation of some cellular organelles also promote NRLP3 activation. Phagocytosis of particulate matter, either endogenous as uric acid and cholesterol crystals or exogenous like silica and asbestos, can cause lysosomal damage, inducing the escape of molecules that lead to inflammasome assembly (Hornung et al., 2008; Orlowski et al., 2015). In addition, molecules released upon mitochondrial dysfunction (e.g. mtROS and mtDNA) have also been observed to induce NRLP3 activation (Zhou et al., 2011; Yabal et al., 2019).

Once signal 2 is detected, NLRP3 molecules oligomerise, a process facilitated by NEK7 (Sharif et al., 2019; Zhao et al., 2020). ASC is then recruited, forming multiple ASC filaments that assemble into a 1-μm structure known as ASC speck. This structure recruits caspase-1 molecules that, due to the proximity to each other, can self-cleave and activate. Caspase-1 catalyses the maturation of the cytokines pro-IL-1β and pro-IL18 into their biologically active forms (Agostini et al., 2004). Additionally, the activation of the NLRP3 inflammasome can lead to pyroptosis, a form of lytic cell death. For this, caspase-1 cleaves gasdermin D (GSDMD) and enables its N-terminal domain to oligomerise and insert into the plasma membrane, forming pores that allow intracellular material to be released (He et al., 2015; Shi et al., 2015; Liu et al., 2016). Pyroptosis facilitates the secretion of cytokines and allows the release of intracellular danger molecules to enhance the response of neighbouring cells, yet it rapidly leads to acute loss of membrane integrity and overall viability of the pyroptotic cell (Evavold et al., 2018; Monteleone et al., 2018).

Although significant progress has been made to determine the basic mechanisms mediating NLRP3 inflammasome formation, the role of additional regulatory mechanisms is not fully understood yet. This is the case for the PTMs cited above or of cellular elements such as the microtubule-organising centre and the dispersion of the trans-Golgi, which have been reported to participate in the coordination of its assembly (Chen and Chen, 2018; Magupalli et al., 2020). Therefore, further research is needed to better understand how the different signals converge into NRLP3 activation and how the process of inflammasome formation is finely controlled both in space and time within the cell (Hamilton and Anand, 2019; Paik et al., 2021).

1.2 Immunobiophysics: the force of the immune system

"The life of immune cells is intensely physical" (Huse, 2017). Adhering to blood vessels, migrating through small interstitial spaces, engulfing dangerous particles and forming signalling synapses with other cells are processes that involve the application of mechanical forces. Moreover, leukocytes not only exert forces but also face dynamic and changing environments where they need to sense and process different pieces of physical information, such as the local stiffness of their surroundings or the shear forces exerted by fluid flow. The development of new biophysical tools and methods during the last decades enabled scientists to start exploring the impact of forces on leukocytes, a field coined with the name "Immunobiophysics" (Fritzsche, 2021; Pfannenstill et al., 2021). The next paragraphs provide some examples on how the application and perception of forces in these different situations control immune cell behaviour.

1.2.1 Exertion of immune cell forces

To perform their function immune cells frequently need to migrate to their target location. Motion implies the generation of forces, and leukocyte migration is no exception. The research published in recent years has begun to unveil the details behind immune cell locomotion, especially in 2D environments. For example, when migrating on surfaces, cells like lymphocytes and neutrophils elongate, forming lamellipodia at their leading edge and a tail-resembling uropod at the rear end. Integrins present on the basal side of leukocytes mediate their adhesion to the substrate (Fig. 1.3A) (Renkawitz et al., 2009; Sánchez-Madrid and Serrador, 2009; Renkawitz and Sixt, 2010). These adhesions behave as "catch bonds", which are defined as bonds whose lifetime increases up until an optimal tensile force is reached. Once this tension is surpassed, the lifetime of the bond decreases (Thomas et al., 2008). In contrast, most biomolecular contacts belong to the so called "slip bonds", whose lifetime is shortened by increasing tensile forces. The formation of adhesion catch bonds enables the formation of a "molecular clutch" composed of the integrin/talin/F-actin system, which constitutes the backbone of the propulsion machinery employed by cells to move forward (Fig. 1.3B) (Chan and Odde, 2008; Vicente-Manzanares et al., 2009). For leukocytes to migrate, upon engagement with their substrates cells exert force against the underlying surface. Distinct 2D traction force profiles have been identified for the different immune cell types. Macrophages and dendritic cells (DCs) apply higher forces near the frontal end of the moving cell and, therefore, are considered to display a "front-wheel drive" locomotion mechanism (Ricart et al., 2011; Hind et al., 2015). Contrarily, neutrophils and T lymphocytes exhibit a rear-wheel drive behaviour, since traction forces peak at the rear part of the cell body (Smith et al., 2007; Stanley et al., 2008).

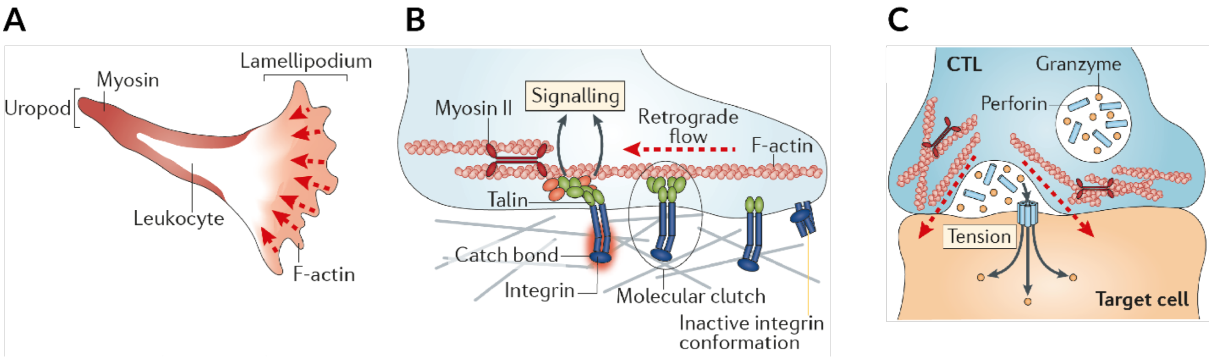

Figure 1.3 | Forces in immune cell locomotion and CTL killing. (A) Shape adopted by leukocytes migrating in 2D. **(B)** Diagram depicting the formation of catch bonds and a molecular clutch upon cell adhesion. **(C)** When in contact with its target cell, CTLs exert tension on its membrane to enhance perforin pore formation and facilitate the entrance of cytotoxic granzymes. Figure adapted and modified from Huse (2017).

In order to kill their target cells, cytotoxic T lymphocytes (CTLs) establish an immune synapse with them and secrete a mixture of toxic proteins in their direction. Among other factors they release perforin, a protein that forms pores in the membrane of the target cell, facilitating the entrance of granzyme proteases and the consequent induction of apoptosis (Stinchcombe and Griffiths, 2007). Interestingly, (Basu et al., 2016) discovered that the pore-forming ability of perforin becomes enhanced upon an increase in the membrane tension of the target cell. Moreover, they observed that CTLs coordinate the release of cytotoxic enzymes and the exertion of force via F-actin on the target cell (Fig. 1.3C). Altogether, the authors of the study suggest that upon the formation of the immune synapse, CTLs apply forces that strain the membrane of their target cell, sensitising it to the activity of perforin and, thus, promoting the destruction of their victim.

Another essential immune process driven by mechanical forces is phagocytosis. Professional phagocytes such as macrophages and neutrophils have the remarkable ability to engulf micron-sized particles, sometimes even larger than themselves (Cannon and Swanson, 1992; Herant et al., 2006). For the successful internalisation of their target, phagocytes first establish adhesions with the particle and begin the formation of a phagocytic cup (Jaumouillé and Waterman, 2020). As depicted in Fig. 1.4, the polymerisation of actin filaments generates the force needed to push against the membrane and form protrusions that extend along the particle (Herant et al., 2006, 2011; Jaumouillé et al., 2019). During the development of the phagocytic cup, this protrusive force has to overcome the resistance generated by the increasing surface tension (Herant et al., 2006, 2011). Simultaneously, the higher membrane tension is compensated by an increase in cell surface area. This is achieved through the flattening of membrane ruffles and folds and the mobilisation of intracellular vesicles to the plasma membrane (Petty et al., 1981; Suzaki et al., 1997; Masters et al., 2013). At its last stage, the phagocytic cup covering the totality of the particle needs to be closed. Current evidence suggests that a mechanochemical process might mediate membrane fission at the edges of the cup, an event that ultimately leads to the formation of the phagosome (Jaumouillé and Waterman, 2020) and later destruction of the target.

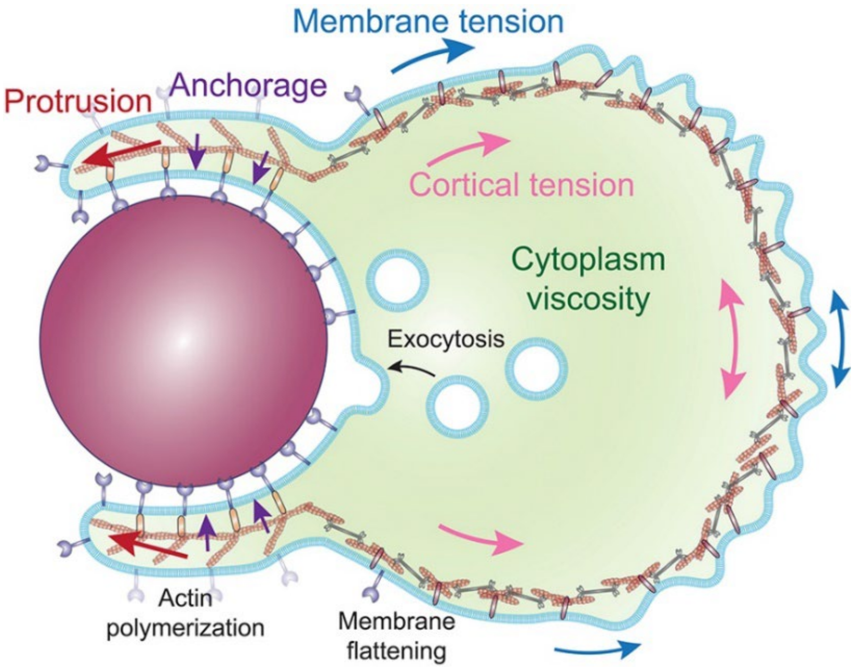

Figure 1.4 | Forces involved during phagocytic target internalisation.
Effective adhesion to the particle and protrusive forces exerted by actin filaments enable drive the formation of the phagocytic cup around the target. The consequent increase in both cortical and membrane tension is compensated by the usage of the available membrane reservoir, consisting of plasma membrane invaginations and the membrane present in intracellular vesicles. Figure adapted from Jaumouillé and Waterman (2020).

1.2.2 Immune cell mechanosensing

Besides generating forces to perform their functions, leukocytes are exposed to a variety of extrinsic biophysical stimuli. These include tissue rigidity, tension, compression and fluid flow shear forces. The ability of cells to perceive the mechanical information provided by their microenvironment is known as "mechanosensing"; and its integration into their signalling networks to elicit a specific cellular response is called "mechanotransduction" (Iskratsch et al., 2014).

For instance, circulating leukocytes are transported through blood and lymphatic vessels. In order to exit them and penetrate into tissues, immune cells first need to adhere to the walls of these conduits. This process, known as "leukocyte rolling", is dependent on hydrodynamic shear forces, since it has been reported that there is an optimal force range for the adhesive bonds to be established (Finger et al., 1996; Yago et al., 2004; Alon and Ley, 2008). The binding to the endothelial cells forming the vessels is mediated by selectins and integrins, which form catch bonds with their ligands (Fig. 1.5). Therefore, above the optimal force range of the circulating fluid, the adhesive bonds do not form and leukocytes increase their rolling speeds. Conversely, if the fluid shear forces are too low, the catch bonds do not remain stable enough to completely stop the cell, a mechanism that could avoid cell clumping in regions with a low flow regime like capillaries (Huse, 2017). Along the same line, Ekpenyong et al., 2017 showed that the *in vitro* mechanical deformation of pre-primed neutrophils induces their depolarisation, suggesting a mechanism that might avoid their over-activation while circulating through narrow blood vessels.

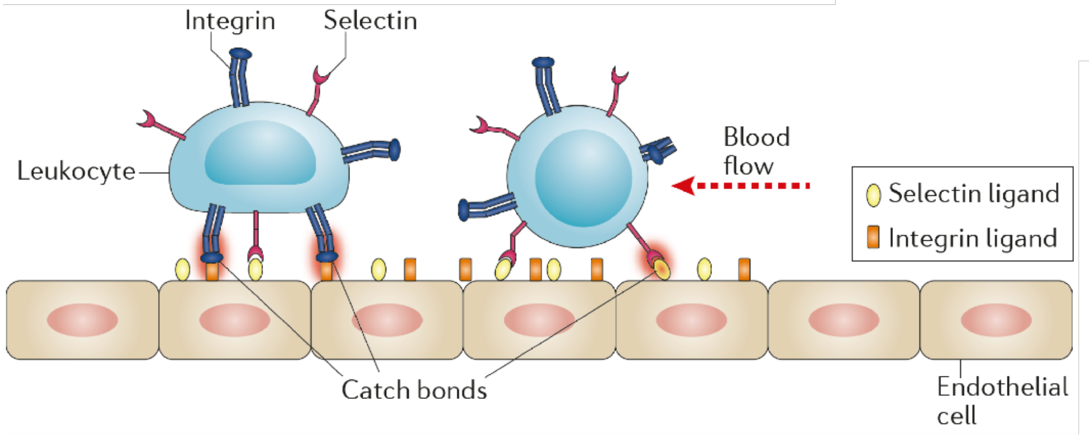

Figure 1.5 | Leukocyte rolling on blood and lymphatic vessels. Circulating leukocytes roll onto vessel walls forming adhesive catch bonds that allow them to stop and start extravasating. Figure adapted and modified from Huse (2017).

Adaptive immune cells are also influenced by external biophysical cues in different manners. B and T lymphocytes make contact with antigen-presenting cells (APCs) to detect the ligands exposed on their surface and generate a specific response against the corresponding threats. For the effective activation of T lymphocytes by APCs, their T cell receptors (TCRs) need to form peptide-MHC-TCR bonds under tension (Liu et al., 2014). Interestingly, the establishment of catch bonds between TCRs and their ligands boosts the ability of T cells to discriminate between bona fide and self-derived antigens (Das et al., 2015). In a similar fashion, B cell activation upon antigen recognition is also enhanced when the engagement of B cell receptors (BCRs) with their ligands occurs under higher tensile forces, yet this seems to be dependent on the BCR subtype (Wan et al., 2015).

Lastly, immune cells are also influenced by the stiffness of their microenvironment. Culturing T lymphocytes in stiffer synthetic matrices enhances their activation, proliferation and migration (Majedi et al., 2020; Meng et al., 2020) and increases their cytokine production and metabolism (Saitakis et al., 2017). B lymphocyte proliferation, activation, class switch and antibody responses are modulated by exposing B cells to different stimuli while in contact with substrates of differing stiffness (Zeng et al., 2015). And the expression of several dendritic cell surface markers like C-type lectin receptors is regulated by substrate stiffness, resulting in varying degrees of antigen internalisation (Mennens et al., 2017).

Research done in the last decades has massively expanded our knowledge on the mechanosensitivity of cells, including which forces are sensed by different cell types and which mechanisms do they use to detect and interpret biophysical cues. The rest of the introduction focuses on describing some of the main mechanotransducing mechanisms cells are equipped with (Section 1.3), and finally presents some of the current knowledge on macrophage mechanosensing (Section 1.4).

1.3 Cellular mechanosensing and mechanotransduction

The stiffness of organs and tissues spans several orders of magnitude (Guimarães et al., 2020), from a few hundred Pascal in the case of CNS tissue (Franze et al., 2013; Arani et al., 2015) to the GPa range in bones (Milovanovic et al., 2012; Mirzaali et al., 2016). Moreover, during the progression of pathologies such as cancer (Emon et al., 2018) or neurodegenerative diseases (Bonneh-Barkay and Wiley, 2009), and during recovery events like liver or spinal cord regeneration (Klaas et al., 2016; Möllmert et al., 2020), the mechanics of the affected tissues are frequently altered. The mechanical properties of the cell niche are mainly determined by the neighbouring cells and the surrounding extracellular matrix (ECM) (Guimarães et al., 2020). Specifically, the rigidity of the matrix largely depends on the combined effect of its molecular composition and the density, distribution and crosslinking degree of its constituents (Bonnans et al., 2014).

The mechanical microenvironment where cells reside influences their phenotype and function, having an impact on processes such as cell growth and differentiation (Handorf et al., 2015) , migration (Barriga et al., 2018) or immune response (Wong et al., 2020). To sense and process extrinsic mechanical signals, cells employ different strategies. The next paragraphs introduce some of them, focusing on the mechanisms responsible for transmitting and processing the mechanical information given by matrix stiffness.

1.3.1 Cell adhesions to the extracellular matrix

When cells interact with their surrounding matrix, some of the well-known mechanosensing structures they develop are cell-ECM adhesions (Jansen et al., 2017; Jo et al., 2020). Among them, focal adhesions have been extensively studied. These multiprotein complexes are not only responsible of ensuring the adequate attachment of cells to their substrate but also act as major sites of force transmission (Geiger and Yamada, 2011).

Integrins are the focal adhesion elements directly in contact with the ECM (Sun et al., 2016). They are transmembrane heterodimers formed by α and β subunits, whose combination results in 24 unique integrins that enable the cell to recognise multiple ECM components (Humphries et al., 2006). The extracellular domain of integrins binds to ECM proteins such as fibronectin, laminin, vitronectin and collagens. The cytoplasmic domain, which is indirectly linked to the F-actin cytoskeleton, mediates integrin signalling in both directions (Humphries et al., 2019) (see Fig. 1.6A). During "inside-out" signalling, molecular stimuli can induce the binding of regulatory proteins to the integrin cytoplasmic side, triggering the switch from a closed inactive state to an open active state and increasing the affinity of integrins for their ECM ligands (Takagi et al., 2002). On the other side, integrins also mediate "outside-in" signalling, since they facilitate the transmission of biophysical and biochemical information from the ECM into the cell by activating several signalling transducers (Horton et al., 2016a).

One of the essential players involved in the propagation of forces throughout the link with the matrix is the F-actin cytoskeleton. Importantly, several actin filaments can bundle together with molecules of myosin II and other crosslinking proteins to form stress fibres (Naumanen et al., 2008). Thanks to the motor activity of myosin II these structures can generate contractile forces, becoming one the crucial elements involved in cell mechanotransduction (Dumbauld et al., 2010). Within the adhesion complex, the transmission of physical information between integrins and the actin cytoskeleton is indirectly also regulated through adaptor proteins. For instance, talin can directly interact with the cytoplasmic domain of integrins as well as with F-actin (Kumar et al., 2016). Therefore, focal adhesion partner proteins not only have a structural function but also play a significant role in mechanosensation (Horton et al., 2015, 2016b).

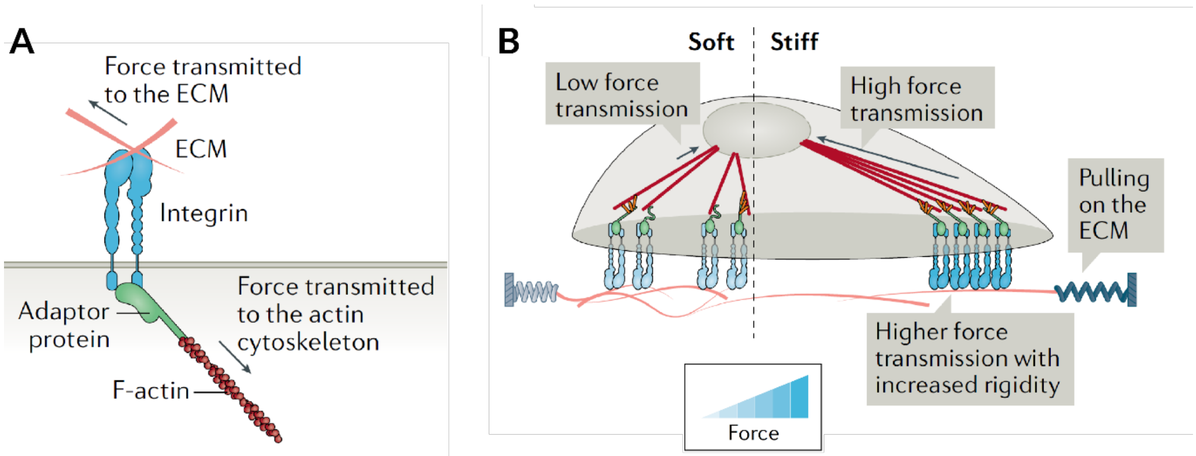
A
Force transmitted to the ECM
ECM
Integrin
Adaptor protein
Force transmitted to the actin cytoskeleton
F-actin
B
Soft
Stiff
Low force transmission
High force transmission
Pulling on the ECM
Higher force transmission with increased rigidity
Force

Figure 1.6 | Force transmission along the ECM – integrin – adaptor protein – F-actin axis. (A) Diagram displaying the basic architecture of matrix-cell adhesions, which enable the bidirectional transmission of forces arising either from the ECM or from the F-actin cytoskeleton. **(B)** Thanks to integrin-mediated adhesions and actomyosin contractility, cells can pull on the matrix and probe its mechanical properties. Higher ECM stiffness results in the reinforcement and maturation of the adhesion and higher force transmission. Figure adapted and modified from Kechagia et al. (2019).

To perceive the mechanical cues provided by their microenvironment, the cell uses the forces exerted by the actomyosin cytoskeleton to pull from the nascent focal adhesions initially established (Changede et al., 2015) (Fig. 1.6B). Depending on parameters such as ECM stiffness, the resulting tension can be lower or higher (Elosegui-Artola et al., 2018). If it reaches a sufficient level, this tensile force not only favours integrins to adopt their open active state but also promotes the formation of catch bonds between certain integrins and their ECM ligands, especially with RGD-containing proteins such as fibronectin (Kong et al., 2009; Elosegui-Artola et al., 2016).

These events promote the strengthening of the mechanical interactions with the ligand ("reinforcement") and the recruitment of additional integrins and adaptor proteins ("maturation"), causing the growth of these focal adhesions and the increase of their mechanical resistance (Galbraith et al., 2002; Roca-Cusachs et al., 2013; Strohmeyer et al., 2017).

As previously mentioned, when the force loading rates distributed across the adhesions are within an optimal range some mechanosensitive events mediated by adaptor and partner proteins can occur (Elosegui-Artola et al., 2016). For instance, talin can unfold and expose cryptic binding sites where vinculin can attach, stabilising the complex (Rio et al., 2009; Hirata et al., 2014). The activity of SRC and FAK, tyrosine kinases initially involved in the maturation of nascent adhesions, is also upregulated (Strohmeyer et al., 2017). FAK promotes the activation of paxillin, a protein that can bind activated vinculin and reinforce the adhesion complex (Qin et al., 2015). Moreover, FAK is also involved in the regulation of actin dynamics and contractility through the regulation of Rho GTPases (Rho, Rac and Cdc-42) (Mitra et al., 2005).

The small GTPase RhoA is of special interest within the context of this thesis (see diagram in Fig. 1.7). Once bound to GTP and, thus, in its active state, RhoA triggers the activation of ROCK (Lessey et al., 2012; Hodge and Ridley, 2016). When active, ROCK performs multiple functions: i) it activates the kinase LIMK, which inhibits the F-actin-severing protein cofilin (Hayakawa et al., 2011); ii) it phosphorylates MLC (myosin light chain) and inhibits MLC phosphatase, events that positively regulate the activity of myosin II (Amano et al., 1996; Kimura et al., 1996). Therefore, the upregulation of ROCK triggered by focal adhesion reinforcement promotes the stabilisation of actin filaments and facilitates the generation of contractile forces. Additionally, RhoA triggers the activation of mDia, a protein that favours F-actin polymerisation and, thus, also supports the activity of the system (Zigmond, 2004).

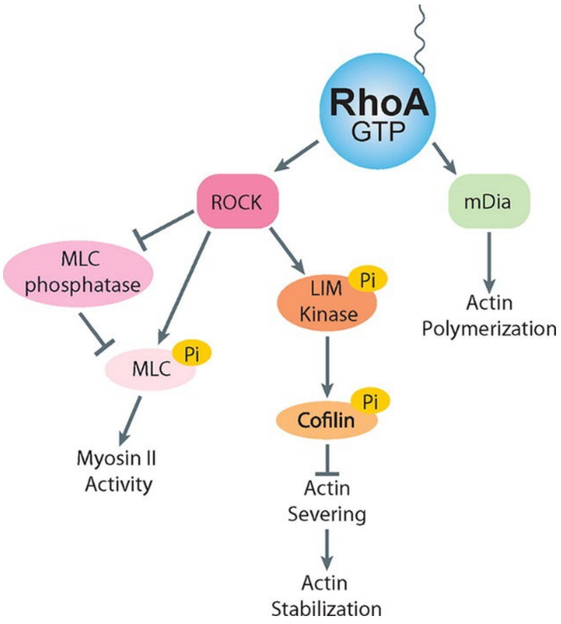

Figure 1.7 | Control of actomyosin activity by RhoA signalling. The activation of RhoA leads to an enhanced stabilisation of F-actin and an increase in actomyosin contractility. ROCK, Rho-associated protein kinase; MLC, myosin light chain; LIMK, LIM kinase; mDia, Diaphanous-related formin-1. Figure adapted from Lessey et al. (2012).

In addition to focal adhesions, some cell types contain other specific classes of cell-matrix contacts. This is the case of macrophages, which are also equipped with distinct adhesive structures known as podosomes (Linder and Wiesner, 2015). Despite sharing some of their molecular components with focal adhesions, their spatial organisation is different (Linder and Wiesner, 2016; van den Dries et al., 2019). Studies done in 2D substrate systems revealed that podosomes present a modular architecture (Fig 1.8), with a core of branched F-actin surrounded by an adhesive ring of integrins and plaque proteins like talin and vinculin (Linder et al., 2000; van den Dries et al., 2013). The top of the core is connected to the ring proteins by unbranched actomyosin filaments ("lateral fibres"), a sort of filament that can also mechanically couple individual podosomes to each other ("dorsal fibres"), forming higher-ordered clusters (Luxenburg et al., 2007; Bhuwania et al., 2012; Labernadie et al., 2014). Finally, a submodule called "cap" and localised on top of the core has been described, likely containing actomyosin regulatory proteins (Linder and Cervero, 2020). Podosomes are capable of mediating adhesion to the ECM, exerting protrusive forces onto the substrate and mechanically probing the cellular microenvironment (Luxenburg et al., 2012; Labernadie et al., 2014). To push on the underlying plasma membrane, the podosome core takes advantage of the forces generated by the Arp2/3-mediated polymerisation of branched F-actin. Simultaneously, the lateral actin fibres coupling the core to the ring produce a counterforce that pulls on the plaque proteins (Gawden-Bone et al., 2010; Luxenburg et al., 2012). Despite still not being fully understood, the mechanosensitive ability of podosome may rely on some of the adaptor proteins localised in the ring. While the core-generated forces could protrude more onto a compliant substrate, this would be hindered on stiffer matrices, transmitting higher tensile forces to the lateral actin filaments and to proteins like talin. This could trigger the opening of vinculin-binding sites and lead to the transduction of mechanical cues (van den Dries et al., 2019).

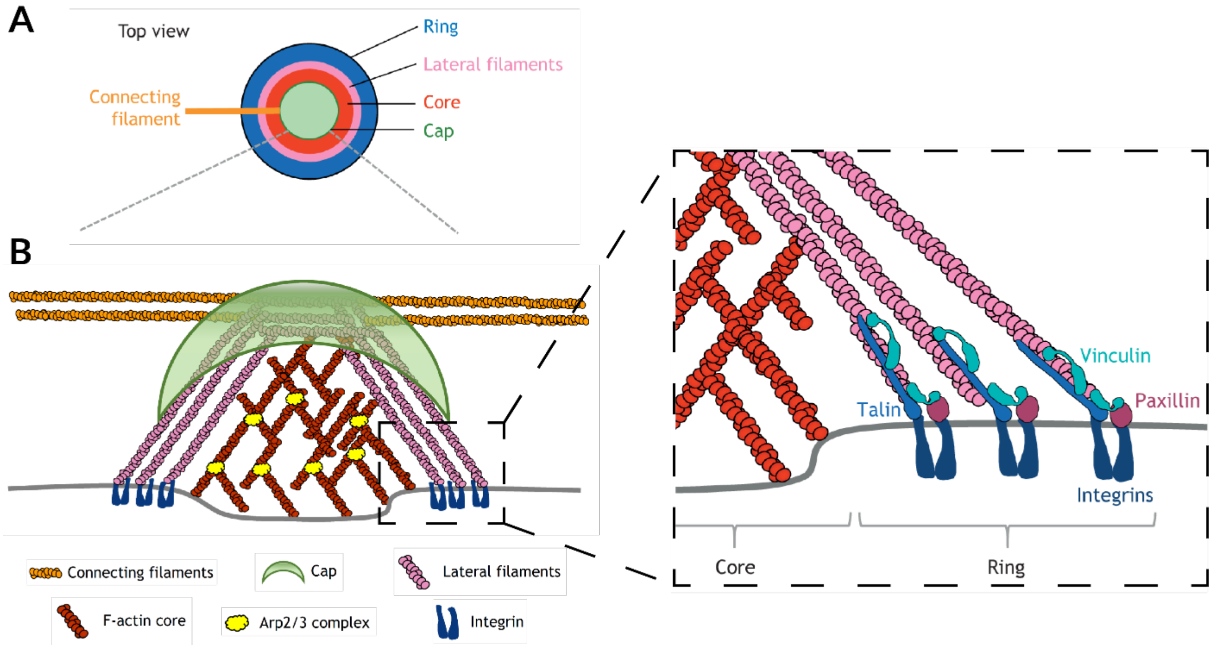

Figure 1.8 | Podosome architecture. (A) Schematic illustration of the modular structure of podosomes. **(B)** The branched F-actin core exerts protrusive forces onto the cell substrate, generating a tension that is propagated through the lateral filaments to the adhesive ring and that can promote conformational changes in mechanosensitive proteins such as talin, vinculin and paxillin. Figure adapted and modified from van den Dries et al. (2019).

1.3.2 Nuclear mechanotransduction

Some of the mechanical signals perceived by cell-matrix adhesions and propagated through the cytoskeleton can be delivered to the nucleus by transducer and effector molecules and have an impact on the regulation of different cellular processes. To date several mechanisms are known to mediate nuclear mechanotransduction.

One of them is the shuttling of mechanoresponsive proteins to the nucleus. For instance, zyxin and paxillin are proteins usually associated to focal adhesions that in response to mechanical stress can detach from the FA complex and translocate into the nucleus (Sathe et al., 2016; Zhou et al., 2017). However, their exact regulatory functions there are still unclear.

Another relevant example and well-studied mechanism is the YAP/TAZ system. YAP and TAZ are homologous proteins which function as mechanosensitive transcriptional activators that can shuttle between the cytoplasm and the nucleus and viceversa (Heng et al., 2021). YAP/TAZ not only mediate the response to stiffness but also to other biophysical cues including adhesive area, strain and shear stress (Dupont et al., 2011; Wang et al., 2016; Nardone et al., 2017). Once inside the nucleus, YAP/TAZ bind to members of the TEAD family of transcription factors and activate genes associated with cell growth, proliferation, cell-matrix interactions, ECM composition and cytoskeleton integrity (Lin et al., 2017; Heng et al., 2021).

A way the cell controls the translocation of YAP/TAZ is through the Hippo pathway, which can integrate several signals of biochemical and biophysical origin. When this pathway is activated, cytosolic YAP/TAZ remain phosphorylated and targeted for proteasomal degradation. If the Hippo pathway is not active, YAP/TAZ become dephosphorylated and able to translocate into the nucleus (Kim and Jho, 2018). As described in Section 1.3.1, stiffer matrices can induce the transmission of higher tensile forces through the cell-matrix adhesion complexes, enhancing the activity of kinases such as FAK and SRC as well as actomyosin contractility. All these factors can then promote the inactivation of the Hippo pathway through different signalling cascades, resulting in the nuclear translocation of YAP/TAZ (Fig. 1.9A) (Serrano et al., 2013; Kim and Gumbiner, 2015).

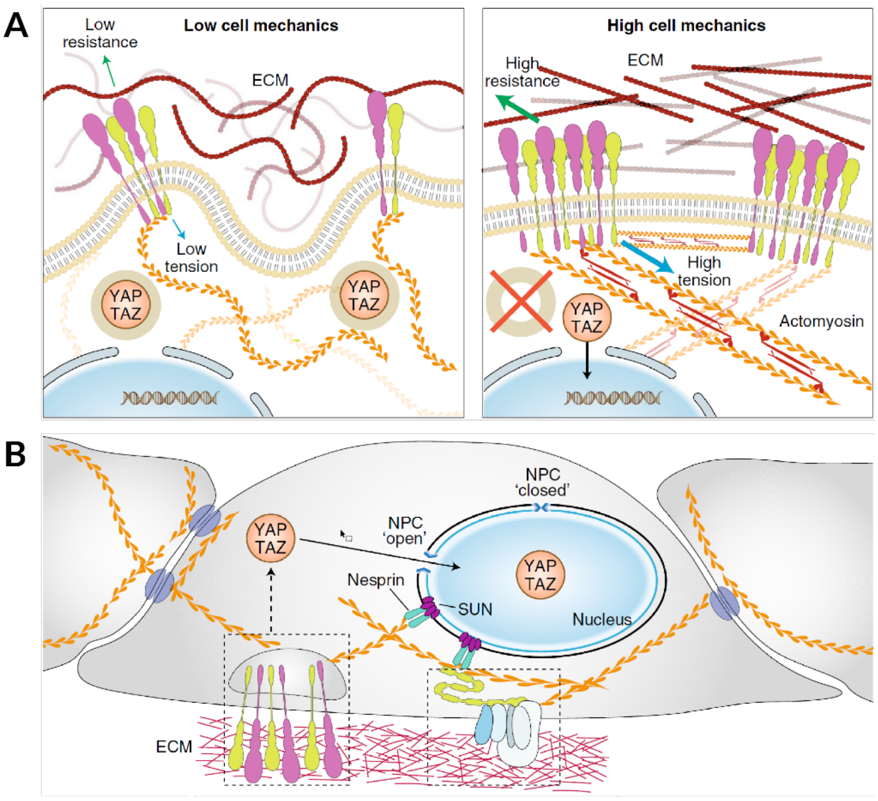
A
Low resistance
Low cell mechanics
ECM
Low tension
YAP TAZ
YAP TAZ
High cell mechanics
High resistance
ECM
High tension
Actomyosin
YAP TAZ
B
NPC 'closed'
YAP TAZ
NPC 'open'
Nesprin
SUN
YAP TAZ
Nucleus
ECM

Figure 1.9 | YAP/TAZ mechanotransduction signalling.
(A) On stiffer matrices, the higher tensile forces propagated through the focal adhesion complexes indirectly promote the dephosphorylation and release of YAP/TAZ, enabling its nuclear translocation. **(B)** Moreover, the tension also propagates to the nucleus, inducing changes in the structure of nuclear pores that enhance the nuclear import of YAP/TAZ into the nucleus. Figure adapted from Totaro et al., (2018).

A second mechanism driving the shuttling of YAP/TAZ is based in the physical link between the nucleus and the F-actin cytoskeleton. In an elegant study, (Elosegui-Artola et al., 2017) showed that on stiffer substrates the tension propagated through actomyosin stress fibres to the nucleoskeleton induces the flattening of the nucleus and an increase in the curvature of the nuclear membrane. Altering the shape of the nucleus induces changes in the architecture of nuclear pores, an event that facilitates the nuclear import of YAP/TAZ rather than their export (Fig. 1.9B).

As illustrated by the case of YAP/TAZ, the mechanical coupling between cell-ECM adhesions, cytoskeleton and nucleus represents one of the key mediators of nuclear mechanotransduction (Pennacchio et al., 2021). Several nuclear components are part of this mechanism (Fig. 1.10). First, the nuclear envelope, which comprises the internal nuclear membrane (INM) and outer nuclear membrane (ONM), separated by a lumen or perinuclear space (Ungricht and Kutay, 2017). Nuclear pore complexes (NPCs) spanning over the nuclear envelope facilitate the bi-directional transport of proteins and RNA (Knockenhauer and Schwartz, 2016). Second, the nuclear lamina, a structure located under the INM that is made of different types of intermediate filaments known as lamins and of other lamin-binding proteins (de Leeuw et al., 2018). This filamentous network is involved in maintaining the structural integrity of the nucleus, determining its size and stiffness (Dahl et al., 2004; Lammerding et al., 2006). Moreover, it is also bound to chromatin and, thus, participates in transcriptional regulation (Solovei et al., 2013; Harr et al., 2015). And third, the LINC complex, which is the main responsible of transmitting forces across the nuclear envelope. Its constituents are nesprin proteins located in the ONM and SUN proteins embedded in the INM (Chang et al., 2015). On the cytoplasmic side, nesprins interact with the different cytoskeletal filaments, and on the lumen side they contain a KASH domain capable of interacting with the SUN domain of SUN1 and SUN2 (Lombardi et al., 2011). Lastly, SUN proteins can propagate the mechanical cues to their binding partners: the nuclear lamina, nuclear pores and chromatin (Jahed et al., 2016; Kirby and Lammerding, 2018).

Recent studies described several final effectors potentially activated through nuclear mechanotransduction (Kirby and Lammerding, 2018). One of them is the translocation of transcriptional regulators from the cytoplasm to the nucleus due to alterations in the permeability of nuclear pores. The shuttling of YAP/TAZ described before is an example of this. Another interesting possibility is the physical reorganisation of chromatin. Heterochromatin – transcriptionally silent DNA tightly wrapped around histones – tends to be localised at the nuclear periphery, while euchromatin – open, transcriptionally active DNA – is frequently found in the interior (Zullo et al., 2012). It has been proposed that the forces propagated from the cytoskeleton to the nucleus could induce changes in the position of certain chromatin regions, altering the transcriptional activity of certain mechanosensitive genes and leading to the modification of gene expression patterns (Uhler and Shivashankar, 2017).

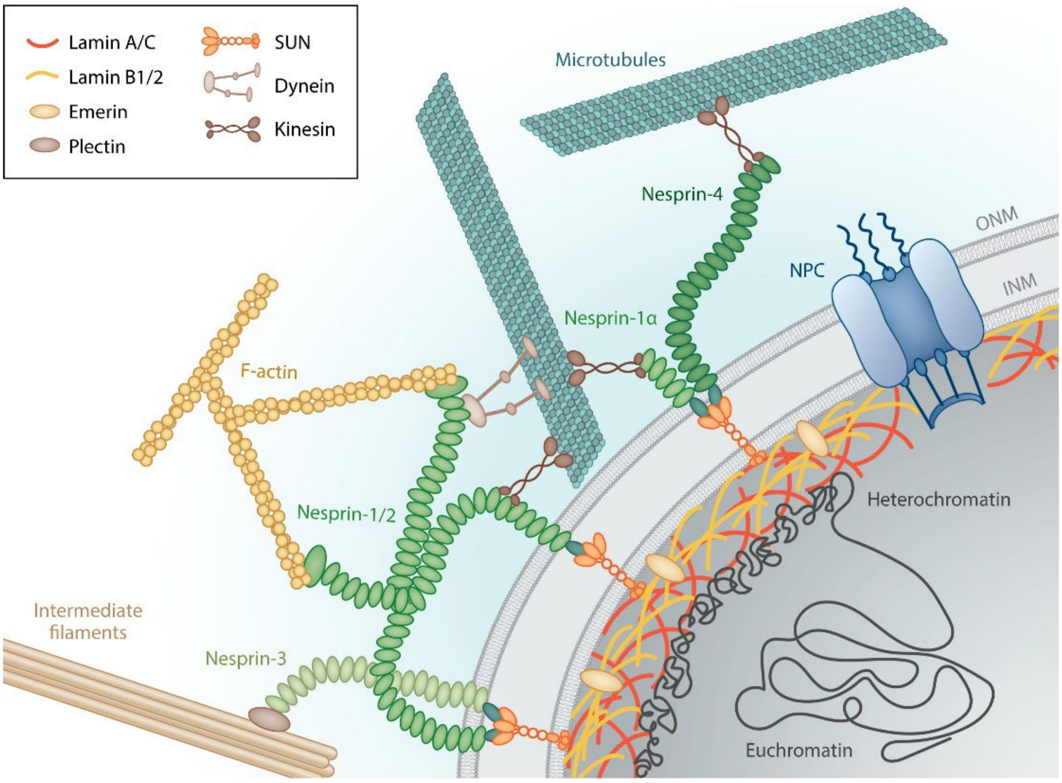
Lamin A/C
Lamin B1/2
Emerin
Plectin
SUN
Dynein
Kinesin
Microtubules
Nesprin-4
ONM
INM
NPC
Nesprin-1α
F-actin
Heterochromatin
Nesprin-1/2
Intermediate filaments
Nesprin-3
Euchromatin

Figure 1.10 | Nuclear components involved in nuclear mechanotransduction.
The LINC complex formed by nesprins and SUN proteins mediate force transmission between the cytoskeleton and the lamins localised underneath the nuclear envelope. The lamin network can then propagate the biophysical information to different structures such as the nuclear pores and the chromatin, modifying their architecture and organisation, respectively. Figure adapted from Maurer and Lammerding (2019).

1.3.3 Membrane mechanosensing elements

The plasma membrane separates the interior of the cell from its surrounding and is an essential regulatory element of the import and export of substances. Importantly, changes in its physical state also serve the cell to detect external mechanical stimuli. The different forces acting on the plasma membrane can exert tensile, compressive and shear stresses (Le Roux et al., 2019).

In the case of tensile stresses, these are commonly caused by changes in osmotic pressure, adhesion to substrates or other cells and by the forces generated by the cytoskeleton. Indeed, the apparent membrane tension experimentally measured through techniques like tether pulling includes both the tension of the lipid bilayer and the tension stored by the underlying cytoskeleton, to which the plasma membrane is coupled (Chichili and Rodgers, 2009; Alert et al., 2015; Sitarska and Diz-Muñoz, 2020). The structure that actually absorbs most of the tensile stress is the cytoskeleton, since the membrane can only stretch between 3 to 5% before rupturing (Morris and Homann, 2001; Lieber et al., 2013).

Several types of elements present in the membrane can react to a tension increase. One of them are the mechanosensitive ion channels (MSCs), which are mechanically gated ion channels whose conformation only changes in response to tensile forces and alterations in the curvature of the membrane (Ridone et al., 2019). Mammalian MSCs include TRP channels, potassium-selective channels such as TREK and TRAAK, and Piezo channels (Ranade et al., 2015). Among them, Piezo channels have especially caught the attention of researchers since they are involved in a wide range of physiological processes: mechanosensation (Woo et al., 2014, 2015), cell-fate determination (Pathak et al., 2014; Sugimoto et al., 2017; He et al., 2018), axon growth and regeneration (Koser et al., 2016; Song et al., 2019), volume regulation (Cahalan et al., 2015) and innate immunity (Solis et al., 2019), among others. Piezos are cationic non-selective channels, meaning they are permeable to Na^+, K^+, Ca^{2+} or Mg^{2+} (Jin et al., 2020). Piezo MSCs have a unique architecture, since they are a homotrimeric complex that forms a channel with a structure resembling a propeller or triskelion (Ge et al., 2015; Saotome et al., 2018; Zhao et al., 2018; Wang et al., 2019a). An increase in the tension of the plasma membrane triggers the activation of the channel, which changes its conformation from a closed to an open state and generates a cationic current (Parpaite and Coste, 2017; Fang et al., 2021).

To compensate the increase in tension, the cell takes advantage of the folds it has in the membrane, such as ruffles, microvilli or caveolae, and other membrane reservoirs like intracellular vesicles (Le Roux et al., 2019). By flattening out these folds and mobilising its endomembrane stores, the cell is capable of buffering the tension arisen in the plasma membrane (Sinha et al., 2011). When the stress ceases, these invaginations can re-form again.

During the last years, the mechanosensitive role of caveolae has raised substantial interest (Nassoy and Lamaze, 2012; Echarri and Del Pozo, 2015; Del Pozo et al., 2021). Caveolae are small invaginations of 50-100 nm in diameter, with a lipid bilayer rich in cholesterol and glycosphingolipids (Lo et al., 2015; Shvets et al., 2015). Their components include proteins of the caveolin and cavin families, which are responsible of stabilising caveolar shape (Rothberg et al., 1992; Kovtun et al., 2015), curvature-generating F-BAR proteins (Kessels and Qualmann, 2020) and EHD2, which localises in the neck of caveolae and prevents their budding (Morén et al., 2012).

The mechanosensing ability of caveolae relies in the ability of some of its proteins to be released and initiate certain signalling (Fig. 1.11). This is for example the case of EHD2, which upon caveolae flattening diffuses into the cytoplasm and becomes imported into the nucleus. There it represses the expression of several genes, including caveolar genes (Torrino et al., 2018). Conversely, caveolae not only enable cells to withstand increases in membrane tension but also compressive stresses. Cell compression or hypertonic shocks can lead to the bending of the plasma membrane and the formation of ruffles and folds (Gervásio et al., 2011). In the case of caveolae, conditions of lower membrane tension favour their reorganisation in structures known as rosettes, which consist of clusters of multiple grouped caveolae (Golani et al., 2019). Finally, it is interesting to note that caveolae may play an additional mechanosensing role by indirectly interacting with other mechanotransduction pathways. For instance, Moreno-Vicente et al. (2018) report that caveolin-1 positively regulates the YAP/TAZ-mediated response to stiffer substrates via the crosstalk with the F-actin cytoskeleton, to which caveolae are also connected (Echarri and Del Pozo, 2015). Altogether, the described examples illustrate the importance of caveolae both as a mechanoprotector and as a mechanosensor. Nevertheless, further research is still needed to completely understand how do caveolae integrate mechanical inputs into cell signalling networks.

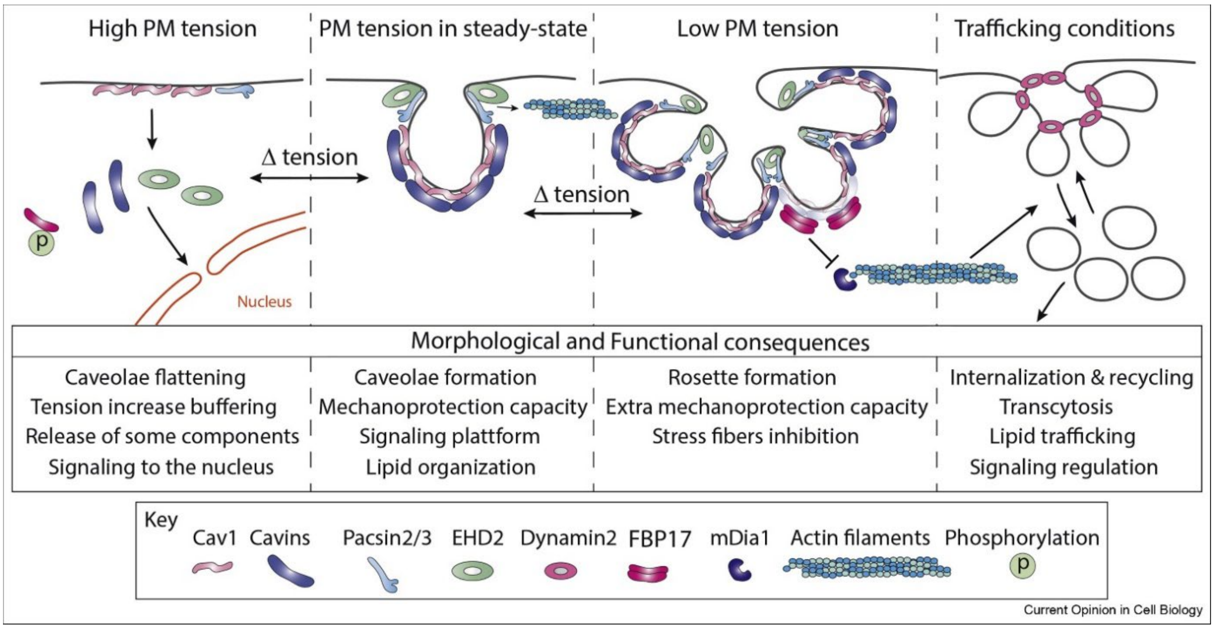
High PM tension
PM tension in steady-state
Low PM tension
Trafficking conditions
Δ tension
Δ tension
P
Nucleus
Morphological and Functional consequences
Caveolae flattening
Tension increase buffering
Release of some components
Signaling to the nucleus
Caveolae formation
Mechanoprotection capacity
Signaling plattform
Lipid organization
Rosette formation
Extra mechanoprotection capacity
Stress fibers inhibition
Internalization & recycling
Transcytosis
Lipid trafficking
Signaling regulation
Key
Cav1
Cavins
Pacsin2/3
EHD2
Dynamin2
FBP17
mDia1
Actin filaments
Phosphorylation
P
Current Opinion in Cell Biology

Figure 1.11 | Response of caveolae to membrane tension and compression. Upon an increase in membrane tension (left) caveolae flatten out, releasing some of its components which can then function as mechanotransducers. Conditions of lower membrane tension promote the formation of caveolae rosettes, which can indirectly also impact the organisation of actin stress fibres. Figure adapted from Del Pozo et al. (2021).

1.4 Macrophage mechanosensing

As described in Section 1.2.2, immune cells are mechanosensitive and macrophages are no exception to this. Extrinsically applied biophysical stimuli such as the modification of cell shape (McWhorter et al., 2013; Jain and Vogel, 2018), hyperosmotic shocks (Ip and Medzhitov, 2015), interstitial flow (Li et al., 2018) and cyclical compression (Cezar et al., 2016) have been reported to impact their phenotype and function. Moreover, while conducting immune surveillance macrophages encounter a variety of mechanically distinct targets and environments that can also affect their behaviour and response.

This is indeed the case of phagocytosis, one of the main macrophage functions and a process in which forces play an essential role (see Section 1.2.1 for further details). It has been extensively documented that not only particle size but also their shape and stiffness influence their internalisation rate (Tabata and Ikada, 1988; Champion and Mitragotri, 2006; Sharma et al., 2010; Leclerc et al., 2012; Möller et al., 2012; Alqahtani et al., 2020). Focusing in the latter parameter, accumulative evidence indicates that macrophages tend to engulf stiffer targets with higher efficiency (Beningo and Wang, 2002; Anselmo et al., 2015; Hui et al., 2020; Vorselen et al., 2020, 2021).

While patrolling organs and tissues conducting immune surveillance, macrophages encounter different local stiffnesses. For example, microglia residing in the human brain are exposed to a shear modulus of a few hundred Pa (Franze et al., 2013), alveolar macrophages in the lung to an elastic modulus of 2 kPa (Booth et al., 2012), macrophages within dermal tissue to a shear modulus of 7-100 kPa (Wang et al., 2017) and bone osteoclasts face an elastic modulus in the GPa range (Mirzaali et al., 2016). In addition, medical interventions such as the introduction of an implant into the body can represent a mechanical challenge to macrophages, since they might need to react against a foreign body that mechanically mismatches the stiffness of the local tissue (Witherel et al., 2019; Carnicer-Lombarte et al., 2021). What is, thus, the impact of microenvironment stiffness on the inflammatory behaviour of macrophages?

Several studies that tried to address this question have shown contradictory results. Some of them reported that increasing substrate stiffness favours macrophage polarisation towards an M1-like phenotype and enhances pro-inflammatory gene expression and cytokine release (Blakney et al., 2012; Hsieh et al., 2019; Meli et al., 2020; Okamoto et al., 2018; Previtera and Sengupta, 2015; Sridharan et al., 2019). In contrast, other publications suggest that when cultured on stiffer materials, macrophages adopt an M2-like phenotype, decrease the production of pro-inflammatory cytokines and increase the secretion of anti-inflammatory factors (Patel et al., 2012;

Scheraga et al., 2016; Gruber et al., 2018; Carnicer-Lombarte et al., 2019; Chen et al., 2020; Xing et al., 2020).

The experimental systems used to investigate macrophage mechanosensing differ across studies and parameters such as stiffness range, adhesive ligand composition and density, cell type or activation stimulus could affect the obtained results. Further research is thus required to decipher how substrate stiffness influences the behaviour of macrophages and how this impacts on their ability to induce and coordinate inflammatory responses.

Limited information is currently available on which macrophage-specific signalling pathways might be influenced by substrate stiffness. A few reports indicate that the inflammasome, one of the main macrophage signalling hubs and mediator of the maturation of major pro-inflammatory cytokines, could be modulated by biophysical cues. For instance, cycling stretch has been shown to negatively regulate the release of IL-1β by inhibiting NLRP3 inflammasome formation (Maruyama et al., 2018) and hyperosmotic shocks have been described to trigger the reverse effect (Ip and Medzhitov, 2015). Moreover, it has been reported that common mechanotransducers such as the cytoskeleton components F-actin (Man et al., 2014; Burger et al., 2016) and microtubules (Magupalli et al., 2020) may play a significant role as regulators of inflammasome assembly. Despite that, whether the mechanical information provided by substrate stiffness affects inflammasome formation and its downstream effects remains still unknown.

AIMS AND SCOPE OF THE THESIS

Despite substantial efforts have been done to understand how substrate stiffness alters macrophage phenotype and function, the data are inconclusive. Moreover, the impact that microenvironment mechanics might have on specific macrophage signalling networks and what elements mediate the transmission of external mechanical cues have not been well characterised.

The work done in this thesis aims to investigate how substrate stiffness affects the inflammatory behaviour of macrophages, with a focus on their pro-inflammatory response. For this, an experimental system where substrate stiffness can be uncoupled from other material parameters and that is compatible with macrophage culture will be established. After this, cells will be challenged with inflammatory stimuli to assess whether they react differently on substrates of varying stiffness. The potential influence of stiffness on the macrophage inflammasome, one of its main pro-inflammatory signalling hubs, will also be tested. Finally, whether certain mechanosensing elements play an important role in the ability of macrophages to perceive and integrate microenvironment stiffness will be studied.

More specifically, this dissertation tries to tackle the following goals:

i. Establish a suitable macrophage 2D culture platform with tuneable mechanical properties within a physiological range and the possibility to control substrate stiffness independently of adhesion ligand density.

ii. Characterise some of the main aspects of the pro-inflammatory response upon macrophage stimulation, such as gene expression and cytokine release.

iii. Determine whether substrate stiffness has any impact on the formation of the NLRP3 inflammasome.

iv. Identify possible mechanosensing elements transducing the mechanical cues given by the microenvironment into the inflammasome pro-inflammatory machinery.

RESULTS

The investigation of macrophage mechanosensing presented in this work followed a reductionist approach in which macrophages were exposed to 2D substrates of tuneable stiffness and their pro-inflammatory response was examined. The first part of the Results describes the establishment of a suitable platform to study substrate stiffness mechanosensing in primary macrophages. The second part explores different aspects of the pro-inflammatory response affected by varying this mechanical input, such as gene and protein expression levels, NLRP3 inflammasome formation and cell pyroptosis. Finally, the last Section attempts to disentangle what cell mechanosensing elements might enable macrophages to integrate the information given by substrate stiffness into their pro-inflammatory machinery. Most of the results shown in this thesis have been published in Escolano et al. (2021).

3.1 Morphological characterisation of macrophages cultured on substrates of varying stiffness

To study the influence of the mechanical properties of the microenvironment on macrophages, 2D flat synthetic hydrogels were used. In particular two different hydrogel chemistries were tested: one based on polyacrylamide (PAA) and an other based on poly(ethylene glycol) and heparin (PEG-Hep). Both of them present the advantages that 1) their elasticity can be easily and independently tuned by changing the proportions of their main components and 2) they can be decorated with the adhesion ligand of choice. This Section presents how these gels were mechanically characterised and tested, how do macrophages initially respond to their stiffness and the results leading to the selection of polyacrylamide gels as the system of choice.

3.1.1 BMDMs adhere and can be cultured on polyacrylamide hydrogels

Polyacrylamide hydrogels have been broadly used to study cell mechanosensing (Janmey et al., 2020), since the elastic modulus of this material can be controlled by modifying the quantities of acrylamide and bisacrylamide. Classically, the addition of adhesion molecules to biofunctionalise PAA gels is done using a sulfo-SANPAH coupling reaction. Nevertheless, this approach provides very poor control over the immobilisation sites because bonds are formed unspecifically with any amine group present in the biomolecule of interest, leading to the presence of non-functional ligands and low reproducibility when performing experiments (Farrukh et al., 2016).

To solve this issue, in this work methylsulfonyl acrylate (MS) monomers are used instead. This strategy enables to independently control ligand density and, thus, produce hydrogels of different stiffness while keeping a similar amount of adhesion sites on their surface (Fig. 3.1A). In this case, cyclic RGD-Phe-Cys was used as adhesion ligand of choice, a molecule that binds through its cysteine residue to the thiol-reactive chemical group provided by the MS monomers. The aminoacid sequence RGD (arginine-glycine-aspartate) is one of the most common adhesion motifs and is present in ECM proteins such as fibronectin, vitronectin and fibrinogen (Bellis, 2011). RGD peptides are recognised by multiple integrin types present in the plasma membrane, mediating the effective adhesion of cells to RGD-functionalised biomaterials (Humphries et al., 2006).

As depicted in Fig. 3.1A, PAA hydrogels were polymerised on round glass coverslips of 13 mm of diameter and had an estimated height of 100 µm, which is sufficient to avoid the influence of the glass underneath on the cultured cells (Buxboim et al., 2010). To evaluate the stiffness of the substrates, elastic moduli were assessed with atomic force microscopy. AFM-based indentation measurements determined that, with the gel production protocol followed in this study, it was possible to produce hydrogels with Young's moduli ranging from 0.2 to 33.1 kPa (Fig. 3.1B). Within this range, three different hydrogel compositions were selected: the most compliant gel with a mean Young's modulus of 0.2 kPa ("compliant"), an intermediate substrate of 14.3 kPa ("intermediate") and the stiffest hydrogel with a modulus of 33.1 kPa ("stiff"). In order to then test whether the density of adhesion ligands was comparable across these stiffnesses, hydrogels coated with FITC-PEG-SH were imaged (Fig. 3.1C) and no major differences in their fluorescence signal were observed (Fig. 3.1D). Altogether, these data indicate that, with the employed chemistry, PAA substrates can be produced within a physiological stiffness range of two orders of magnitude and with similar cRGD coating levels, making it a potentially suitable hydrogel system for the culture of macrophages.

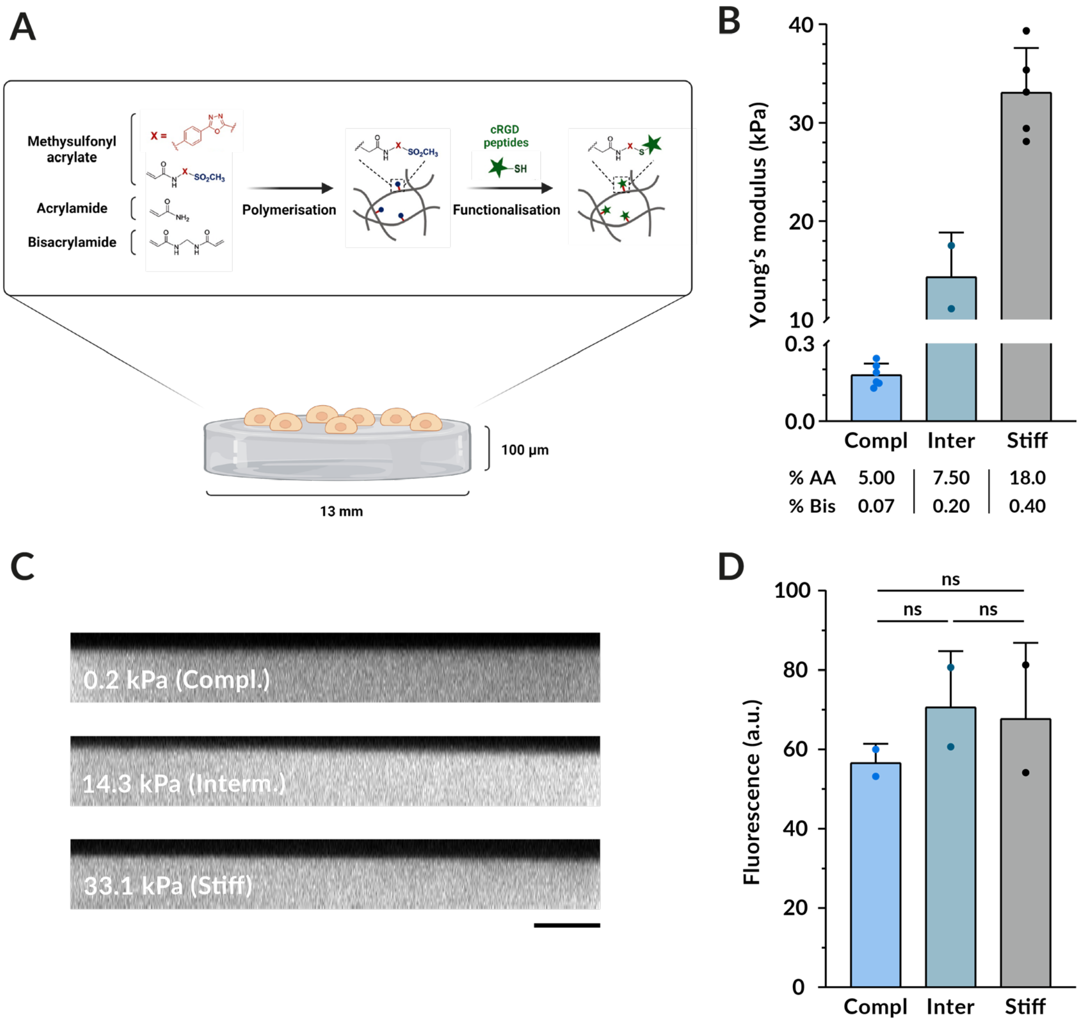

Figure 3.1 | PAA gels are a suitable biomaterial to investigate macrophage mechanosensing. (A) Scheme depicting the composition of PAA hydrogels. The stiffness of the gels is tuned by modifying the amounts of acrylamide and bisacrylamide, and the reactive groups created by the incorporation of MS monomers are afterwards coupled with cRGD. **(B)** Young's moduli of different PAA hydrogels produced. The mean ± SD was 0.18 ± 0.04 kPa for compliant, 14.32 ± 4.54 kPa for intermediate, and 33.07 ± 4.55 kPa for stiff gels. **(C)** Representative fluorescence confocal images of hydrogels functionalised with FITC-PEG. Scale bar, 50 µm. **(D)** Quantification of the fluorescent signal as a proxy of ligand density. Mean ± SD is displayed and each dot indicates the mean intensity obtained from 5 different regions of a single hydrogel. Statistical analysis was performed using a Kruskal-Wallis ANOVA followed by Dunn's post hoc analysis to obtain the multiple comparison *p*-values. ns, non-significant.

The cells used to perform all the experiments in this thesis were murine bone marrow-derived macrophages (BMDMs). These cells represent a useful macrophage model to study primary cell function since they can be generated in large quantities after differentiating for 6 days bone marrow progenitors collected from young mice (see Methods Section 5.4 for a detailed description). Besides a high differentiation yield, the obtained macrophage populations are highly pure (98.8% as measured in Appendix Fig. A.1) and with relatively homogeneous characteristics, contributing to achieve adequate experimental reproducibility.

After their complete differentiation, BMDMs were seeded on PAA hydrogels at a confluence always below 100% to prevent the potential influence of cell-cell contacts occurring upon cell crowding. After culturing the cells for 14-18 h, BMDMs were well adhered to all substrates, with few cells floating in the medium. After overnight culture, cells displayed notable morphological differences across varying stiffnesses (Fig. 3.2). Moreover, manipulation of the samples such as medium exchange or transfer to another culture plate did not cause major cell detachment, making this PAA hydrogel system well suited to continue studying macrophage mechanosensing.

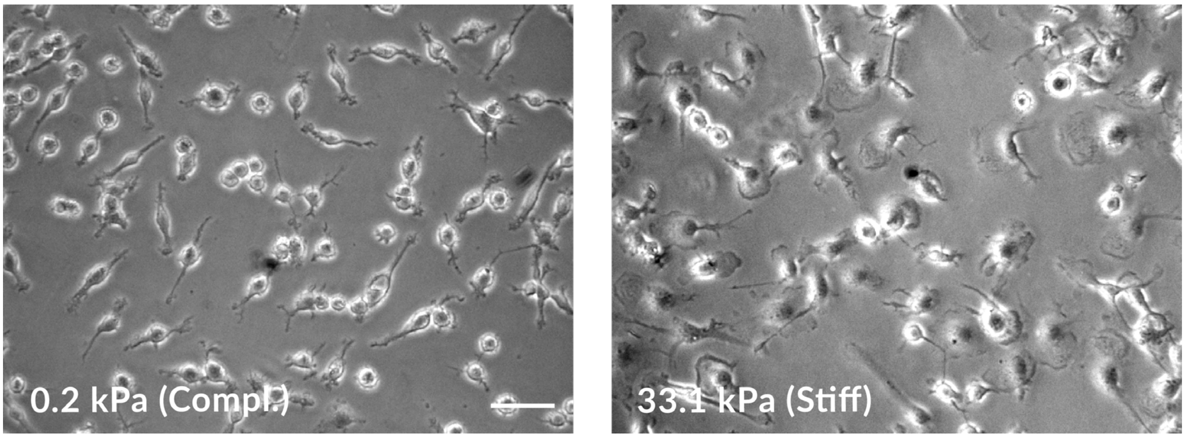

Figure 3.2 | Macrophages are compatible with PAA gels. Representative phase contrast images of differentiated BMDMs cultured for 14-18 h on 0.2 and 33.1 kPa hydrogels. Scale bar, 50 µm.

3.1.2 Macrophage morphology is influenced by substrate stiffness

Given the recognisable morphological differences displayed by macrophages on substrates of varying rigidities, initial experiments focused on characterising them. To this end, cell nuclei and F-actin were imaged by fluorescence confocal microscopy (Fig 3.3A). While BMDMs on the most compliant gels (0.2 kPa) were rounder and less spread, macrophages on the stiffest substrates (33.1 kPa) adopted a remarkably larger area, longer extensions and higher actin density in some clusters. Quantification of several cell shape parameters is shown in Fig. 3.3B-D. Macrophages on the stiffest PAA gels displayed a 229% larger mean spreading area, a 202% higher perimeter and 57% lower circularity. These results confirm that upon culture on stiffer substrates, macrophages increase their cell area, developing more cell processes and becoming less round. Out of the three gel stiffnesses tested, the most compliant and the stiffest were chosen for the remainder of this study because they were the most distant from each other and they consistently caused major differences in macrophage morphology.

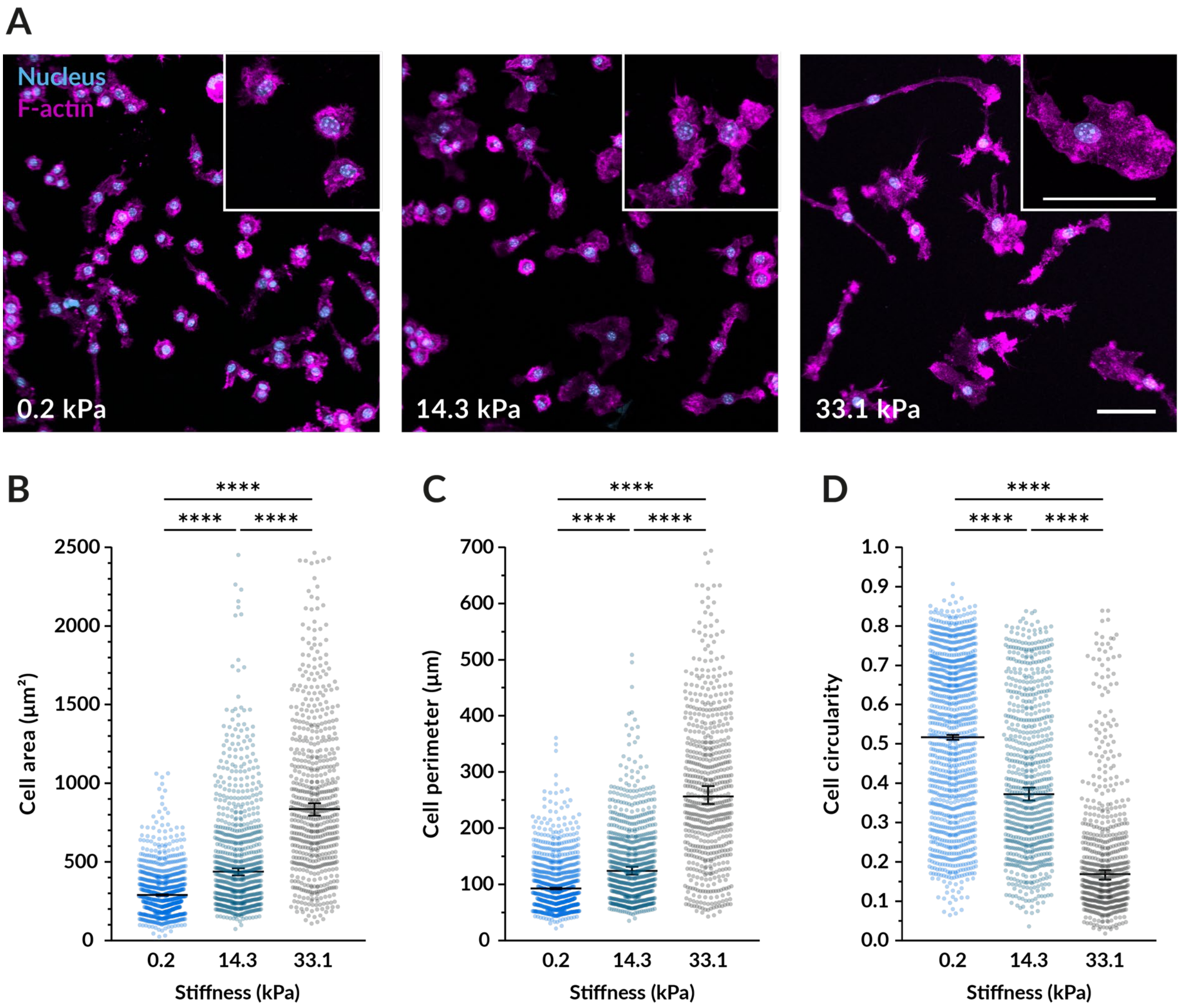

Figure 3.3 | Macrophages on compliant substrates become smaller and rounder.
(A) Representative confocal microscopy images of fluorescence BMDMs cultured for 14-18 h on the different hydrogels. Nuclei shown in blue (DAPI) and F-actin in magenta (phalloidin-TRITC). Enlarged examples of cells of each condition are displayed in the insets. Scale bars, 50 µm. **(B-D)** Quantification of the cell area (B), perimeter (C) and circularity (D) from images taken under the same conditions as Fig. 3. In all pots, each dot represents a cell and black bars indicate mean ± SEM. The number of analysed cells was 1117 for compliant, 771 for intermediate and 629 for stiff. Data were obtained from three independent experiments done with cells from three different mice. Statistical analysis was performed using a Kruskal-Wallis ANOVA followed by Dunn's post hoc analysis to obtain the multiple comparison *p*-values. **** $p < 0.0001$.

3.1.3 PEG-Hep hydrogels induce similar morphological differences as PAA substrates but do not constitute a suitable macrophage culture platform

The second hydrogel system tested was one based in PEG-Heparin (Fig. 3.4A). These hydrogels consist of 4-arm star-shaped poly(ethylene glycol) covalently cross-linked with heparin, and their stiffness can be tuned by modifying the PEG:Heparin ratio (γ) used when polymerising them (Freudenberg et al., 2009). As done with PAA substrates, PEG-Hep gels were polymerised on 13 mm coverslips and had an estimated height of 150 µm. These gels were as well mechanically characterised using AFM. As shown in Fig. 3.4B, analysis of the force-indentation curves determined that that the maximum range of achievable stiffnesses ranged from a mean apparent Young's modulus of 4.0 kPa (γ = 1) to 46.0 kPa (γ = 6). Moreover, the values obtained approximately matched the storage moduli obtained by shear rheometry in previous reports (Welzel et al., 2011).

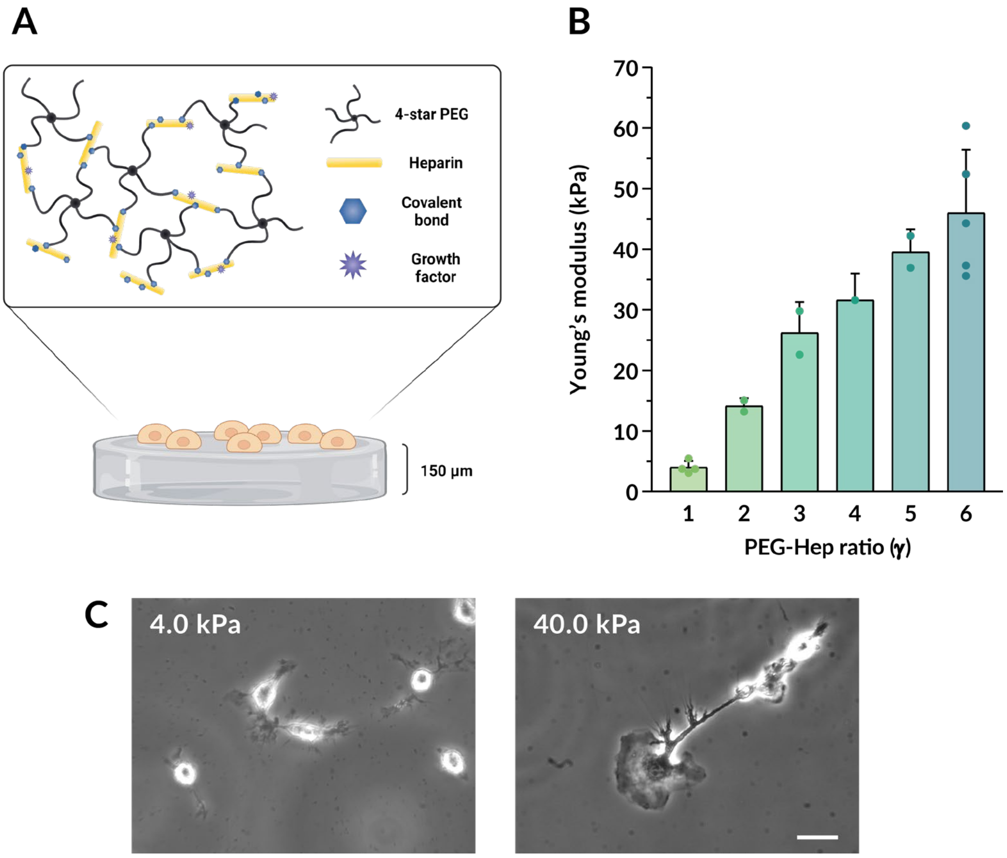

Figure 3.4 | PEG-Heparin hydrogels as an alternative hydrogel substrate.
(A) Scheme depicting the composition of the hydrogels, where 4-arm starPEG is crosslinked with heparin and material stiffness can be modified by altering the ratio between the two main components. Additionally, heparin offers reactive groups to functionalise the gels with peptides of interest as well as negative charges that also link growth factors and other proteins present in the culture medium. Figure modified from (Freudenberg et al., 2009). **(B)** Young's moduli of different PEG-Hep hydrogels produced. The mean ± SD for γ = 1 was 4.0 ± 1.0 kPa; for γ = 2, 14.1 ± 1.3 kPa; for γ = 3, 26.2 ± 5.1 kPa; for γ = 4, 31.6 ± 0 kPa; for γ = 5, 40.0 ± 3.7 kPa; and for γ = 6, 46.0 ± 10.4 kPa. **(C)** Representative phase contrast images of BMDMs cultured for 14-18 h on PEG-Hep hydrogels of 4.0 (γ = 1) and 40.0 kPa (γ = 5). Scale bar, 20 µm.

BMDMs were cultured on PEG-Hep gels of varying stiffness, first without coupling any specific adhesive ligand protein to their surface. After a few hours, cells were attached to the substrates and after overnight culture they displayed different morphologies (Fig. 3.4C). To quantify this observation, BMDMs were fixed and their F-actin cytoskeleton was stained (Fig. 3.5A). Assessment of morphological parameters showed that on average BMDMs on 40.0 kPa gels had a larger spreading area and perimeter (Fig. 3.5B-C), resembling the trends observed on polyacrylamide substrates. However, in the case of PEG-Hep cell circularity was similar between 4.0 and 40.0 kPa (Fig. 3.5D). This was probably due to the fact that BMDMs on stiffer PEG-Hep did not display as many long processes as previously observed on stiffer PAA gels. Besides cell morphology, preliminary data on the mechanical properties of BMDMs on PEG-Hep gels of varying stiffness were also acquired, showing that macrophages on 40.0 kPa substrates became stiffer compared to cells grown on 4.0 kPa gels (Appendix Fig. A.2).

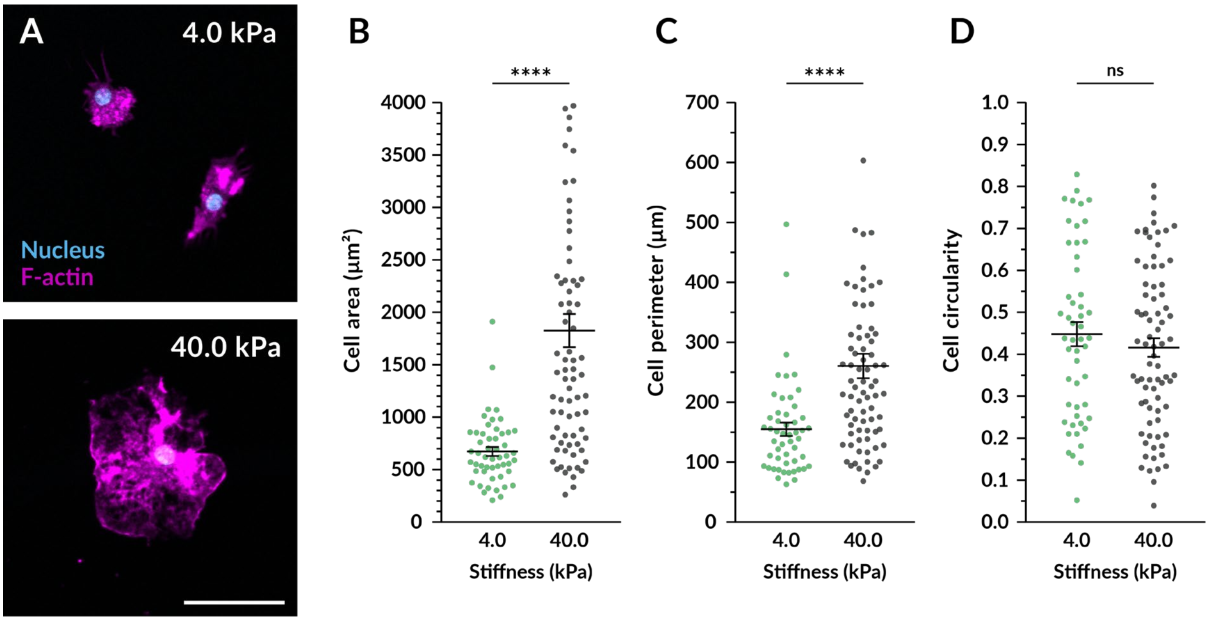

Figure 3.5 | BMDMs on stiffer PEG-Hep hydrogels become more spread.
(A) Representative confocal microscopy images of BMDMs cultured for 14-18 h on PEG-Hep hydrogels of 4.0 ($\gamma = 1$) and 40.0 kPa ($\gamma = 5$). Nuclei shown in blue (DAPI) and F-actin in grey (phalloidin-TRITC). Scale bar, 50 µm. **(B-D)** Quantification of the cell area (B), perimeter (C) and circularity (D) from images acquired under the same conditions as (A). In all plots, each dot represents a cell and black bars indicate mean ± SEM. The number of analysed cells was 51 for 4.0 kPa and 77 for 40.0 kPa. Data was obtained from one independent experiment with two different replicates. Statistical analysis was performed using a Mann-Whitney test. **** $p < 0.0001$; ns, not significant.

Despite the fact that a preliminary characterisation of BMDMs on PEG-Hep hydrogels could be performed, any experimental manipulation done on live cells after their initial culture led to the detachment of a large amount of macrophages. This indicated their weak attachment to the substrate and hindered the collection of any reproducible and reliable data from experiments done with these samples. As an attempt to improve the system, the hydrogels were functionalised with RGD peptides and tested again with BMDMs. Nevertheless, the problem persisted and cells were still detaching easily when handling the samples or exchanging the medium. In conclusion, PEG-Hep hydrogels induced similar morphological changes on macrophages but did not represent an adequate hydrogel platform to culture BMDMs and study their mechanoresponse. Therefore, this material was not used for the rest of this work and PAA was the substrate of choice to continue with the study.

3.1.4 Substrate stiffness affects membrane architecture.

To better visualise how substrate stiffness influenced the morphology of macrophages and, specifically, to observe possible differences in membrane topography, fixed gold sputter-coated samples were imaged using scanning electron microscopy (SEM). Representative SEM images of BMDMs cultured overnight on 0.2 and 33.1 kPa PAA gels are shown in Fig. 3.6. Macrophages on compliant hydrogels commonly showed ruffles and folds. In contrast, cells on stiff gels displayed a smoother membrane with less topographical features and a few visible folds on the cell periphery. The fact that macrophages on stiffer substrates accompanied their larger cell area with a flatter plasma membrane suggested that macrophages might use their membrane to maximise their spreading. Moreover, as described in the Introduction Section 1.3.3, it should be considered that changes in parameters such as membrane curvature and tension can trigger the activation of certain mechanosensing elements like caveolae or mechanically-gated ion channels (Sinha et al., 2011; Ranade et al., 2015; Cox et al., 2016; Del Pozo et al., 2021). Consequently, could the increase in cell spreading and membrane smoothness observed on stiffer hydrogels activate any membrane-related signalling elements and, thus, play a role in macrophage mechanosensing? This is a question addressed later on in the Section 3.3.1.

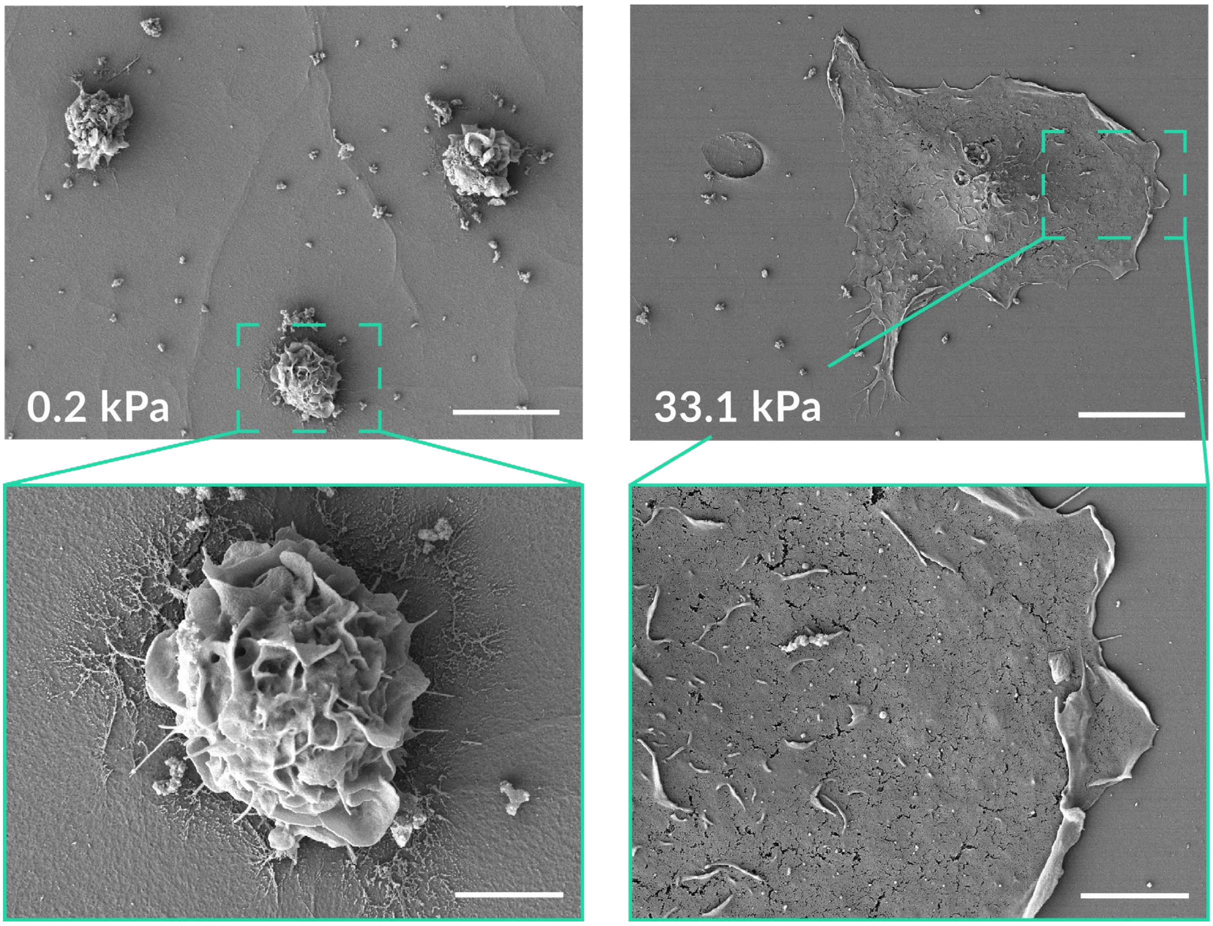

Figure 3.6 | Substrate stiffness induces changes in membrane morphology. Scanning electron micrographs of BMDMs cultured for 14-18 h on compliant and stiff gels. Scale bars on top, 50 µm, and bottom, 20 µm.

Summing up, initial efforts of this work focused on establishing a suitable system to investigate substrate stiffness mechanosensing in macrophages. As shown so far, the polyacrylamide gels used here 1) provide substrates with Young's moduli within a physiologically relevant range; 2) compared to other functionalisation chemistries, offer the advantage that ligand density can be uncoupled from material stiffness and can, thus, be kept equal; and 3) enable an adequate attachment and culture of macrophages on the material, representing a reliable platform to study their mechanoresponse. Finally, when culturing BMDMs on more compliant substrates, they adopted a smaller and more circular shape and presented considerably more membrane invaginations than when grown on stiffer hydrogels.

3.2 Impact of substrate stiffness on the pro-inflammatory response of macrophages

Besides engulfing harmful particles, one of the main functions of macrophages is to detect the presence of dangerous entities and orchestrate the onset of the immune response by secreting different cytokines and chemokines. Some of them promote inflammation and the recruitment of other immune cells, and others favour tissue repair and ultimately lead to the recovery of tissue homeostasis (see Introduction 1.2 for further details). There is still considerable ambiguity with regard to how the mechanical properties of the microenvironment affect the inflammatory behaviour of macrophages. Moreover, whether stiffness influences important pro-inflammatory signalling elements like the inflammasome is still unknown. The following Section describes how the established hydrogel platform was used to study the influence of substrate stiffness on the macrophage pro-inflammatory response and on some of its major signalling players.

3.2.1 The morphological differences induced by different stiffness persist after macrophage priming

As described in the Introduction Section 1.1.3, to detect different microbial and endogenous danger molecules macrophages take advantage of multiple subtypes of TLRs. These receptors recognise different DAMPs and initiate downstream signalling events that lead to macrophage activation and pro-inflammatory gene expression. In this study, the compound employed for this initial priming step was lipopolysaccharide (LPS), a molecule present in the wall of gram-negative bacteria that binds and activates the TLR4 receptors present in the membrane of macrophages (Park et al., 2009).

First, whether the morphological changes promoted by substrates of different stiffness remained after LPS challenge was tested. To this end, BMDMs cultured on PAA gels were incubated with LPS for 4.5 h, fixed and imaged as previously described (Fig. 3.7A). The relative differences in morphology between the compliant and stiff hydrogels observed in non-primed macrophages persisted upon LPS priming (Fig. 3.7B-D). Nevertheless, when compared to untreated, LPS-primed cells became larger on both stiffness. On 0.2 kPa substrates, LPS-treated macrophages had an 83% larger area, an 85% longer perimeter and a 40% lower circularity compared to untreated controls. On 33.1 kPa gels, their spreading area was only 38% higher, their perimeter 8% longer and their circularity was similar to non-primed. It is worth noting that the LPS-induced increase in spreading area and perimeter and the decrease in circularity were more notable in the cells cultured on the compliant than on the stiffer substrate. As previously reported

(Jain and Vogel, 2018), LPS tends to promote cell spreading and, since macrophages were already well spread on the stiff gels before their priming, it seems coherent that more pronounced changes were detected in the 0.2 kPa gels.

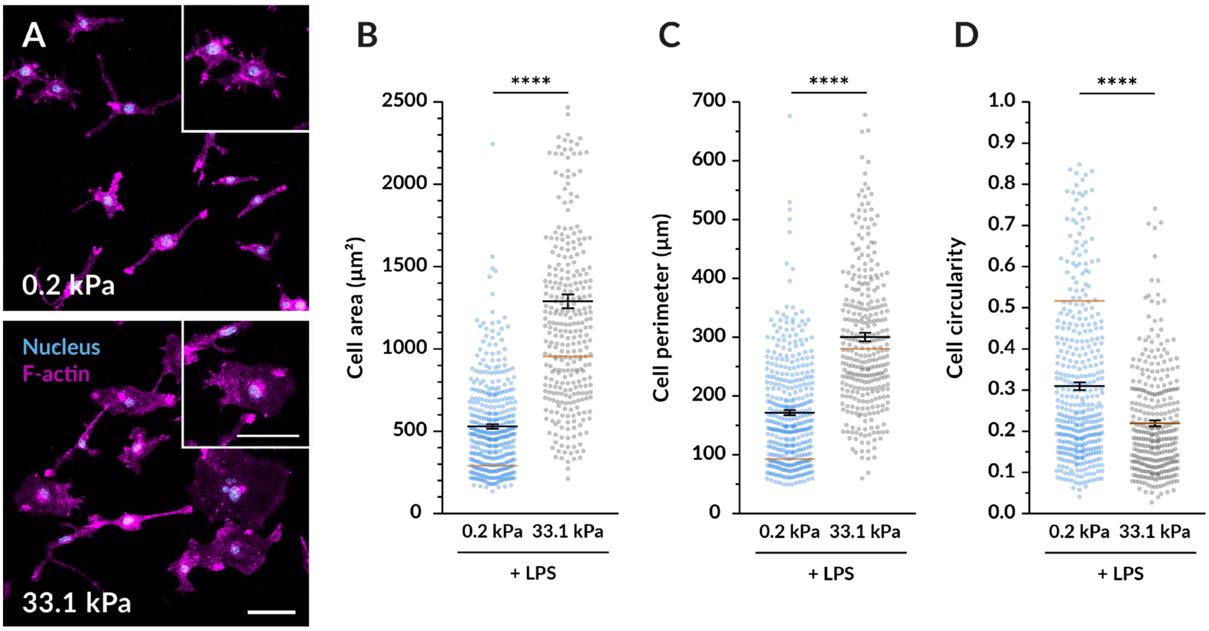

Figure 3.7 | Stiffness-induced morphological differences persist after macrophage LPS priming. (A) Representative fluorescence microscopy images of BMDMs cultured for 14-18 h on 0.2 and 33.1 kPa gels and primed for 1.5 h with 100 ng/ml LPS. Nuclei shown in blue (DAPI) and F-actin in magenta (phalloidin-TRITC). Enlarged examples of cells in each condition are displayed in the insets. Scale bars, 50 µm. **(B-D)** Quantification of the cell area (B), perimeter (C) and circularity (D) from images taken under the same conditions as (A). In all plots, each dot represents a cell, the black bars indicate the mean ± SEM, and the reference orange bar indicates the mean of the non-primed macrophages in Fig. 1D-F. The number of analysed cells was 390 for compliant and 322 for stiff; and data were obtained from three independent experiments done with different animals. Statistical analysis was performed using a Mann-Whitney test. **** $p < 0.0001$.

3.2.2 Tuning substrate stiffness does not cause major changes in the expression of pro-inflammatory genes

The interaction of TLR4 with its ligand LPS triggers the activation of a signalling cascade that leads to the translocation of the transcription factor NFκB into the nucleus, which promotes the transcription of pro-inflammatory genes (Bauernfeind et al., 2009; Kuzmich et al., 2017; Zamyatina and Heine, 2020). To begin studying the effect of substrate stiffness on the pro-inflammatory behaviour of macrophages, quantitative RT-PCRs were performed to quantify the expression of several genes representing some of the major mediators and effectors of the pro-inflammatory response. Specifically, the expression of the genes encoding for the cytokines TNF-α, IL-1β and IL-6; the pro-inflammatory molecule NOS2; the chemokines CXCL2 and CXCL9; and the receptors TLR2 and TLR4 were tested.

In absence of LPS, the expression of all the genes was minimal except for *Tlr4* and no differences were observed between BMDMs cultured on compliant and stiff hydrogels (Fig. 3.8). Upon LPS priming, an increase in the expression levels of most of the above-mentioned genes was observed. Interestingly, when comparing the two stiffnesses, a statistically significant higher expression of *Tnf-α* was detected when culturing the macrophages on compliant substrates. Despite not being significant, the cytokine genes *Il6* and *Il1b* were also higher in the 0.2 kPa gels, and *Tlr2* and *Cxcl2* followed the same trend. There were no differences in the expression levels of *Nos2*, *Tlr4* and *Cxcl9*. Therefore, under the chosen experimental conditions, these data indicate that substrate stiffness does not have a major influence on the expression of pro-inflammatory genes.

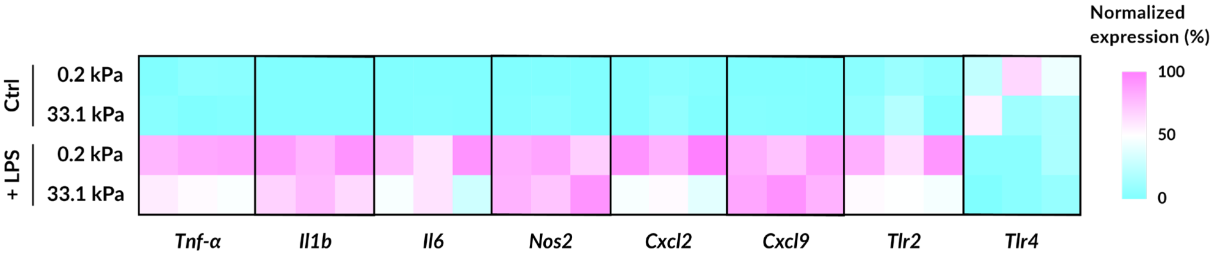

Figure 3.8 | Modifying substrate stiffness does not significantly influence macrophage pro-inflammatory gene expression. Relative gene expression levels of pro-inflammatory genes in non-treated macrophages and in cells primed with 100 ng/ml LPS for 6 h. Normalised data are presented as heatmaps (see Appendix Fig. A.3 for absolute fold changes).

3.2.3 Lower substrate stiffness upregulates the secretion of the cytokines IL-6 and IL-1β

After the activation of the genes encoding for pro-inflammatory cytokines, a series of events still needs to occur before these factors are released into the extracellular environment and have an effect on other cells. These steps, which include protein synthesis, maturation, transport and secretion, can also be modulated by multiple regulatory signals (Netea et al., 2010; Wolf et al., 2014; Afonina et al., 2015; Monteleone et al., 2018). Therefore, although macrophage gene expression was not strongly affected by substrate stiffness, whether it influenced the production and release of the pro-inflammatory cytokines IL-6 and IL-1β remained a question of interest.

Priming of macrophages with LPS alone leads to the synthesis and secretion of IL-6, which can be detected via ELISA (Barton and Medzhitov, 2003; Lee et al., 2015). In this experiment, BMDMs on PAA hydrogels were treated for 4.5 h with LPS and the amount of IL-6 released into the culture supernatant was assessed (Fig. 3.9A). A representative experiment is shown in Fig. 3.9B and a heatmap displaying the trends across different independent experiments is included in Fig. 3.9C.

On average, 11% higher concentrations of IL-6 were detected when macrophages were cultured on compliant substrates compared to those primed on stiff gels.

As previously described in Section 1.1.3, to secrete major amounts of IL-1β macrophages need to be 1) primed with LPS and 2) provided with a second stimulus that triggers the final maturation and release of the cytokine. In this work, the chosen stimulus was nigericin: a potent inducer of K^+ efflux that triggers the assembly of the NLRP3 inflammasome. This multiprotein signalling hub mediates the final processing of IL-1β, which is then released outside the cell (Martinon et al., 2002; Agostini et al., 2004). Following the same trend as with IL-6, after 1.5 h of nigericin stimulation macrophages on 0.2 kPa hydrogels consistently secreted higher amounts of IL-1β, representing a mean 44% increase over cells cultured on 33.1 kPa hydrogels (Fig. 3.9D-E).

Interestingly, the collected data reveal that while pro-inflammatory gene expression levels of macrophages were not significantly altered on varying PAA stiffness, both the secretion of IL-6 and IL-1β became upregulated at lower substrate stiffness.

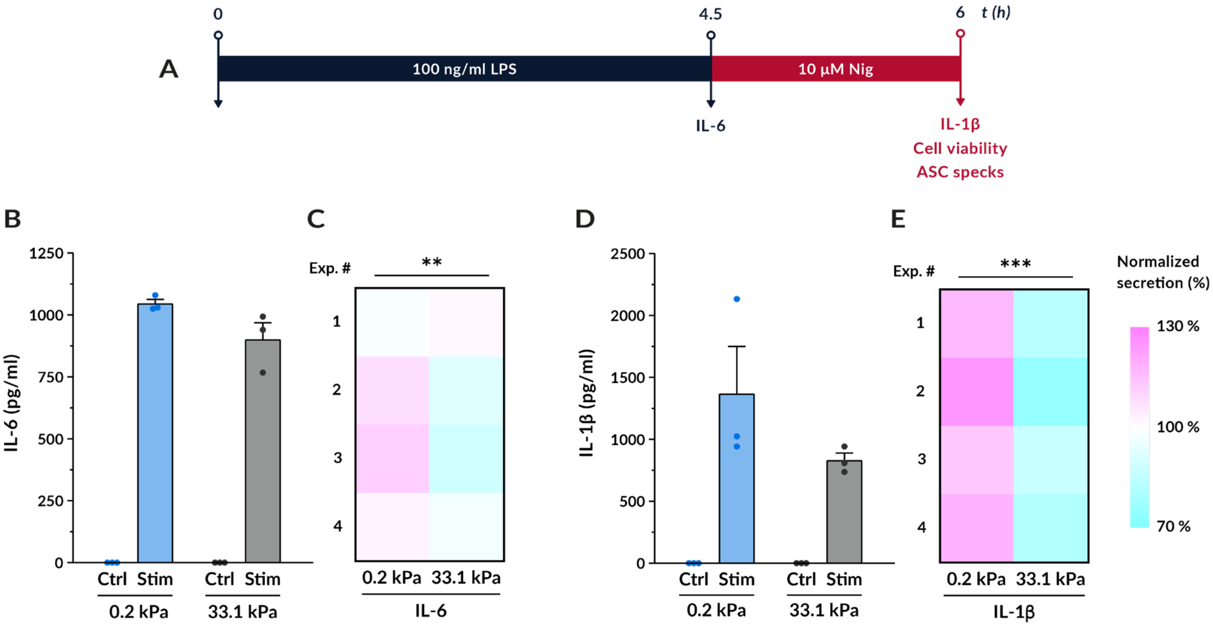

Figure 3.9 | Macrophages secrete higher levels of the cytokines IL-6 and IL-1β on compliant substrates. Quantification by ELISA of the protein levels of IL-6 and IL-1β secreted by BMDMs on compliant and stiff polyacrylamide gels. **(A)** Scheme of the experimental treatment applied in (B-E). Cells were cultured for 14-18 h on hydrogels, primed for 4.5 h with 100 ng/ml LPS and stimulated for 1.5 h with 10 µM nigericin. To measure IL-6, supernatants were collected after LPS priming and to assess IL-1β, samples were taken after nigericin treatment. **(B, D)** Results of one representative experiment for IL-6 (B) and IL-1β (D). Mean ± SEM is displayed and each dot indicates one replicate. **(C, E)** Heatmaps of the IL-6 (C) and IL-1β (E) cytokine quantification performed as described in (A). Each square represents an independent experiment, which were repeated four times using cells from four different mice, with similar results. Statistical analysis was performed using a 1D linear mixed model and p-values were determined by a likelihood ratio test. ** $p < 0.01$; *** $p < 0.001$.

3.2.4 Stiffer substrates diminish macrophage pyroptotic cell death

Another downstream effect of nigericin stimulation is the onset of pyroptosis, a process defined as caspase-1-mediated cell death. During this lytic process, the cleavage of the effector protein gasdermin D (GSDMD) forms pores in the plasma membrane, initially inducing cell swelling quickly followed by cell lysis and release of intracellular contents (de Vasconcelos et al., 2019). Indeed, the same was observed in the preliminary data obtained in our lab and shown in Annex Fig. A.4, where BMDMs grown and stimulated on plastic were monitored by optical diffraction tomography (ODT) for 70 min. The results indicated that dry mass started decreasing 10 min after the onset of the treatment and continued doing so up to the final 70 min. In addition, cell volume steadily increased up to 40 min post-nigericin, point at which starts decreasing until the last measured timepoint. These changes in the measured volume could be due to the formation of blebs commonly observed upon nigericin stimulation and their later burst, but further data would be needed to confirm it.

Macrophage pyroptosis further contributes to the extracellular release of some of the cytokines produced upon pro-inflammatory activation such as IL-1β and IL-18. According to this, could the enhanced secretion of IL-1β observed on compliant gels be accompanied by an increase in cell death? To answer this question, cell viability was determined by measuring the levels of lactate dehydrogenase (LDH), an enzyme released by cells upon cell death. In control (unstimulated) samples, cell viability was equally high in both compliant and stiff substrates (Fig. 3.10A), confirming that the hydrogels do not have a considerable negative impact on cell survival. After 90 min of incubation with nigericin, LDH release was notably affected, and a significantly lower viability was detected in macrophages grown on 0.2 kPa gels, indicating that pyroptosis was enhanced on compliant gels. Moreover, additional time course data (Fig. 3.10B) indicated that the differences in cell death were already noticeable 60 min after nigericin exposure and still detectable 6 h after the onset of the treatment. Nevertheless, the 90 min time point was used for the remainder of the study because at this stage the macrophage pyroptotic response was robust enough but still submaximal.

Altogether, these results show that gels with a lower Young's modulus upregulated both nigericin-induced pyroptotic cell death and cytokine release, and highlight the importance of investigating which macrophage signalling components could mediate this mechanotransduction.

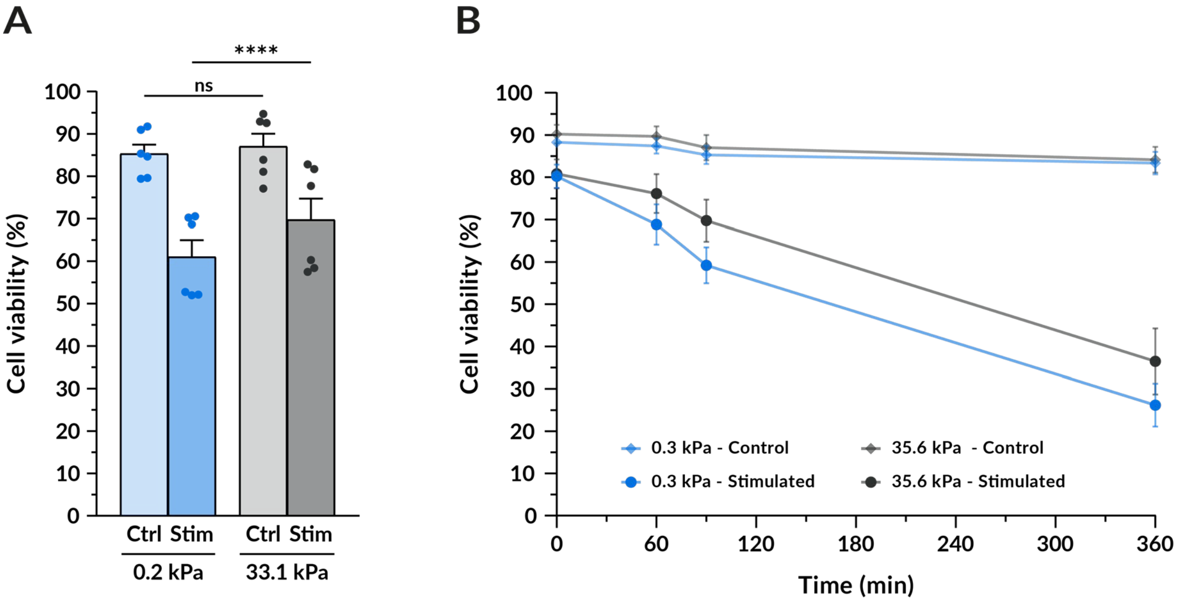

Figure 3.10 | Nigericin-induced macrophage pyroptosis increases on compliant substrates. (A) Assessment of cell viability determined by LDH assay in untreated BMDMs (control) and after macrophage priming and stimulation (stimulated) done as previously described. Mean ± SEM are shown and each dot represents a replicate obtained from three independent experiments. Statistical analysis was performed using a 1D linear mixed model and p-values were determined by a likelihood ratio test. ns, not significant; **** $p < 0.0001$. **(B)** Time-course assessment of cell viability at 0, 60, 90 and 360 min after macrophage priming and stimulation. Mean ± SEM are shown and data corresponds to 2 independent experiment with 3 replicates per condition.

3.2.5 Compliant substrates enhance NLRP3 inflammasome formation

The data presented above suggest that the upstream signalling events leading to cytokine maturation and release may become upregulated when macrophages are cultured on more compliant substrates. Among these, one of the most relevant signalling elements is the NRLP3 inflammasome, which is the corresponding inflammasome activated by the K^+ efflux induced by nigericin (Pétrilli et al., 2007; Muñoz-Planillo et al., 2013). As mentioned in the introductory Section 1.1.3, this macromolecular complex is comprised of three different proteins – the sensor protein NLRP3, the adaptor ASC and the effector pro-caspase-1 – that cluster together, mediating the activation of the latter. By fluorescent immunostaining of ASC it is possible to image and clearly detect bright 1-µm "ASC specks" (Franklin et al., 2014), which correspond to assembled inflammasomes (Fig. 3.11A). This approach, thus, allows to easily and reliably quantify in a single-cell manner macrophages containing formed inflammasomes (Stutz et al., 2013; Beilharz et al., 2016).

As shown in Fig. 3.11A, in cells that did not contain a maturely formed inflammasome the fluorescence signal corresponding to ASC was distributed across all the cytoplasmic and nuclear areas and the F-actin distribution matched the organisation commonly observed in BMDMs (Jain and Vogel, 2018) . In contrast, macrophages with an assembled inflammasome had a distinct and clearly visible punctum, usually in a perinuclear region. These ASC speck-positive cells tended to display weaker F-actin staining. Moreover, the quantification of cell area showed that cells with an assembled inflammasome were typically smaller, which was particularly evident for the more spread cells on stiff gels (Fig. 3.11B). These observations are explained by the fact that treating macrophages with nigericin triggered the onset of pyroptotic cell death, inducing the impairment of the F-actin cytoskeleton and the loss of integrity of the whole cell. This cellular rupture may also be the reason why a few ASC specks were released by macrophages and were observed isolated, with no visible cellular components surrounding them, which is in line with previous reports such as (Franklin et al., 2014). As shown in Appendix Fig. A.5, approximately only 20% of the observed ASC specks were extracellular, a percentage that did not substantially vary across the different conditions used in this study. For these reasons, both intra- and extracellular specks were included in the final analysis (see Methods Section 5.5.3 for a detailed description of the procedure).

As in previous experiments, BMDMs were primed with LPS for 4.5 h and stimulated with nigericin for 1.5 h, and the ratio of ASC-positive specks to cell number was determined. Remarkably, macrophages on 0.2 kPa polyacrylamide gels displayed a ratio of 48%, representing 4 times more ASC specks than cells on 33.1 kPa (Fig. 3.11C). These data strongly indicate that the formation of the NLRP3 inflammasome was upregulated in macrophages cultured on compliant substrates.

Summing up, the results presented in this Section show that more compliant substrates enhance the assembly of macrophage NLRP3 inflammasomes, the secretion of the pro-inflammatory cytokines IL-1β and IL-6 and the release of the pyroptotic marker LDH. Besides supporting the idea that macrophages and their inflammatory response are mechanosensitive, these data suggest that substrate stiffness may modulate the formation of the inflammasome and the downstream activation of the pyroptotic machinery. Furthermore, these findings pose the question of which cellular components could serve as a link between substrate stiffness and the NLRP3 inflammasome. This is an issue that Section 3.3 attempts to tackle.

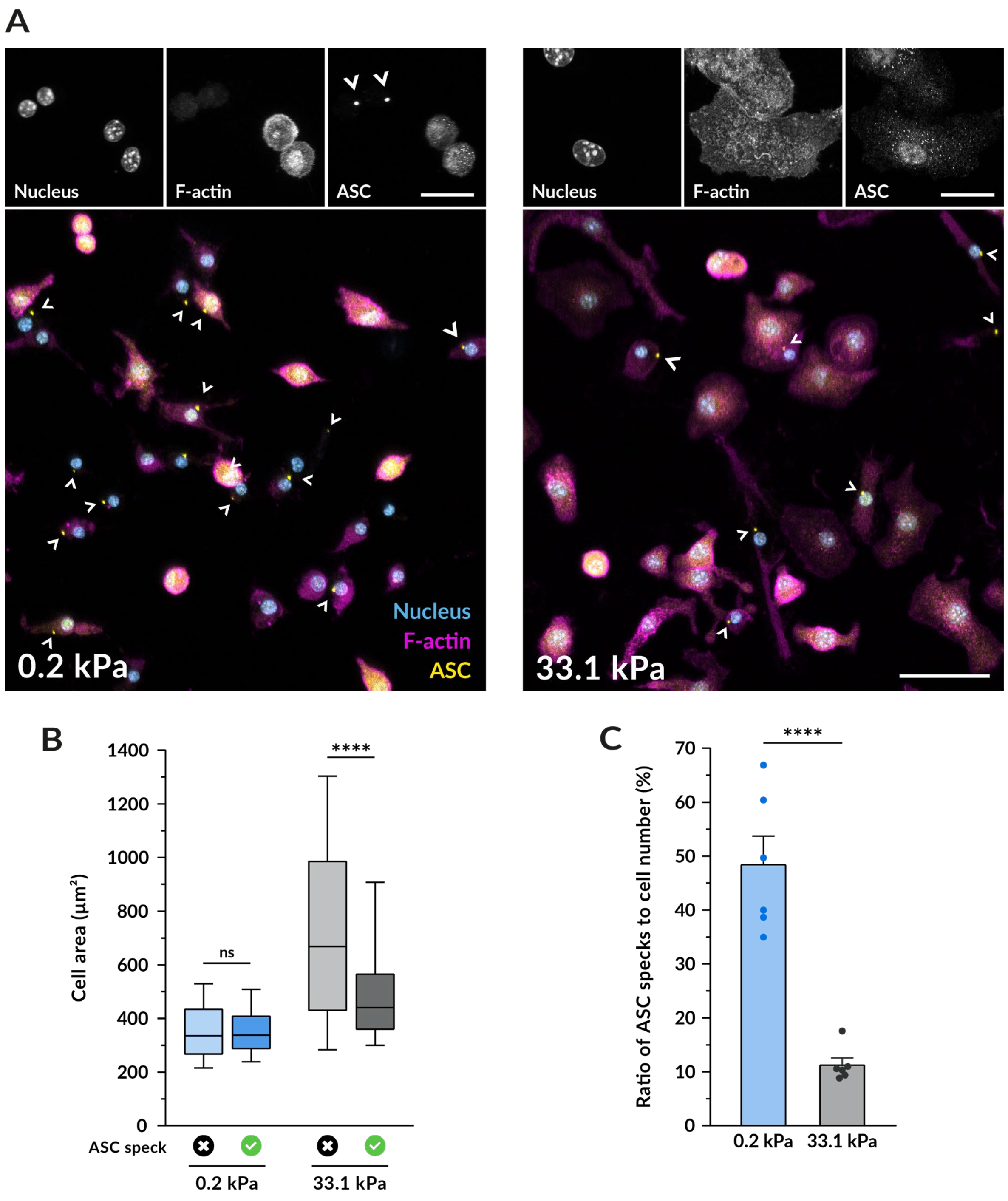
A
Nucleus
F-actin
ASC
Nucleus
F-actin
ASC
Nucleus
F-actin
ASC
0.2 kPa
33.1 kPa
B
Cell area (µm²)
1400
1200
1000
800
600
400
200
0
ns
****
ASC speck
0.2 kPa
33.1 kPa
C
Ratio of ASC specks to cell number (%)
70
60
50
40
30
20
10
0
****
0.2 kPa
33.1 kPa

Figure 3.11 | NLRP3 inflammasome formation is enhanced on hydrogels of lower stiffness.
(A) Representative confocal microscopy images of ASC specks as a measure of inflammasome formation. BMDMs were primed and stimulated as described in Fig. 3.10A. Top, separate channels of higher magnification examples on each stiffness; scale bar, 20 µm. Bottom, merged channels of lower magnification images with nuclei shown in blue (DAPI), F-actin in magenta (phalloidin-TRITC) and the inflammasome linker protein ASC in yellow. White arrowheads indicate ASC specks, markers of inflammasome assembly. Scale bar, 50 µm. **(B)** Quantification of the spreading area of ASC speck-positive and negative cells for images taken under the same conditions as (A). **(C)** Quantification of the ratio of ASC specks to cell number. Mean ± SEM are shown and each dot indicates one of the different replicates obtained from three independent experiments. The total number of cells analysed was 4327 for compliant hydrogels and 5030 for stiff hydrogels. Statistical analysis was performed using a 1D linear mixed model and p-values were determined by a likelihood ratio test. ns, not significant; ** $p < 0.01$; *** $p < 0.001$; **** $p < 0.0001$.

3.3 Investigation of macrophage mechanotransducing elements

One of the goals of this dissertation was to distinguish which mechanisms enable macrophages to perceive matrix stiffness. A few other publications have also reported that mechanical stimuli affect inflammasome formation (Ip and Medzhitov, 2015; Maruyama et al., 2018), but how the information given by biophysical cues is transmitted into the inflammasome machinery is still unclear. As explained in the Introduction Section 1.3, several cell mechanosensing elements have been described, including cell-substrate adhesion complexes such as focal adhesions (Jansen et al., 2017) and membrane constituents like caveolae (Del Pozo et al., 2021) and mechanically gated ion channels (Ranade et al., 2015). Whether these mechanosensors could contribute to regulate inflammasome assembly and activation was of particular interest to the present study, and the experimental results presented in the following pages aim to address this.

3.3.1 Limiting cell spreading alone does not recapitulate the effects induced by stiffness on inflammasome formation

As reported in Section 3.1.1, the effects of substrate stiffness on the pro-inflammatory behaviour of macrophages are accompanied by notable differences in the morphology adopted by cells upon culture on PAA hydrogels. In light of the strong impact of stiffness on cell shape, could the distinctly low spreading area of macrophages on compliant substrates represent an initial mechanosensitive trigger of downstream signalling events that lead to an enhanced response? To tackle this question, a micropatterning-based approach was employed to test whether cell spreading alone affects inflammasome formation.

Specifically, BMDMs were cultured on fibronectin-coated round islands patterned on glass. The islands had a diameter of 20 µm and, thus, an area of 314 µm^2, resembling the mean spreading area adopted by macrophages on 0.2 kPa gels. These confined macrophages were then compared to cells grown on a glass surface functionalised with non-patterned fibronectin, a situation where they could extensively spread and that mimicked the morphology observed on 33.1 kPa substrates (Fig. 3.12A). To compare the response in both conditions, the detection of formed inflammasomes was chosen since it is a reliable, single-cell, microscopy-based readout. As in previous experiments, cells were primed with LPS, stimulated with nigericin and ASC specks were quantified as a proxy of inflammasome assembly (Fig. 3.12B).

Surprisingly, macrophages confined on 20 µm islands had on average significantly less ASC specks than cells grown on an unconfined area (21% *vs* 40%, respectively). Under these conditions, limiting cell spreading did not recapitulate what had been observed on compliant polyacrylamide gels since it did not increase inflammasome formation but actually reduced it. Therefore, cell spreading alone does not seem to be the factor positively modulating the enhanced response of macrophages on more compliant substrates. This observation reduces the possibilities that membrane-related elements such as caveolae or mechanosensitive ion channels play a crucial role in substrate stiffness macrophage mechanosensing and, consequently, other possible mechanosensing components were investigated.

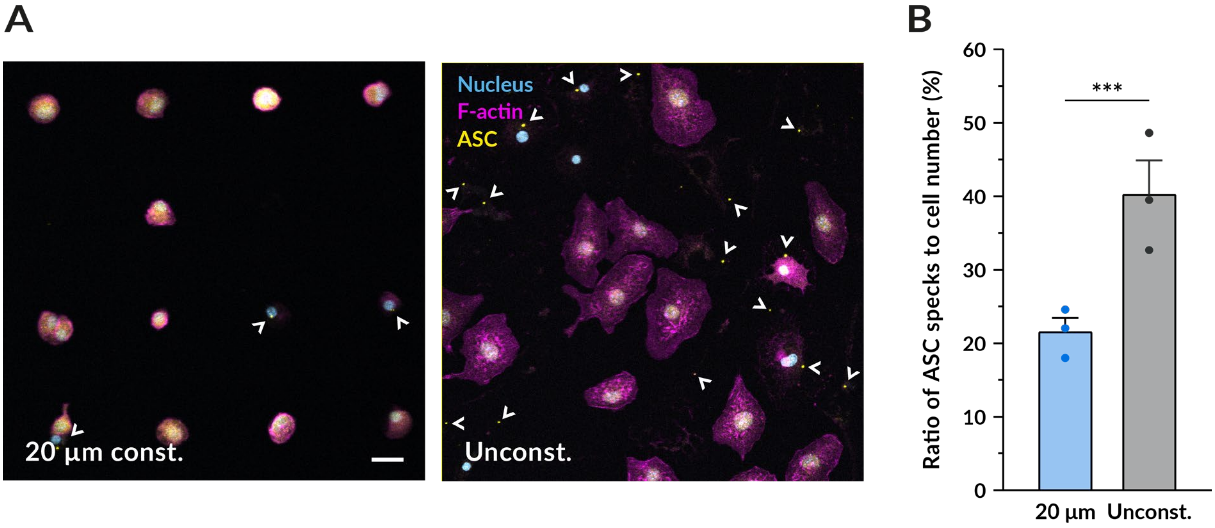

Figure 3.12 | Limiting cell spreading does not recapitulate the differences induced by stiffness on inflammasome formation. (A) Representative confocal microscopy images of inflammasome formation under cell confinement. Constrained BMDMs were cultured on fibronectin-coated circular islands with a diameter of 20 µm micropatterned on glass substrates. Unconstrained cells were grown on fibronectin-coated glass coverslips in an unconfined manner. After 14 – 18 h of culture, they were primed and stimulated as done in previous experiments. Nuclei shown in blue (DAPI), F-actin in magenta (phalloidin-TRITC) and ASC in yellow. Scale bar, 20 µm. **(B)** Quantification of the ratio of ASC specks to cell number. Mean ± SEM are shown and each dot indicates an independent experiment done with BMDMs from different mice. The total number of cells analysed was 1560 for the 20 µm constrained and 1524 for the unconstrained adhesion area. Statistical analysis was performed using a 1D linear mixed model and p-values were determined by a likelihood ratio test. **** $p < 0.0001$.

3.3.2 Actomyosin contractility may play a role in transducing the mechanical cues given by substrate stiffness

The F-actin cytoskeleton is one of the most well-known mechanotransducing elements as actomyosin not only enables cells to generate forces but it also contributes to integrate mechanical signals from the microenvironment (Elosegui-Artola et al., 2018). Given the observations that the F-actin architecture was also altered by substrate stiffness, the potential mechanosensing role of actomyosin contractility in macrophages was investigated.

For this, a pair of small molecule inhibitors were used to determine the effect of interfering with actomyosin contractility on NLRP3 inflammasome formation on polyacrylamide hydrogels. BMDMs were treated with blebbistatin, a non-muscle myosin II inhibitor, or with Y-27632, a molecule that blocks ROCK1 and ROCK2. As shown in the schematic in Fig. 3.13A, the inhibitors were added 1 h prior to the start of macrophage priming and stimulation and were kept during all the procedure. After all the treatment, cells were fixed and the ratio of ASC specks to cell number was determined. Fig. 3.13B contains some representative images of nigericin-stimulated macrophages treated with the different actomyosin contractility inhibitors and Fig. 3.13C shows the quantification of spreading area of the cells in these images. It is interesting to note that the treatment with blebbistatin did not induce notable morphological changes in BMDMs. This is in line with (Jain and Vogel, 2018), who reported a similar effect even using higher concentrations of blebbistatin for longer times. By contrast, Y-27632-treated macrophages were thinner and had some elongated processes, being especially noticeable upon imaging the cells cultured on stiff 33.1 kPa gels.

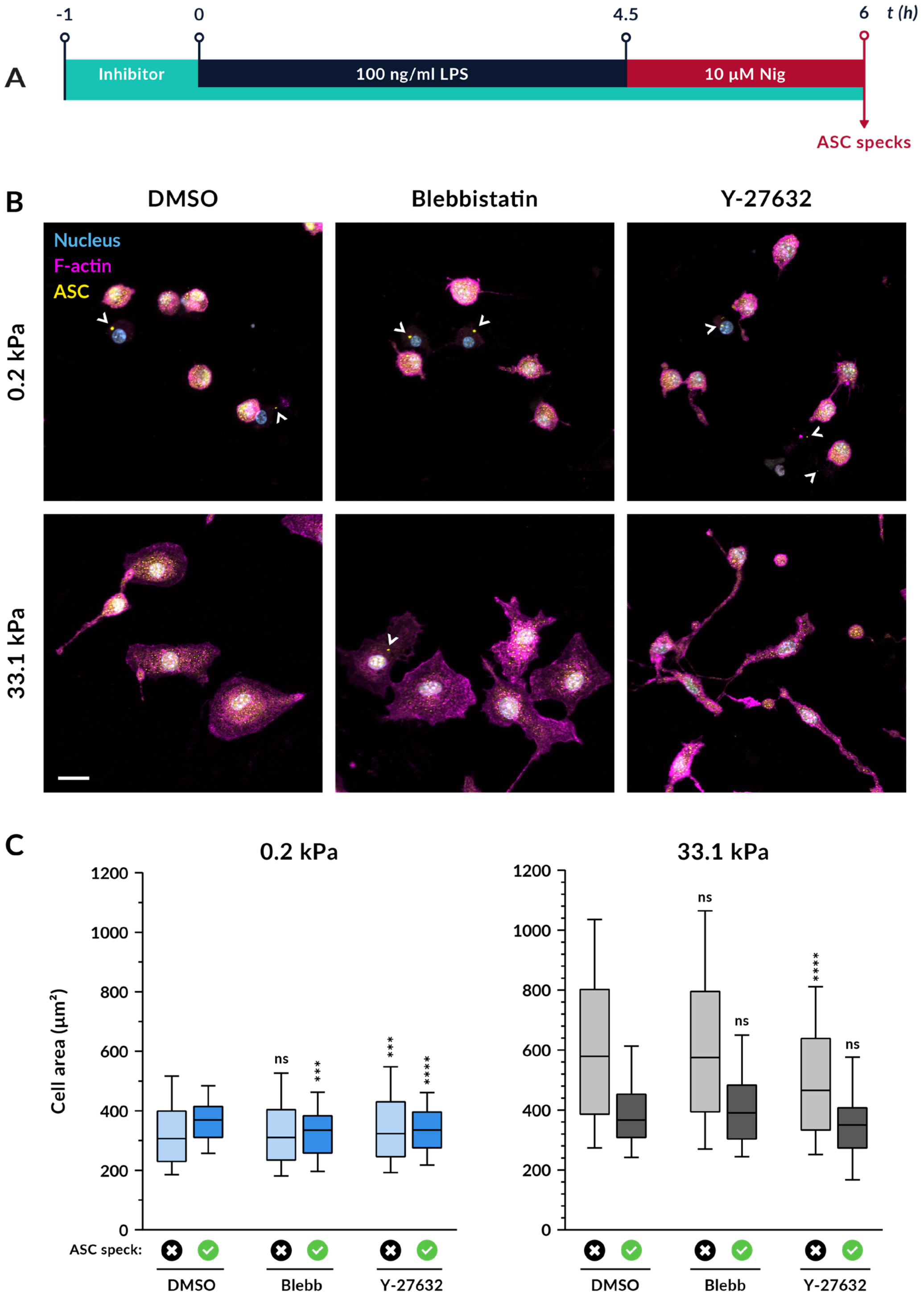

Figure 3.13 | Interfering with ROCK activity induces a decrease in macrophage spreading area.
(A) Scheme of the experimental treatment applied in Fig. 12B and Fig. 13. BMDMs cultured on hydrogels for 14 -18 h were pre-treated with either 1:1700 DMSO as a control, 10 µm blebbistatin or 10 µm Y-27632 for 1 h. While keeping the respective inhibitor molecules, cells were then primed with 100 ng/ml LPS for 4.5 h and 10 µm nigericin for 1.5 h. **(B)** Representative confocal microscopy images of inflammasome formation under actomyosin inhibition. Nuclei shown in blue (DAPI), F-actin in magenta (phalloidin-TRITC) and ASC in yellow. Scale bar, 20 µm. **(C)** Quantification of the spreading area of ASC speck-positive and negative cells for images taken under the same conditions as (B). Statistical analysis was performed using a Kruskal-Wallis test followed by Dunn's post hoc analysis to obtain the multiple comparison p-values. ns, not significant, * $p < 0.05$; *** $p < 0.001$; **** $p < 0.0001$. Symbol on top of each bar indicates the comparison with its corresponding DMSO-control ASC-positive or negative condition.

The quantification of inflammasome formation, displayed in Fig. 3.14, revealed that on compliant gels both blebbistatin and Y-27632 treatments reduced the ratio of ASC specks. In contrast, on stiff hydrogels there were no differences to the DMSO control. Interestingly, when comparing each treatment between the two stiffnesses, treating the cells with blebbistatin strongly diminished the differences in inflammasome formation between 0.2 and 33.1 kPa substrates. Inhibiting ROCK, however, did not suppress the differences between both stiffnesses.

These results indicate that interfering with actomyosin contractility with blebbistatin had a significant impact on the enhanced capacity of BMDMs on compliant substrates to assemble the NLRP3 inflammasome in response to nigericin stimulation, decreasing inflammasome formation and equalising it to the one on stiff hydrogels. This suggests that actomyosin contractility might play a role in the mechanotransduction process and might mediate the modulatory effect of stiffness on macrophage inflammasome formation.

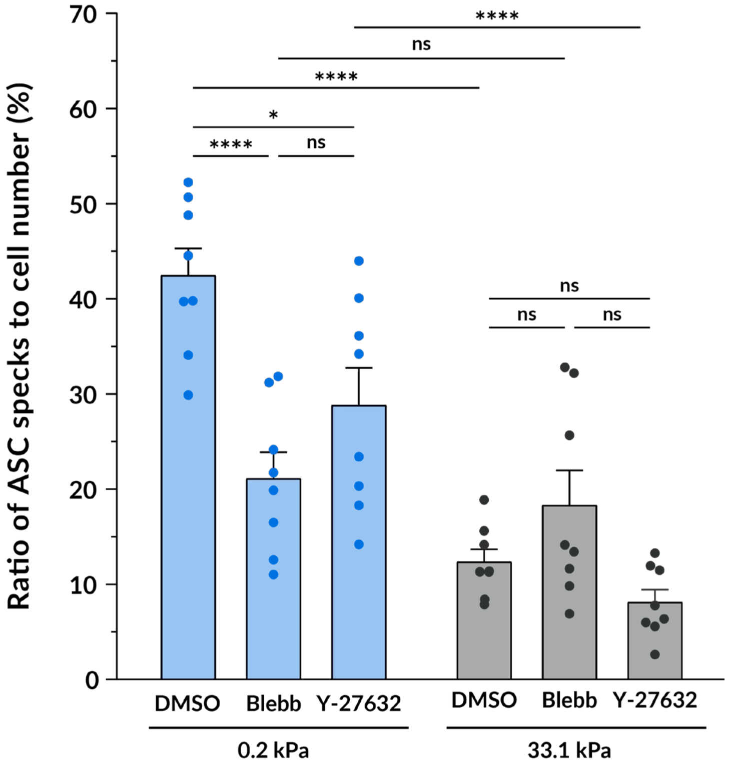

Figure 3.14 | Inhibiting myosin diminishes the differences induced by stiffness on inflammasome formation. Quantification of the ratio of ASC specks to cell number for images taken under the same conditions as Fig. 3.13. Mean ± SEM are shown and each dot indicates one of the different replicates obtained from three independent experiments. The total number of cells analysed was, for compliant gels, 4673 (DMSO), 3528 (blebbistatin) and 5182 (Y-27632); and for stiff gels, 4859 (DMSO), 5447 (blebbistatin), and 5214 (Y-27632). Statistical analysis was performed using a one-way ANOVA followed by Bonferroni's post hoc analysis to obtain the multiple comparison p-values. ns, not significant, * $p < 0.05$; *** $p < 0.001$; **** $p < 0.0001$.

DISCUSSION AND CONCLUSIONS

As cells of the innate immune system, macrophages are not only present in most tissues of the body but also migrate towards lesion areas and sites of infection. This implies that they are not only exposed to the native biophysical properties of tissues but also experience the mechanical changes that result from tissue damage and disease. In the present study, the influence of microenvironment stiffness on the pro-inflammatory response of macrophages was explored. Primary macrophages were exposed to substrate stiffness in the range of 0.2 to 33.1 kPa and the results revealed that more compliant substrates increase the sensitivity of BMDMs to pro-inflammatory stimuli, enhancing inflammasome formation, pyroptosis onset and cytokine release, and that this might be mediated through actomyosin contractility. The following paragraphs comment on these results and puts them in the context of the current literature. Parts of this discussion have also been published in Escolano et al. (2021).

4.1 Compliant substrates enhance the macrophage pro-inflammatory response

The initial work shown in this dissertation focused on searching an adequate platform to study macrophage mechanosensing. Among the different biomaterials tested, PAA-based substrates resulted to be the best option. The thiol-group functionalisation done by incorporating methysulfone acrylate (MS) monomers in the acrylamide mix enabled to tune hydrogel stiffness while maintaining comparable RGD coating, an advantage that classical PAA functionalisation methods do not offer (Farrukh et al., 2016). Primary macrophages attached well to the hydrogel surfaces and could be successfully cultured on all stiffnesses in a stable and reproducible manner, with minimal cell detachment and a viability of ≥ 85% after 1 day on the substrates (Fig 3.10). The hydrogel elasticities mainly used in this work (0.2 vs. 33.1 kPa) were chosen for different reasons. First, this range covers the stiffness values found in multiple tissues where macrophages are present, including brain, adipose, lung, liver, kidney, cardiac and dermal tissues (see the respective review of Guimarães et al., 2020 for a list of values). Second, the morphological characterisation of macrophages on the three different Young's moduli used in Fig. 3.3 pointed towards a linear response to substrate stiffness within this range. Since the 0.2 and 33.1 kPa gels encompass a change of two orders of magnitude and showed consistent and substantial effect differences at the onset of the study, these two most distant stiffnesses were chosen to continue with the study. Moreover, these values approximately matched the lower and upper limits reported for the elastic moduli of bone marrow by Ivanovska et al. (2017), being 0.1 kPa in the central part and more vascularised regions and 30-100 kPa near the bone surface.

The characterisation of different morphological metrics, including spreading area, circularity and membrane topography, indicated that varying substrate stiffness had an impact on macrophages. BMDMs grown for a day on stiffer hydrogels displayed a larger area, smaller circularity and a smoother plasma membrane. All these changes are in line with what has been reported in several polyacrylamide stiffness ranges and different macrophage cell types, including murine BMDMs (Gruber et al., 2018), RAW 264.7 murine cells (Blakney, et al., 2012; Patel et al., 2012), human THP-1-differentiated macrophages (Sridharan et al., 2019a; Xing et al., 2020) and human monocyte-derived macrophages (Adlerz et al., 2016).

The experimental results described in this thesis confirmed that substrate stiffness influences the pro-inflammatory response of macrophages. Despite culturing BMDMs on PAA with different Young's moduli did not induce major changes in the expression of pro-inflammatory genes, macrophages primed and stimulated on 0.2 kPa hydrogels released higher amounts of the cytokines and IL-6 and IL-1β than cells on 33.1 kPa matrices.

Different studies using polyacrylamide hydrogels within a similar stiffness range also described an enhanced release of pro-inflammatory cytokines on more compliant substrates. For example, Scheraga et al. (2016) cultured BMDMs on fibronectin-coated PAA with elastic moduli between 1 and 25 kPa. Upon a 24 h LPS challenge, they quantified higher concentrations of IL-1β on the compliant substrates and, additionally, increased levels of the anti-inflammatory cytokine IL-10 on the stiffest hydrogels - a factor not measured in the present work -. Using the same sort of cells, gels and stimulus, Gruber et al. (2018) detected higher levels of the pro-inflammatory cytokine TNF-α on 1 kPa hydrogels than on 20 and 150 kPa materials. In this case, though, the amount of IL-10 was higher on the compliant substrates. And following the same trend but using different cell lines, Patel et al. (2012) exposed murine RAW 264.7 and human U397 macrophages to poly-D-lysine (PDL)-coated PAA gels between 0.3 to 150 kPa. In both cell types their results showed that the levels of TNF-α released after LPS priming became higher when decreasing substrate stiffness.

By contrast, there are other reports stating that stiffer microenvironments are the ones upregulating the pro-inflammatory behaviour of macrophages (Blakney, et al., 2012; Previtera and Sengupta, 2015; Okamoto et al., 2018; Hsieh et al., 2019; Sridharan et al., 2019; Meli et al., 2020). For instance, Previtera and Sengupta (2015) cultured for 24 h murine BMDMs on polyacrylamide gels with Young's moduli ranging from 0.3 to 230 kPa. After LPS treatment they detected higher levels of secreted IL-1β, TNF-α and NO on stiffer substrates, observing the same trend with different hydrogel coatings. This discrepancy in the response of macrophages across different studies might be caused by the choice of different cell lines, substrate material, adhesion proteins, their coating densities or the specific type of stimulatory challenge. In the present work it should be noted that the samples used to quantify IL-6 were collected only after 4.5 h of LPS priming and, unlike all the mentioned studies, the release of IL-1β was induced with the ionophore nigericin. Given this variability in the experimental settings, the comparison of results obtained by different laboratories should be done with care. Moreover, the ongoing progress in the design of hydrogels and artificial matrices may help recreate better the structural and mechanical features of the native tissues where macrophages reside, thus improving the physiological relevance of future mechanobiology studies (Caliari and Burdick, 2016).

In addition to this, a limitation of the present work is that most experiments were only performed using two different stiffness. It is important to consider the possibility that macrophages might not respond to substrates of differing stiffness in a monotonous manner. Sridharan and colleagues (2019) reported that in THP-1-derived macrophages the effect of material stiffness on their phagocytic ability and on several M1-associated genes and cytokines followed a biphasic response. The data obtained by Gruber et al. (2018) in RAW 264.7 cells displayed a similar behaviour in LPS-induced TNF-α release. The biphasic response to substrate mechanics has already been described in other cell types such as fibroblasts (Wang et al., 2019b) and, therefore, the existence of a non-linear relationship between substrate stiffness and macrophage behaviour should not be discarded until more data is collected.

While the results described in this thesis indicate that lower substrate stiffness upregulates the pro-inflammatory response of macrophages, the limited amount of gene expression data obtained does not allow to completely understand how their phenotype is affected. Complementing this, other publications have focused their attention on assessing the influence of substrate stiffness on their polarisation state. Carnicer-Lombarte et al. (2019) cultured BMDMs for 3 days on PDL-coated PAA gels between 0.1 and 50 kPa, and performed RNAseq to evaluate the expression levels of a wide panel of pro-inflammatory (M1) and anti-inflammatory (M2) genes. Their data indicated that macrophages underwent a phenotype switch, becoming more M1-like on compliant substrates and M2-like on the stiffer ones. Similarly, Chen et al. (2020) grew BMDMs for 3 and 5 days on PAA gels of approx. 3, 35 and 64 kPa, detecting at both culture time-points an increase of M1 genes (such as *Il1b* and *iNos2*) on the 3 kPa hydrogels and an increase of M2 genes (like *Arg1* and *Tgfb*) on 35 and 64 kPa. In line with this, Xing et al. (2020) reported that THP-1-derived macrophages cultured for 2 days on PAA-collagen between 6 and 16 kPa enhanced their

M2 polarisation on stiffer substrates. In all these studies, macrophages were cultured for several days on the different hydrogels before analysing their phenotypic markers and gene profiles. Despite the mechanical cues given by substrates may be transduced into the nucleus and influence the expression of certain macrophage polarisation genes, the fact that in this thesis BMDMs were only cultured for 1 day on the hydrogels might explain why no significant differences were detected when quantifying pro-inflammatory gene expression across varying stiffness. To clarify this, future work should thus include the acquisition of further data at additional timepoints.

4.2 Substrate stiffness influences the formation of the NLRP3 inflammasome

The inflammasome represents a supra-molecular signalling hub activated in macrophages upon inflammatory stimuli that leads to the activation of caspase-1, enzyme that catalyses the maturation of certain interleukins such as IL-1β and IL-18. Although most of the described inflammasome regulators consist of biochemical signals (Swanson et al., 2019), recent studies suggest that mechanical cues could also be modulating its formation (Ip and Medzhitov, 2015; Maruyama et al., 2018).

The present dissertation provides evidence for the first time that microenvironment stiffness can also influence the formation of the NLRP3 inflammasome. To test whether varying substrate stiffness affected its assembly, the presence of ASC specks was quantified as a proxy of inflammasome activation. The data showed that upon LPS priming and nigericin stimulation the more compliant substrates remarkably enhanced inflammasome formation. Moreover, this was accompanied by an increase in the number of cells entering pyroptotic cell death, as indicated by the higher levels of LDH detected in the supernatant of cells stimulated on 0.2 kPa hydrogels.

Together, these results might suggest an upregulation of the activity of pyroptotic effectors, such as caspase-1. On the one hand, more active caspase-1 could potentially process more pro-IL-1β into its mature form IL-1β (Agostini et al., 2004). On the other hand, active caspase-1 could trigger the cleavage of gasdermin D (GSDMD) and enhance the formation of membrane pores by its N-terminal domain, facilitating the release of molecules such as IL-1β, IL-6 and LDH (He et al., 2015; Shi et al., 2015; Liu et al., 2016). All these effects could be caused by a decrease in the inflammasome activation threshold, the existence of different macrophage subpopulations or by higher assembly rates, but in this study the quantification of inflammasome formation was only performed at a single time point. Therefore, more resolved time-dependent data and the monitoring of additional events such as the cleavage and activation of caspase-1 and GSDMD would be necessary to understand the specific dynamics behind this process.

The fact that the expression of pro-inflammatory genes was not strongly altered upon LPS treatment suggests that the increase in cytokine secretion on compliant gels could be caused by an effect on pathways involved in interleukin maturation and processing. Indeed, the obtained results seem to point in this direction, supporting the hypothesis that under the experimental conditions employed here substrate stiffness does not considerably affect the priming pathway (signal 1) but has a strong impact on the activating pathway (signal 2). Nevertheless, as mentioned earlier, other studies where macrophages have been cultured on hydrogels of differing stiffness for longer times show that their gene expression patterns are modified. Moreover, in this thesis data on the expression of genes that could have a direct impact on inflammasome formation such as *Nlrp3* were not collected. To better dissect the different responses of macrophages to substrate stiffness future experiments should also consider these possibilities.

In conclusion, the work presented here proves that substrate stiffness modulates the formation of the NLRP3 inflammasome, and proposes that more compliant substrates may induce the inflammasome to be more “sensitive” to the effect of activating stimuli, enhancing its assembly and the consequent activation of the pyroptotic machinery, to finally upregulate the processing and release of pro-inflammatory cytokines.

4.3 Exclusively altering cell spreading does not explain the differences induced by substrate stiffness

One of the most relevant questions originating out of the described findings was: how do macrophages integrate the mechanical cues given by substrate stiffness into the inflammasome regulatory network?

The first explored possibility was the potential mechanosensing role of cell shape. This was motivated by the fact that one of the first discernible effects of substrate stiffness on macrophages was the change in cell morphology and membrane topography, and that in studies like McWhorter et al. (2013) their polarisation state could be modified by simply forcing them to adopt certain cell geometries.

Based on this, whether there is a relationship between macrophage spreading and inflammasome formation was tested. As seen in this work and others, BMDMs on stiffer substrates spread considerably more, which could indirectly cause an increase in membrane curvature and tension that mechanosensing elements like caveolae and mechanically-gated ion channels could detect (Le Roux et al., 2019). To determine whether the lower spreading that macrophages adopted on more compliant hydrogels enhanced the formation of the NLRP3 inflammasome, BMDMs were confined using a micropatterning-based approach. While the area of constrain was chosen to match the one of cells on compliant hydrogels, the spreading area of unconfined macrophages resembled the area of cells cultured on stiff hydrogels. Unexpectedly, limiting cell area on a stiff substrate did not promote inflammasome formation but rather reduced it, indicating that reducing cell spreading alone may not recapitulate the downstream inflammatory effects observed on hydrogels with varying Young's moduli.

Despite the limitations given by constraining cell spreading on a glass substrate instead of directly on hydrogels, the followed approach still enables to uncouple spreading area from cues provided by substrates of differing stiffness in a well-controlled manner. Moreover, it allows for comparison to previous work such as the one done by Jain and Vogel (2018), who observed that decreasing the spreading area of macrophages negatively regulated their pro-inflammatory response. Specifically, they spatially confined BMDMs on a glass surface and observed a downregulation of pro-inflammatory genes *Il6*, *Cxcl9*, *Il1b* and *Nos2* and the subsequent secretion of TNF-α, IL-6 and IL-12 via the indirect modulation of chromatin compaction. Following the same trend, the data presented in this work supports the idea that limiting cell spreading has a negative impact in the response of macrophages to pro-inflammatory stimuli and implies that the NLRP3 inflammasome is another – so far unacknowledged – inflammatory signalling components affected by cell confinement.

4.4 Actomyosin contractility as a potential macrophage mechanotransducer element

Macrophages are highly motile cells that exert traction forces on their substrates to adhere, spread and migrate through tissues. The magnitude of these forces increases with substrate stiffness and their generation is dependent on the contraction of the actin cytoskeleton (Hind et al., 2015). Since actomyosin contractility has been described as one of the key elements of the stiffness mechanotransduction machinery (Elosegui-Artola et al., 2018), this work tested whether interfering with it would have any impact on the formation of the NLRP3 inflammasome in BMDMs exposed to different material stiffness. Blocking non-muscle myosin II's motor activity with blebbistatin during macrophage priming and stimulation strongly decreased the percentage of inflammasome-activated cells on the compliant substrates and slightly increased it on the stiff ones, diminishing the original differences between both stiffness. Inhibiting ROCK1 and ROCK2 with Y-27632 also reduced inflammasome assembly on compliant hydrogels but in a less substantial manner than blocking myosin II alone.

The different results obtained by using these two small molecule inhibitors might be explained by the fact that while blebbistatin specifically blocks the motor activity of myosin II, pharmacologically inhibiting ROCK1 and ROCK2 with Y-27632 not only impedes the phosphorylation of myosin but also promotes F-actin destabilisation (Maekawa et al., 1999; Horváth et al., 2020). This would also justify the notable morphological differences observed after incubating the cells with Y-27632 but not detected when using blebbistatin. Moreover, Hind et al. (2016) showed that the generation of traction forces in M1-polarised macrophages requires the activity of myosin II but is independent of upstream ROCK activation. As they proposed, perhaps other myosin II regulatory proteins such as MLCK contribute to promote actin contractility, also helping to explain why the effect observed in this thesis when blocking ROCK is not of the same magnitude as when directly inhibiting myosin II.

It could be speculated that there might be an optimal level of actomyosin contractility at which inflammasome assembly is enhanced and that macrophages on more compliant substrates might be closer to it, leading to an increase in inflammasome formation and in the downstream activation of pro-inflammatory effectors. To investigate this hypothesis, future experiments should aim at assessing in more detail how substrate stiffness affects actomyosin contractility in macrophages. Despite previous studies such as Mih et al. (2012) indicate that stiffer substrates promote an increase in contractility, determining how it is altered within the specific stiffness range and cell type used in this work should be empirically characterised. This could be done by imaging the structure of the actin cytoskeleton via fluorescence microscopy, by detecting phospho-myosin through biochemical assays or also by taking advantage of AFM-based approaches, and would aid interpret the results on inflammasome formation in a more complete manner.

Collectively, the findings of this study suggest that actomyosin contractility may play an important role in the integration of mechanical cues into the NLRP3 inflammasome regulatory pathways, but further work is needed to dissect the exact sequence of events required to couple them. A few additional studies have also proposed that the actin cytoskeleton may participate in the control of inflammasome activation. Using BMDMs infected with *Salmonella typhimurium*, Man et al. (2014) proved that actin polymerisation is necessary for NLRC4 inflammasome formation, pyroptosis onset and IL-1ß release. And Burger et al. (2016) showed that F-actin interacts with NLRP3 and ASC and downregulates the activity of the NLRP3 inflammasome.

Besides actin, other cytoskeletal components have also been described as regulators of inflammasome activation. For instance, dos Santos et al. (2015) reported that the intermediate filament vimentin also associates with NLRP3 and participates in the control inflammasome assembly. And in an excellent study, Magupalli et al. (2020) showed that the NLRP3 inflammasome is assembled at the centrosome (or microtubule-organising centre (MTOC)) and that the dynein adaptor HDAC6 is required for the microtubule retrograde transport of NLRP3 towards it. Overall, they propose that, upon an activation stimulus, NLRP3 molecules pre-packed in trans-Golgi network vesicles are transported through microtubules to the MTOC. This would then facilitate the association of NLRP3 with positive regulators of the inflammasome residing in the MTOC, such as the kinase NEK7, and the subsequent assembly of the entire inflammasome together with ASC and caspase-1. Given this and given that the MTOC (Raab and Discher, 2017) and microtubule architecture (Rong et al., 2021) may also be influenced by substrate stiffness, future experiments should also address the possibility that these components might contribute to transduce the mechanical information given by substrate stiffness into the inflammasome signalling hub. Additionally, actin and microtubule filaments are not completely independent structures but also crosstalk to each other. This includes not only the existence of shared regulator molecules (Krendel et al., 2002; Rafiq et al., 2019) but also other interactions like actin-microtubule crosslinks that enable actin filaments to guide and redirect microtubule growth (López et al., 2014). Therefore, further studies should also consider the possibility that the actin cytoskeleton could play a synergistic role together with other cytoskeletal systems to bring together inflammasome components and, thus, facilitate inflammasome assembly. What the exact link between mechanical cues, cytoskeleton activity and inflammasome activation is remains an open question to be addressed in the field and the importance the cytoskeleton may have as an additional inflammasome regulator has just begun to be uncovered.

4.5 Potential impact of the study in the context of cancer

The increasing understanding of immune mechanosensing may also provide a better insight into pathologies that are associated with alterations in tissue mechanical properties. For instance, the downregulation of the pro-inflammatory response of macrophages on substrates with higher stiffness described in this work could be relevant in the context of cancer.

Tumour-associated macrophages (TAMs) are one of the major components present in the tumour microenvironment and can represent up to 50 % of the tumour mass (Azizi et al., 2018). An elevated infiltration of this immune cell type into the primary tumour tends to correlate with poor prognosis as well as a decrease in the response to standard-of-care therapies (Jung et al., 2015; Yeung et al., 2015; Zhou et al., 2019). These macrophages, when located within the tumour stroma, tend to adopt an M2-like phenotype and perform several functions. They expose surface receptors and secrete chemokines, cytokines, growth factors and proteolytic enzymes that, on one side, favour tumour initiation and growth and, on the other, facilitate immune evasion (Lin et al., 2019). Therefore, TAMs play a dual role both as tumour promotors and immune suppressors.

Compared to their healthy tissue counterparts, primary tumours are often associated with higher tissue stiffness (Nia et al., 2020). For instance, in murine breast cancer the elastic modulus raises from an average of 0.17 kPa in a normal mammary gland to 4 kPa in mammary tumours (Paszek et al., 2005). And in human brain tumours the Young's modulus can increase from a few hundred Pa in non-cancerous tissue up to 13.5 kPa in advanced glioblastomas (Miroshnikova et al., 2016). In light of what has been reported in this and the other studies previously mentioned (Alonso-Nocelo et al., 2018; Carnicer-Lombarte et al., 2019; Chen et al., 2020; Xing et al., 2020), it could be possible that, in conjunction with soluble factors, the stiffening experienced by malignant tissues decreases the M1-like response of TAMs and induces a polarisation switch towards an M2 phenotype, promoting cancer survival and growth.

The targeting of TAMs as a therapeutic strategy is progressively attracting more attention (Xiang et al., 2021). An example of this is zoledronic acid, an agent able to reverse the phenotype of cancer macrophages from M2 to M1-like which has shown positive results against early-stage breast cancer (Gnant et al., 2011; Comito et al., 2017). Nevertheless, there are still many fundamental questions to be solved to really understand how to modulate the behaviour of these cells. Understanding the response of TAMs to mechanical cues given by the tumour microenvironment could, thus, help to refine of treatments that aim at supressing the macrophage phenotype conversion into M2 and contribute to broaden the landscape of available cancer immunotherapies.

4.6 Potential impact of the study in the context of implant design

The implant of an external device or prosthesis represents one of the clearest examples of a situation where macrophages might encounter a material with considerably different mechanical properties than their native tissue. The clinical success or failure of implants frequently depends on the inflammatory response of the body against them, which comprises a series of events known as Foreign Body Response (FBR) (Anderson et al., 2008). Briefly, following the implantation of a biomaterial proteins from the damaged tissue adsorb onto its surface and platelets accumulate and activate the complement system, forming a provisional matrix around the implant (Wilson et al., 2005). This is also thought to trigger the recruitment of innate immune cells, including neutrophils and macrophages, which initiate an acute inflammatory response (Franz et al., 2011). From this early point onwards, macrophages are essential since first they clear debris, bacterial and dead cells and, some days later, they polarise towards an M2-like phenotype and secrete signals that recruit additional cells such as fibroblasts (Klopfleisch, 2016). Once fibroblasts reach the lesion site, they proliferate and produce new ECM proteins – especially collagen – to repair the damaged tissue around the implant (Hinz, 2016). This can result in two different outcomes: either a) the new ECM integrates well with the biomaterial and supports the correct regeneration of the tissue or b) a chronic inflammation state promotes excessive deposition of ECM, which ends up encapsulating the foreign body and can potentially hinder the long-term functionality of the implant (Witherel et al., 2019; Carnicer-Lombarte et al., 2021).

In synergy with biochemical cues, other properties of the biomaterial such as geometry, stiffness, porosity or its surface topography can also affect macrophage behaviour during the FBR (Sridharan et al., 2015; Carnicer-Lombarte et al., 2021). This is of particular interest in the case of neural implants, in which the physical and mechanical mismatch often occurring between the neural tissue (which is a few hundred Pa (Sack et al., 2008; Christ et al., 2010; Elkin et al., 2010)) and the implanted device (often some orders of magnitude stiffer) seems to worsen the fibrotic response against it (Lacour et al., 2016).

One of the studies that motivated the present work, undertaken by Moshayedi et al. (2014), showed that microglia are mechanosensitive. After implanting a PAA body with two segments of differing stiffness, microglial cells became more attracted towards the stiffer 30 kPa region than towards the compliant 0.1 kPa one. Complementing this, Carnicer-Lombarte et al. (2019) characterised the influence of PAA between 0.1 and 50 kPa on fibroblasts and macrophages within the context of the FBR. When cultured *in vitro*, BMDMs adopted an M1-like gene profile on the compliant gels and an M2-like on the stiffer substrates, which is in line with the results reported in this dissertation. Importantly, when implanted both in subcutaneous and nerve injury locations, the biomaterials coated with 0.1 kPa PAA significantly reduced the fibrotic FBR. By contrast, stiffer materials presented a remarkably higher amount of fibroblasts, collagen and macrophages forming a thicker capsule around them.

In the case of implants that offer not a flat surface but a scaffold where cells can infiltrate and proliferate in all directions, the specific cell mechanoresponse to 3D environments should be considered. Despite that the behaviour of macrophages in these two situations may not be exactly the same (Friedemann et al., 2017), compared to 2D studies, not much work has been done so far using this immune cell type in a 3D context. The few respective publications point into a similar direction as this dissertation and, among them, the work done by Jiang et al. (2019) is of special relevance. They cultured BMDMs on collagen 3D scaffolds with controllable pore size and elastic modulus (E = 20, 70 and 190 kPa), observing that while cells within compliant materials adopted an M1-like phenotype and secreted higher amounts of pro-inflammatory cytokines, macrophages in their stiffest scaffolds favoured the polarisation towards M2. Moreover, when implanted subcutaneously in mice, compliant scaffolds induced a pro-inflammatory response and the stiffest material promoted a wound healing, fibrotic response, resembling *in vivo* what they had observed *in vitro*.

The described studies illustrate that minimising the mechanical mismatch between the biomaterial and native tissue may help to suppress chronic inflammation and permit regeneration, a strategy that has been extensively tested with positive results in the case of neural devices (Nguyen et al., 2014; Kolarcik et al., 2015; Lacour et al., 2016). The ongoing development of new tools and biomaterials should allow immune cell biologists to extend the knowledge obtained in the last 10 years by culturing macrophages in 2D and dissect their mechanoresponsive behaviour in 3D microenvironments. This could for example lead to the improved design of mechanically adaptive materials (Harris et al., 2011; Hess et al., 2011; Capadona et al., 2012; Ware et al., 2012) and, in the long-run, enable to better control the immune reaction against implants, increasing their long-term compatibility and functionality.

4.7 Conclusions of the study

i. RGD-coated polyacrylamide hydrogels constitute an adequate system to study the influence of substrate stiffness on macrophages.

ii. More compliant substrates upregulate the secretion of the pro-inflammatory cytokines IL-1β and IL-6 and increase the release of the pyroptotic marker LDH.

iii. Substrate stiffness modulates the formation of the NLRP3 inflammasome formation, with more compliant substrates enhancing its assembly.

iv. Actomyosin contractility may contribute to integrate the mechanical cues given by substrate stiffness into the inflammasome regulatory machinery.

MATERIALS AND METHODS

5.1 Production of polyacrylamide (PAA) hydrogels

5.1.1 Silanisation of glass coverslips

To achieve a stable and permanent bonding of polyacrylamide to the glass underneath them, hydrogels were produced on aminosilanised glass coverslips. Briefly, 13 mm round glass coverslips were washed with 0.1 M NaOH for 15 min, washed with ethanol and water and dried. They were incubated for 20 min in a solution of 0.1% (v/v) allyltrichlorosilane and 0.1% (v/v) triethylamine diluted in chloroform, washed and dried. Finally, they were covered with 0.5% glutaraldehyde for 30 min, washed and dried.

5.1.2 Polymerisation of PAA hydrogels

To obtain hydrogels with a range of different stiffness, acrylamide (AA) and N,N′-methylenebisacrylamide (BisA) were pre-mixed in different proportions. For compliant gels 5% AA and 0.07% BisA were used; for intermediate 12% AA and 0.2% BisA; and for stiff 18% AA and 0.4% BisA (all v/v and dissolved in PBS). Tetramethylethylenediamine (TEMED) was added to the pre-mixes to a final concentration of 0.3% (v/v). The mixture was degassed for 10 min.

Custom-made methylsulfone acrylate (MS) monomers were used as a thiol-reactive compound for functionalization with adhesion molecules, as recently described in Farrukh et al., 2016. The MS monomers are incorporated to the AA/BisA mix and after the gels are polymerised they can react with the thiol group present at the Cys residue of the employed adhesion peptide. This strategy enables the uncoupling of polyacrylamide stiffness from adhesion ligand density, ensuring a comparable density of peptides between different hydrogels. MS monomers were dissolved at 32 mg/ml in dimethylformamide (DMF).

To initiate the polymerisation, a final mixture 1:8 (v/v) of MS monomers and the AA/BisA pre-mixes was prepared and ammonium persulfate (APS) was added to a final concentration of 0.1% (w/v). 9.3 µl of the solution were placed between a glass coverslip and a flexible hydrophobic polyester sheet to gel for 30 min. Polymerised hydrogels were peeled off, immersed in water in a 24-well plate to swell for a minimum of 1 h, washed, UV-sterilized for 30 min and washed again. Hydrogels were functionalised with 0.5 mg/ml of cRGD-Phe-Cys diluted in ddH_2O at room temperature overnight. They were finally washed and then stored in water at 4° C for a maximum of 14 days until they were used for either mechanical characterization or cell culture.

Materials:

Substance	Working concentration	Supplier	Ref. number
NaOH	0.1 M	Sigma-Aldrich	S5881
Allyltrichlorosilane	0.1% (v/v)	Sigma-Aldrich	107778
Triethylamine	0.1% (v/v)	Sigma-Aldrich	T0886-100ML
Chloroform	99.8% (solvent)	Sigma-Aldrich	366927
Glutaraldehyde	0.5% (v/v)	Sigma-Aldrich	G6257
Polyacrylamide	see recipe table	Sigma-Aldrich	01697
Bis-acrylamide	see recipe table	Bio-Rad	1610142
APS	see recipe table	Sigma-Aldrich	A3678
TEMED	see recipe table	Sigma-Aldrich	T9281
Methylsulfone acrylate (MS)	32 mg/ml	Custom-made	-
Dimethylformamide	99.8% (solvent)	Sigma-Aldrich	227056
cRGD-Phe-Cys peptide	0.5 mg/ml	Pepnet	PCI-3686-PI

Pre-mix recipe:

Gel	Final % AA (w/v)	Final % Bis (w/v)	PBS (µl)	40 % AA (µl)	2 % Bis (µl)	TEMED (µl)
Compliant	5	0.07	4200	625	175	15
Interm.	7.5	0.2	3562	938	500	15
Stiff	18	0.4	1750	2250	1000	15

5.2 Production of polyethylenglycol-heparin (PEG-Hep) hydrogels

5.2.1 PE-MSA polymer coating of glass coverslips

To achieve a stable and permanent bonding of PEG-Heparin to the glass underneath them, the coverslips were chemically treated to create reactive groups on their surface. Briefly, 13 mm round glass coverslips were pre-cleaned by submerging them in ethanol, keeping them under ultrasonic treatment for 30 min and rinsing with ddH_2O. Then, an RCA-clean step was done, where coverslips were incubated in a solution of hydrogen peroxide, ammonium peroxide and water mixed in a 1:1:5 (v/v) manner, for 10 min at 70^o C. After rinsing with water and drying them, they were incubated for 2 h in a 9:1 (v/v) solution of 3-aminopropyltriethoxysilane in isopropanol, thoroughly rinsing with isopropanol once the time had passed. The coverslips were dried for at least 60 min at 120° C and then directly spin-coated for 30 s at 4000 rpm with a 0.15% (v/v) PE-MSA solution prepared in 1:2 acetone:tetrahydrofurane. Finally, the coated coverslips were kept in a dry environment at room temperature until used.

5.2.1 Polymerisation of PEG-Hep hydrogels

The necessary amounts of PEG, heparin, NHS and EDC were precisely weighed and dissolved in cold ddH_2O (see amounts in the recipe below). PEG solutions were kept in the ultrasonic bath to help the compound dissolve well. While always keeping the solutions in ice, the necessary volumes of NHS and EDC were added to the heparin-containing tube to start the 15 min of activation time, pipetting vigorously to mix the components well. Once the time passed, the PEG solution was added into the heparin tube, mixing it well by vortexing the tube 5 s and spinning it down. Per gel, 20 µl of this polymerising solution were quickly distributed on hydrophobic glass slides and sandwiched with the PE-MSA-coated glass coverslips. The PEG-Hep hydrogels were left polymerising overnight inside a wet chamber and the next day were peeled off and kept swelling in PBS. After 5x washes with PBS, the hydrogels were UV-sterilised for 40 min and kept at 4° C for a maximum of 14 days until used.

Materials:

Substance	Working concentration	Supplier	Ref. number
EtOH	Solvent	Sigma-Aldrich	34852-M
Hydrogen peroxyde	35 % (v/v)	Panreac AppliChem	147145.1211
Ammonium peroxide	0.1 % (v/v)	Thermo Fisher Scientific	205840100
Isopropanol	-	Thermo Fisher Scientific	10366430
3-Aminopropyltriethoxysilane (Fluka)	0.5 % (v/v)	Sigma-Aldrich	440140
Tetrahydrofuran	Solvent	Sigma-Aldrich	186562
PE-MSA (MW = 125 000)	0.15 % (w/v)	Sigma-Aldrich	188050
4arm-PEG-NH2 (MW = 1000)	see recipe table	JenKem	Custom-made
Heparin (MW = 14 000)	see recipe table	Millipore	375095
Sulfo-NHS	0.1 mg/ml	Sigma-Aldrich	56485
EDC	0.1 mg/ml	Iris Biotech	RL-1022.0250

Recipe:

PEG/Hep ratio (γ)	PEG (mg)	$H_2$0 to PEG (µl)	Heparin (mg)	$H_2$0 to Hep (µl)	EDC (mg)	$H_2$0 to EDC (µl)	NHS (mg)	$H_2$0 to NHS (µl)
1	11.67	70.00	16.33	111.98	1.79	17.89	1.01	10.13
2	16.47	70.00	11.53	100.44	2.53	25.26	1.43	14.31
3	19.09	70.00	8.91	94.14	2.93	29.28	1.66	16.58
4	20.74	70.00	7.26	90.18	3.18	31.81	1.80	18.01
5	21.88	70.00	6.13	87.45	3.35	33.55	1.90	19.00
6	22.70	70.00	5.30	85.47	3.48	34.82	1.97	19.72

5.3 Mechanical characterisation of hydrogels and macrophages

5.3.1 Characterisation of PAA and PEG-Heparin hydrogels

Hydrogels bound to the glass coverslips were mounted on a 35 mm dish using vacuum grease and covered with PBS at room temperature. The characterisation was performed with a Nanowizard 4 (JPK Instruments) using cantilevers equipped with 5 µm diameter polystyrene beads and calibrated with the thermal noise method. Gels were probed in liquid with an indentation speed of 5 µm/s and a relative force setpoint ranging from 0.6 to 8 nN to achieve comparable indentation depths of approximately 2 µm. The obtained force-distance curves were analysed using the JPK data processing software. Parts of the curves corresponding to the first 2 µm of indentation depth were fitted using the Hertz/Sneddon model for a spherical indenter and Poisson ratio of 0.5 was assumed (Hertz, 1881; Sneddon, 1965).

5.3.2 Characterisation of BMDMs on PEG-Heparin hydrogels

In the case of BMDMs on PEG-Heparin gels, a similar approach was followed. Cells were seeded at a density of approximately 50 000 cells/cm^2 on hydrogels placed in 35 mm dishes and cultured for 14 - 18 h. Culture medium was exchanged for complete CO_2-independent medium prior to the experiments and measurements were done at 37° C. The same setup, cantilever type and indenter as the ones used with hydrogels were employed. Single cells were probed in liquid with an indentation speed of 5 µm/s and a relative force setpoint of 1 nN to achieve indentation depths of approximately 1 µm. The obtained force-distance curves were also analysed using the JPK data processing software. Parts of the curves corresponding to the first 0.5 µm of indentation depth were fitted using the Hertz/Sneddon model for a spherical indenter and Poisson ratio of 0.5 was assumed (Hertz, 1881; Sneddon, 1965).

Materials:

Substance	Supplier	Ref. number
35 mm TPP cell culture dishes	Ilona Schubert Laborfachhandel	TPP93040
Arrow TL1 cantilevers	Nanoworld	ARROW-TL1-50
5 µm polystyrene beads	microParticles GmbH	PS-R-5.0

5.4 Isolation and culture of bone marrow-derived macrophages (BMDMs)

5.4.1 Production of L929-supplemented media

L929 fibroblasts secrete factors needed by bone marrow progenitor cells to differentiate into macrophages, such as M-CSF (Heap et al., 2021). In order to provide these factors to the isolated progenitors, L929-supplemented medium was produced.

L929 fibroblasts (ATCC #CCL-1) were thawed and seeded on tissue-culture grade plastic (T25) using complete basal culture media. They were incubated at 37° C and 5% CO_2 and progressively expanded. Splitting was done incubating the cells with trypsin-EDTA for 3 min and transferring them into larger flasks, first T75 and later T175. Cells were then kept in 50 ml of complete media and, to provide enough time for the fibroblasts to secrete factors, the supernatant was collected after 10 days. This enriched solution was finally filtered through a 0.22 µm pore membrane, distributed in 30 ml aliquots and frozen at -80° C.

To prepare the “macrophage complete medium” used to culture both the bone marrow progenitors and the differentiated macrophages, 20% (v/v) L929-supplemented medium was prepared by mixing 30 ml of full L929-derived medium with 120 ml of basal medium.

Formulation of the basal medium:

Substance	Final concentration	Supplier	Ref. number
DMEM + GlutaMAX	4.5 g/l glucose	Thermo Fisher Scientific	61965026
FBS	5 % (v/v)	Thermo Fisher Scientific	10270106
Penicillin / Streptomycin	100 U/ml	Thermo Fisher Scientific	15140-122
Sodium Pyruvate	1mM	Thermo Fisher Scientific	11360070

Cell culture solutions:

Substance	Supplier	Ref. number
Trypsin-EDTA (0.25%), phenol red	Thermo Fisher Scientific	25200056
Cell dissociation buffer	Thermo Fisher Scientific	13151014
1x PBS	BIOTEC media kitchen	-

5.4.2 Isolation of bone marrow progenitors and differentiation into macrophages

Bone marrow was obtained from C57BL/6J female mice with an age ranging between 16 and 24 weeks old. The rodents were purchased from Janvier Labs under (ethics approval number DD24.1-5131/396/9, Landesdirektion Sachsen) and maintained by the animal facility of the Centre for Regenerative Therapies (CRTD) of the TU Dresden.

Isolation of bone marrow progenitors was done adapting the protocols described by (Manzanero, 2012; Davis, 2013; Trouplin et al., 2013) and according to the welfare animal laws. Briefly, mice were sacrificed by cervical dislocation and their tibiae and femurs were carefully harvested. To reduce the collection of other cell types, flesh and muscle adhered to the bone surface were gently removed without breaking them. The bones were transferred to a 6-well plate containing ice-cold, sterile PBS, immersed in EtOH for 1 min and back to PBS. To extract the bone marrow, the bones were crushed in warm basal cell culture medium using a mortar and a pestle. The solution was flushed through a 0.22 µm pore filter, centrifuged at 180 x *g* for 10 min, the supernatant was discarded and the cells in the pellet were resuspended in complete macrophage medium.

Cell concentration was determined with a cell counter and $5{\cdot}10^5$ cells were seeded on sterile 10 cm petri dishes with complete macrophage medium. In this case, sterile bacterial-grade plastic dishes were used to negatively select the rest of the cell types that are not macrophages, since they cannot adhere to non-tissue culture plastic. Cultured bone marrow progenitors were incubated at 37° C and 5% CO_2, and 5 ml of fresh macrophage medium were added on days 3 and 5.

After 6 days of differentiation, between $8{\cdot}10^6$ and 10^7 mature macrophages were adhered to the surface of the dish. Old medium was removed and fresh complete medium was added every 2 days. The purity of macrophages was determined during the initial protocol optimisation via fluorescence flow cytometry. By immunolabelling the macrophage-specific markers CD11b and F4/80 it was determined that 98.8% of the cells obtained after 6 days where macrophages (Appendix Fig. A.1). Differentiated macrophages were used to perform the experiments between days 6 and 10 of culture, always using complete macrophage medium unless specified otherwise.

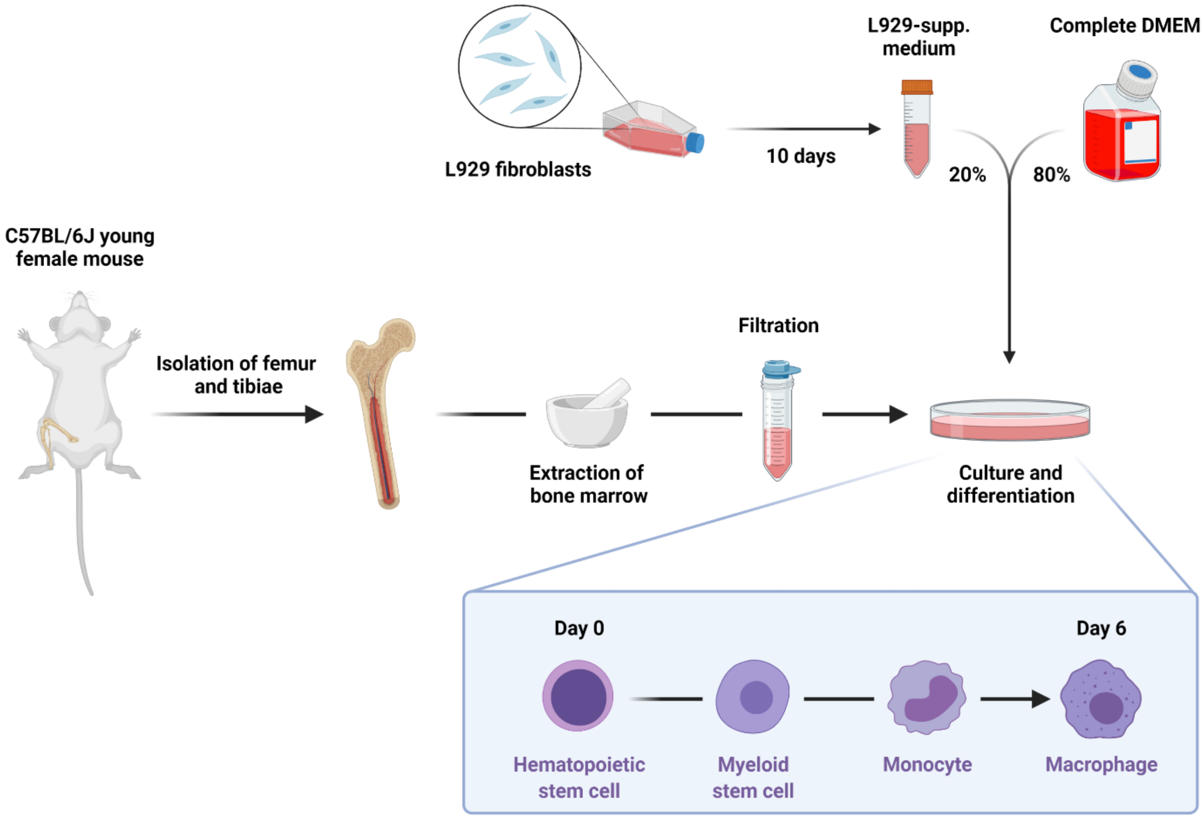
L929 fibroblasts
10 days
L929-supp.
medium
Complete DMEM
20%
80%
C57BL/6J young
female mouse
Isolation of femur
and tibiae
Extraction of
bone marrow
Filtration
Culture and
differentiation
Day 0
Day 6
Hematopoietic
stem cell
Myeloid
stem cell
Monocyte
Macrophage

Figure 5.1 | Production of bone marrow-derived macrophages. Bone marrow progenitors are isolated from murine femur and tibiae and differentiated during 6 days towards mature macrophages by culturing them with L929-supplemented medium.

5.4.3 Culture of macrophages on the hydrogels

Bone marrow-derived macrophages (BMDMs) were detached from the plastic culture dishes using cell dissociation buffer and resuspended in fresh complete macrophage medium. Cell concentration was determined using an automatic cell counter and the number of cells specified for each experimental approach was seeded onto the hydrogels placed in 24-well plates. BMDMs on gels were incubated for 14-18 h to let them adhere and spread adequately. In case further treatments were done to the cells, the hydrogels with the macrophages were transferred to new wells to get rid of the cells adhered on the border of the well.

5.4.4 Priming and stimulation of BMDMs

Macrophages were primed using 100 ng/ml ultrapure lipopolysaccharide (LPS) from *Escherichia coli* diluted in macrophage complete medium. Cells were challenged with LPS for 4.5 h for most of the experiments and for 6 h for the gene expression experiments.

After priming, LPS-containing medium was gently removed and macrophages were stimulated for 1.5 h with the ionophore nigericin (Nig) diluted at 10 µM in macrophage complete medium.

Materials:

Substance	Final concentration	Supplier	Ref. number
LPS	100 ng/ml	InvivoGen	tlrl-3pelps
Nigericin	10 µM	InvivoGen	tlrl-nig

5.4.5 Inhibition of actomyosin contractility

To interfere with actomyosin contractility, 0.06% DMSO, 10 µM blebbistatin or 10 µM Y-27632 were used. BMDMs were pre-treated with the inhibitors for 1 h, and the inhibitors were kept in the medium during the subsequent LPS priming and nigericin stimulation steps.

Materials:

Substance	Final concentration	Supplier	Ref. number
DMSO	0.06% (v/v)	Sigma-Aldrich	D2650
Blebbistatin	10 µM	Sigma-Aldrich	B0560
Y-27632	10 µM	Sigma-Aldrich	Y0503

5.5 Fluorescence confocal microscopy

To characterise the morphological features adopted by BMDMs on hydrogels of differing stiffness and determine the formation of ASC specks, fluorescence confocal microscopy was employed. Moreover, this imaging approach was also used to infer the density of adhesion ligands on cRGD-functionalised PAA hydrogels.

5.5.1 Immunocytochemistry

Cells were seeded at a density of approximately 50 000 cells/cm^2 on hydrogels placed in a 24-well plate and cultured for 14-18 h. Samples were carefully pre-washed with PBS with Mg^{2+}/Ca^{2+}, fixed using 4% paraformaldehyde (v/v in PBS 2X) for 10 min at 37° C and then washed 3 times with PBS. In the case antibody labelling was later used, samples were permeabilised with

0.2% Triton™ X-100 (v/v in PBS) for 10 minutes at room temperature and washed 3 times with PBS. Blocking was then done for 1 h with 10% goat serum, 0.1% bovine serum albumin (v/v, diluted in PBS). To visualise ASC specks, samples were incubated with anti-ASC antibody overnight at 4 °C and Alexa Fluor 488 anti-rabbit for 1 h at room temperature, washing 3 times with PBS after each antibody incubation. The same procedure was followed to immunolabel the fibronectin coating on the micropatterns, but with anti-FN and StarRED anti-mouse antibodies. Nuclei and F-actin were stained with DAPI and phalloidin-TRITC during in the same step as the secondary antibodies. Samples were stored at 4° C until imaged.

Materials:

Substance	**Final concentration**	**Supplier**	**Ref. number**
Paraformaldehyde	4% (v/v)	Thermo Fisher Scientific	28908
PBS	1X and 2X	BIOTEC media kitchen	-
PBS with Mg2+/Ca2+	1X	BIOTEC media kitchen	-
TritonX	0.2%	Sigma-Aldrich	T8787
Goat serum	10%	Abberior	005-000-121
Bovine serum albumin (BSA)	0.1%	Sigma-Aldrich	A9418
Anti-ASC; pAb (AL177)	2.5 µg/ml (1:400)	Adipogen	AG-25B-0006-C100
Alexa Fluor® 488 goat anti-rabbit IgG (H+L)	5 µg/ml (1:400)	Thermo Fisher Scientific	A11034
Anti-fibronectin HFN 7.1	1:400	Dev. Stud. Hybrid. Bank	HFN 7.1
Goat anti-Mouse IgG (H+L) - StarRED	10 µg/ml (1:200)	Thermo Fisher Scientific	A-21237
DAPI	1:2000	Cell Biolabs Inc.	112002
Phalloidin-TRITC	1:800	Sigma-Aldrich	P1951

5.5.2 Image acquisition

The fluorescence imaging of all samples was performed using confocal laser scanning microscopy. Specifically, an LSM700 (Zeiss) was used. Samples were mounted by inverting them over a #1.5 glass coverslip with a PBS drop to avoid excessive drying and imaged as follows:

i. Samples comprising PAA hydrogels coated with FITC-PEG were imaged with a 40×/1.2 objective (Zeiss). 5 regions of interest (ROIs) per hydrogel were measured, acquiring a z-stack with 5 µm steps in each ROI to image both above and below the gel surface plane.

ii. Samples containing BMDMs on hydrogels were imaged with a 20×/0.8 objective (Zeiss). Since the hydrogels were not completely flat but presented some topographical irregularities, z-stacks with 0.89 µm steps in each ROI were acquired to image the whole volume of the cells present in the field of view.

The excitation laser and detected emission range used are detailed in the following table:

Dye	Excitation laser	Detection range
DAPI (channel 1)	405 nm	400-490 nm
TRITC (channel 1)	555 nm	560-615
Alexa 488 / FITC (channel 2)	488 nm	400-555
StarRED (channel 2)	639 nm	640-720

5.5.3 Image analysis

Image post-processing and analysis were done using the software Image J/Fiji (Schindelin et al., 2012; Schneider et al., 2012) and Ilastik (Berg et al., 2019).

To determine whether the functionalisation of PAA hydrogels was similar across differing stiffness, the fluorescence signal of FITC-PEG was used as a proxy of adhesion ligand density. The hydrogel surface was manually identified and the intensity signal of 2 planes below the surface was measured.

To characterize cell morphology, cell nuclei and cell body were automatically segmented based on the intensity signal of the DNA and the F-actin labelling, respectively, and morphological parameters were extracted. Circularity was calculated as $4\pi \frac{Area}{Perimeter^2}$.

The ratio of ASC specks to cell number was determined semi-automatically. Briefly, ASC specks were quantified manually, considering only mature, clearly formed single specks, with an approximate diameter of 1 µm. Cells which presented numerous smaller yellow punctae across all the cytoplasm were not considered to have a mature formed speck and, thus, were not included in the speck count. Since pyroptosis causes the release of cytoplasmic material out of the cell, both intra- and extracellular specks were included in the analysis. Macrophages with more than one mature speck were highly rare, counted as single-specked and also included. The number of cells per image was obtained by automatically segmenting their nuclei.

5.6 Scanning electron microscopy (SEM)

SEM sample preparation was kindly done by Thomas Kurth, leader of the electron microscopy facility of the Centre for Molecular and Cellular Bioengineering (CMCB) of the TU Dresden. Samples were fixed in 1 % glutaraldehyde in 100 mM phosphate buffer for at least 2 hours at room temperature and then washed in buffer (2x) and in water (4x). They were postfixed in 1% osmium tetroxide in water, washed several times in water, dehydrated in ascending ethanol concentrations (30, 50, 70, 90, 96% ethanol, 3x 100% EtOH on molecular sieve), and critical-point-dried using the Leica CPD300 drier (Leica Microsystems). Samples were mounted on 12 mm aluminium stubs, sputtered with gold (60 mA, 60 sec) and analysed with a Jeol JSM 7500F cold field emission scanning electron microscope (Jeol Germany GmbH; acceleration voltage: 5 kV, emission: 10 µA, working distance: 8 mm, detector: lower secondary electron detector).

5.7 Gene expression analysis using quantitative real-time PCR (qRT-PCR)

Total RNA was extracted from $1.2 \cdot 10^6$ BMDMs grown on compliant or stiff gels for 14-18 h using the RNeasy Mini Kit. For this, 6 wells with $2 \cdot 10^5$ cells each were pooled for every experimental condition. For each stiffness, 6 wells were primed with lipopolysaccharide while 6 wells received no treatment.

qPCRs were kindly performed by our technical assistant, Christine Schweitzer. Reverse transcription of 1 µg RNA was performed with iScript™ Advanced cDNA Synthesis Kit, using a combination of oligo(dT) and random hexamer primers. qRT-PCR was performed at 56 °C using GoTaq qPCR Mastermix on a Stratagene cycler Mx3005P system. Several primers of pro-inflammatory genes were used (see attached table). Samples were run in duplicates and expression levels were normalized to the geometric mean of β-*actin*, *gpdh* and *m18S* rRNA controls. Relative expression values were calculated as $2^{(-\Delta\Delta CT)}$ (relative to geometric mean of housekeeping genes and plastic controls). Fold-changes can be found in Fig. A.3. For heatmaps, relative expression values were normalised to values between 0 and 100% for each gene. Heatmaps were generated in R (R Core Team, 2020).

Materials:

Substance	Supplier	Ref. number
RNeasy Mini Qit	Qiagen	74104
iScript™ Advanced cDNA Synthesis Kit	Bio-Rad	1725037
GoTaq qPCR Mastermix	Promega	6002

Primers:

Oligo name	**Primer sequence (5' --> 3') FWD**	**Primer sequence (5' --> 3') REV**	**Concentrated stock**	**Working stock**	**Species**
mACTB	GATCAAGATCATTGCTCCTCCTG	CGCAGCTCAGTAACAGTCCG	100 µM	3 µM	*Mus musculus*
mGAPDH	GTTGTCTCCTGCGACTTCA	GGTGGTCCAGGGTTTCTTA	100 µM	3 µM	*Mus musculus*
m18SrRNA	AGAAACGGCTACCACATCCAA	GGGTCGGGAGTGGGTAATTT	100 µM	3 µM	*Mus musculus*
mTLR2	CGCCCTTTAAGCTGTGTCTC	CGTCAAAGAGCCTGAAGTGG	100 µM	3 µM	*Mus musculus*
mTLR4	CCAACATCATCCAGGAAGGC	GGACTTCTCAACCTTCTCAAG	100 µM	3 µM	*Mus musculus*
mCXCL2	GCCTGAAGACCCTGCCAAG	AACCAGGGGGGCTTCAGGG	100 µM	3 µM	*Mus musculus*
mTNFa	ACGCTCTTCTGTCTACTGAAC	TTGTCTTTGAGATCCATGCC	100 µM	3 µM	*Mus musculus*
mIL1b	GATCCCAAGCAATACCCAAAG	CTTTGTGCTCTGCTTGTGAGG	100 µM	3 µM	*Mus musculus*
mNOS2	GCAGCACTTGGATCAGGAAC	ACCATCTCCTGCATTTCTTCC	100 µM	3 µM	*Mus musculus*
mIL6	AGCCAGAGTCCTTCAGAGAG	GTCCTTAGCCACTCCTTCTG	100 µM	3 µM	*Mus musculus*
mCXCL9	CTGTTCTTTTCCTCTTGGGCA	GGCAGGTTTGATCTCCGTTC	100 µM	3 µM	*Mus musculus*

5.8 Cytokine quantification assays

To quantify the amount of the inflammatory proteins IL-6 and IL-1ꞵ secreted by macrophages cultured on different substrates, we made use of enzyme-linked immunosorbent assays (ELISAs).

BMDMs were seeded at a density of approximately 100 000 cells/cm^2 (2·10^5 in a 24-well plate). Supernatants from cell cultures were collected after LPS priming (for IL-6) and after nigericin stimulation (for IL-1ꞵ) and dead cells removed by centrifugation. All the samples were stored at -80° C until ELISAs were performed.

Commercial sandwich ELISA kits were employed and assays were done following the manufacturer's instructions. Briefly, 96-well plates were coated with capture antibody overnight at 4° C. Blocking solution was applied for 1 h at room temperature and samples and standard protein to generate a standard curve were loaded into the wells and incubated overnight at 4° C. The next day, the detection antibody was applied for 1 h at room temperature to create a sandwich. Then, the wells are incubated with Avidin-HRP for 30 min at room temperature, which binds to the detection antibody. To detect the presence of the target molecule, TMB solution was pipetted into the wells for 15 min at room temperature and a stop solution made of 2N H_2SO_4 was finally added. The plate was transferred to a plate-compatible spectrophotometer (TECAN Infinite Pro) and absorbance at 450 nm was recorded, subtracting the 570 nm signal from it.

Materials:

Substance	Supplier	Ref. number
IL-6 Mouse Uncoated ELISA Kit	Thermo Fisher	88-7064-88
IL-1β Mouse Uncoated ELISA Kit	Thermo Fisher	88-7013-88

5.9 Cell viability assay

To assess the impact of substrate stiffness on nigericin-induced pyroptosis, the levels of lactate hydrogenase (LDH) in the cell culture medium were used as a proxy of cell death. LDH is a soluble cytosolic enzyme that is released into the supernatant upon the loss of integrity of the plasma membrane. LDH activity was measured using the LDH-Glo™ Cytotoxicity assay according to the manufacturer's instructions. In this assay, LDH catalyses the first of a series of reactions that leads to the production of luminescence.

For this assay, BMDMs were also cultured at density of approximately 100 000 cells/cm^2 (2·10^5 in a 24-well plate). After priming and stimulation, 5 µl of cell culture medium were collected and diluted 1:200 in LDH storage buffer, being kept at -80° C until assays were performed.

To measure LDH activity, samples were mixed 1:1 with LDH detection reagent, which contains the necessary enzyme mix and reductase substrate to perform the assay. Bioluminescence was recorded with a GloMax™ 96 microplate luminometer (Promega). Total amount of cells was inferred by lysing cells with Triton™ X-100 at the end of the experiments and comparing the signal values to the ones of an included standard curve.

Materials:

Substance	Supplier	Ref. number
LDH-Glo Cytotoxicity assay	Promega	J2380

5.10 Culture of BMDMs on micropatterns

Micropatterned glass slides were purchased from the company 4Dcell. These had a diameter of 22 mm and a thickness of #1.5, and they were compatible to be used for fluorescence confocal imaging. The glass slides consisted of different areas with adhesion disks of a specific diameter ranging from 10 to 100 µm and non-adherent surface was passivated with PEG.

Prior to seeding the cells, the slides were incubated with 1 mg/ml fibronectin for 1 h at room temperature. To create a comparable substrate where macrophage spreading was not constrained, the same was done with regular sterile glass coverslips. Afterwards, all the slides were cleaned with sterile water and transferred to 6-well plates. BMDMs were seeded at an approximate density of 10 400 cells/cm^2 (10^5 in a 6-well plate) and incubated overnight. The next day, unattached cells were gently washed out before the start of the experiment.

5.11 Optical diffraction tomography (ODT)

ODT experiments were performed together with Dr. Kyoohyun Kim. BMDMs were seeded at a density of approximately 25 000 cells/cm^2 on 35-mm glass-bottom dishes the day prior to the measurements. The day of the experiment, cells were primed with 200 ng/ml LPS for 3 h. Afterwards, culture medium was exchanged for complete CO_2-independent medium and samples were transferred to the acquisition setup, where they were kept at 37° C with a petri dish heater during all the procedure. Several regions of interest (ROIs) with 2-3 cells were selected and initial tomograms were acquired. To induce pyroptosis, a solution containing nigericin was added to achieve a final concentration of 10 µM. Tomograms were acquired every 10 min in each of the ROIs up to 90 min.

Formulation of the CO_2-independent medium:

Substance	Final concentration	Supplier	Ref. number
CO_2-indep. DMEM	4.5 g/l glucose	Thermo Fisher Scientific	18045054
FBS	5 % (v/v)	Thermo Fisher Scientific	10270106
Penicillin / Streptomycin	100 U/ml	Thermo Fisher Scientific	15140-122
Sodium Pyruvate	1mM	Thermo Fisher Scientific	11360070
GlutaMAX	100 mM	Thermo Fisher Scientific	35050061

5.11.1 Optical setup

The three-dimensional (3D) refractive index (RI) distribution of macrophages was reconstructed by optical diffraction tomography (ODT). The detailed optical setup was described previously (Kim and Guck, 2020). Briefly, ODT employs Mach-Zehnder interferometry to measure multiple complex optical fields from various incident angles. A laser beam (λ = 532 nm, frequency-doubled Nd-YAG laser, Torus, Laser Quantum Inc.) was coupled into an optical fibre and divided into two paths using a 2 × 2 single-mode fibre-optic coupler (TW560R2F2, Thorlabs). One beam was used as a reference beam and the other beam passed through a tube lens (f = 175 mm) and a water-dipping objective lens (NA = 1.0, 40×, Carl Zeiss AG) to illuminate the sample on the stage of a home-built inverted microscope. The beam diffracted by the sample was collected with a high numerical aperture objective lens (NA = 1.2, 63×, oil immersion, Carl Zeiss AG) and a tube lens (f = 200 mm). To reconstruct a 3D RI tomogram of the sample, the sample was illuminated from 150 different incident angles scanned by a dual-axis galvano-mirror (GVS012/M, Thorlabs Inc.) located in the conjugate plane of the sample. The diffracted beam interfered with the reference beam at an image plane, and generated a spatially modulated hologram, which was recorded with a CCD camera (FL3-U3-13Y3M-C, FLIR Systems, Inc.). The total magnification of the setup was 57×, and the field-of-view (FOV) of the camera covers 86.2 μm × 86.2 μm.

5.11.2 Tomogram reconstruction and quantitative analysis

The complex optical fields of light scattered by the samples were retrieved from the recorded holograms by applying a Fourier transform-based field retrieval algorithm (Cuche et al., 2000). The 3D RI distribution of macrophages was reconstructed from the retrieved complex optical fields via the Fourier diffraction theorem, employing the first-order Rytov approximation (Wolf, 1969; Sung et al., 2009). A more detailed description of tomogram reconstruction can be found elsewhere (Kim et al., 2013).

On the reconstructed tomograms, Otsu's thresholding method (Otsu, 1979) was used to segment the region occupied by the macrophages from the background and vacuoles inside cells, and quantitative analysis was performed to calculate mean RI value in the individual BMDMs. The mass density of the cells was directly calculated from the mean RI value, since the RI value in biological samples, $n(x,y,z)$, is linearly proportional to the mass density of the material, $\rho(x,y,z)$, as $n(x,y,z) = n_m + \alpha\rho(x,y,z)$, where nm is the RI value of the surrounding medium and α is the RI increment (dn/dc) with $\alpha = 0.190$ ml/g for proteins and nucleic acids (Zhao et al., 2011; Zangle and Teitell, 2014). The RI of the medium was measured using an Abbe refractometer (2WAJ, Arcarda GmbH).

5.12 Statistical analysis and data visualisation

Statistical tests are indicated in each plot. Linear mixed model analysis was performed using R (R Core Team, 2020) and the rest of statistical analyses were performed using GraphPad Prism 6 (GraphPad Software). All data are presented as mean ± SEM unless specified. In all cases, p values 0.05 were considered statistically significant (ns, not significant; * $p < 0.05$; ** $p < 0.01$; *** $p < 0.001$; **** $p < 0.0001$).

Most data was plotted using GraphPad Prism 6 and heatmaps were produced using R. Figures were prepared with Adobe Illustrator CC 2015 (Adobe) and diagrams were done with BioRender.

APPENDIX

Figure A.1 | Characterisation of macrophage purity after differentiation from murine bone marrow progenitors.

Bone marrow-derived macrophages differentiated for 6 days were immunolabelled with CD11b-APC and F4/80-FITC and their relative quantities assessed via fluorescence cytometry. The quadrant corresponding to double-positive cells (Q2) indicate that a BMDM purity of 98.8% was achieved. Data was obtained from one independent experiment.

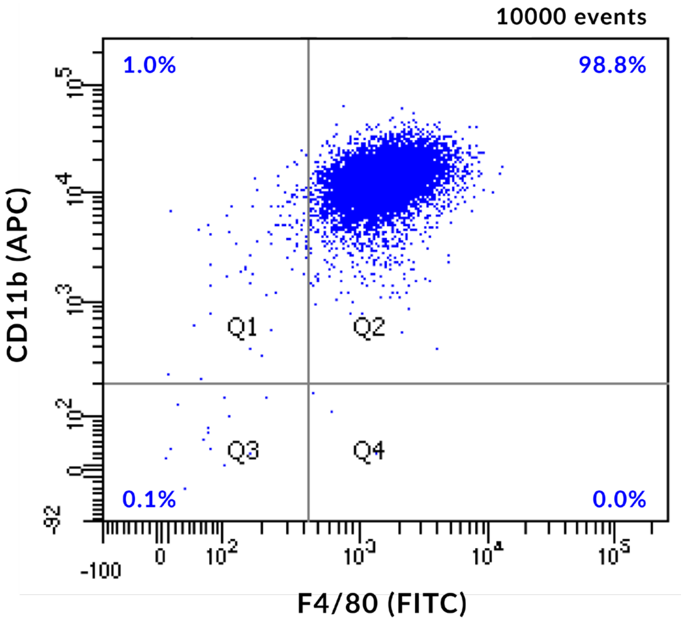

Figure A.2 | Influence of PEG-Hep substrate stiffness on the mechanical properties of macrophages.

Young's moduli of BMDMs cultured for 14-18 h on PEG-Hep hydrogels of 4.0 kPa (compliant) and 40.0 kPa (stiff) determined by AFM. Each dot represents a cell and black bars indicate mean ± SEM. The number of analysed cells was 134 for the compliant gels and 172 for the stiff substrates. Data was obtained from one independent experiment with two different samples per condition. Statistical analysis was performed using a Mann-Whitney test. **** $p < 0.0001$.

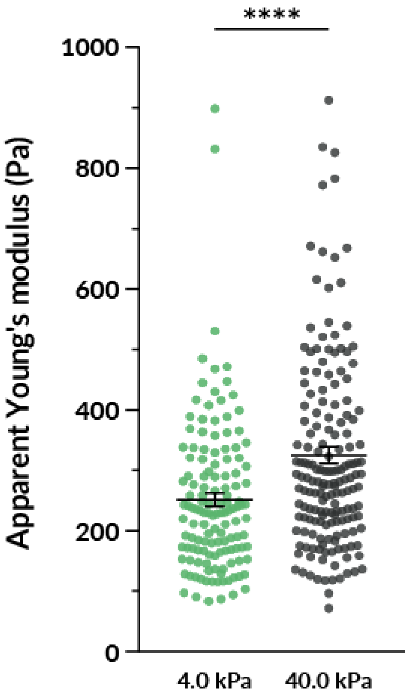

Figure A.3 | Relative gene expression levels of pro-inflammatory genes in non-treated macrophages and in primed cells.

BMDMs were cultured on PAA hydrogels for 14-18 h and treated with 100 ng/ml of LPS for 6 h. Three independent experiments were conducted with cells from three different mice. Triplicates were done in each experiment. Relative expression was calculated as 2(-$^{\Delta\Delta}$CT) (relative to the geometric mean of housekeeping genes β-*actin*, *Gapdh* and *18S rRNA* and plastic controls. Mean ± SEM are shown and each dot represents an independent experiment. Statistical analysis was performed using a t-test. ** $p < 0.01$.

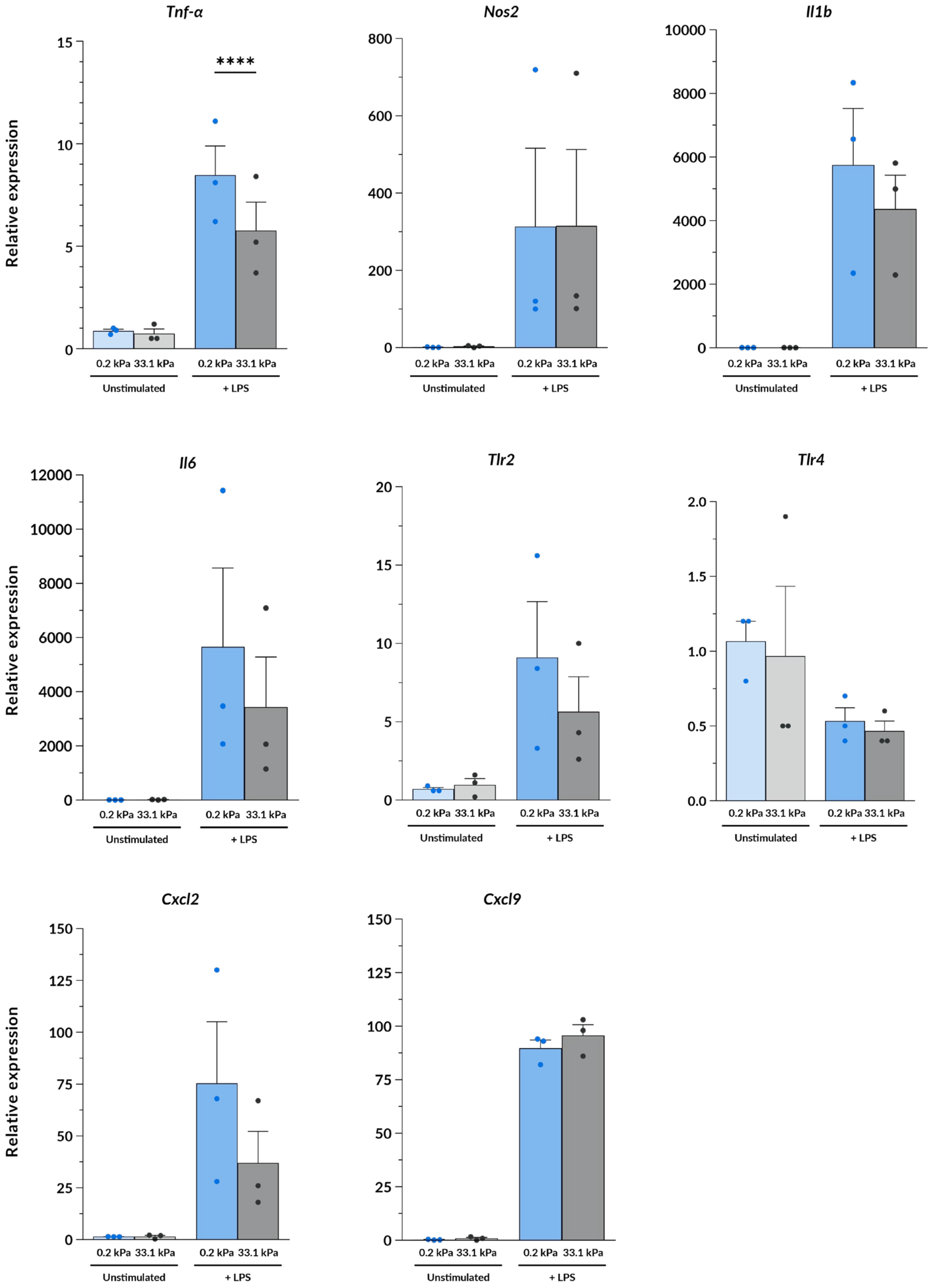

Fig. A.4 | Refractive index changes during macrophage pyroptosis.

Pharmacologically-stimulated macrophages were measured by optical diffraction tomography (ODT). This technique enables to reconstruct the 3D refractive index of cells, a parameter which in biological samples is linearly proportional to the mass density of the material (Zhao et al., 2011; Zangle and Teitell, 2014). (A) Representative time course refractive index images of BMDMs cultured on TCP, primed with 200 ng/ml LPS for 3 h and stimulated with 10 µM nigericin. Time indicates the minutes after nigericin addition. Scale bar is 20 µm. (B) Refractive index (RI) contrast, volume and dry mass normalised values extracted from the images as taken in (A). Mean ± SD are indicated. In total, 18 cells were analysed from different samples measured within one experiment.

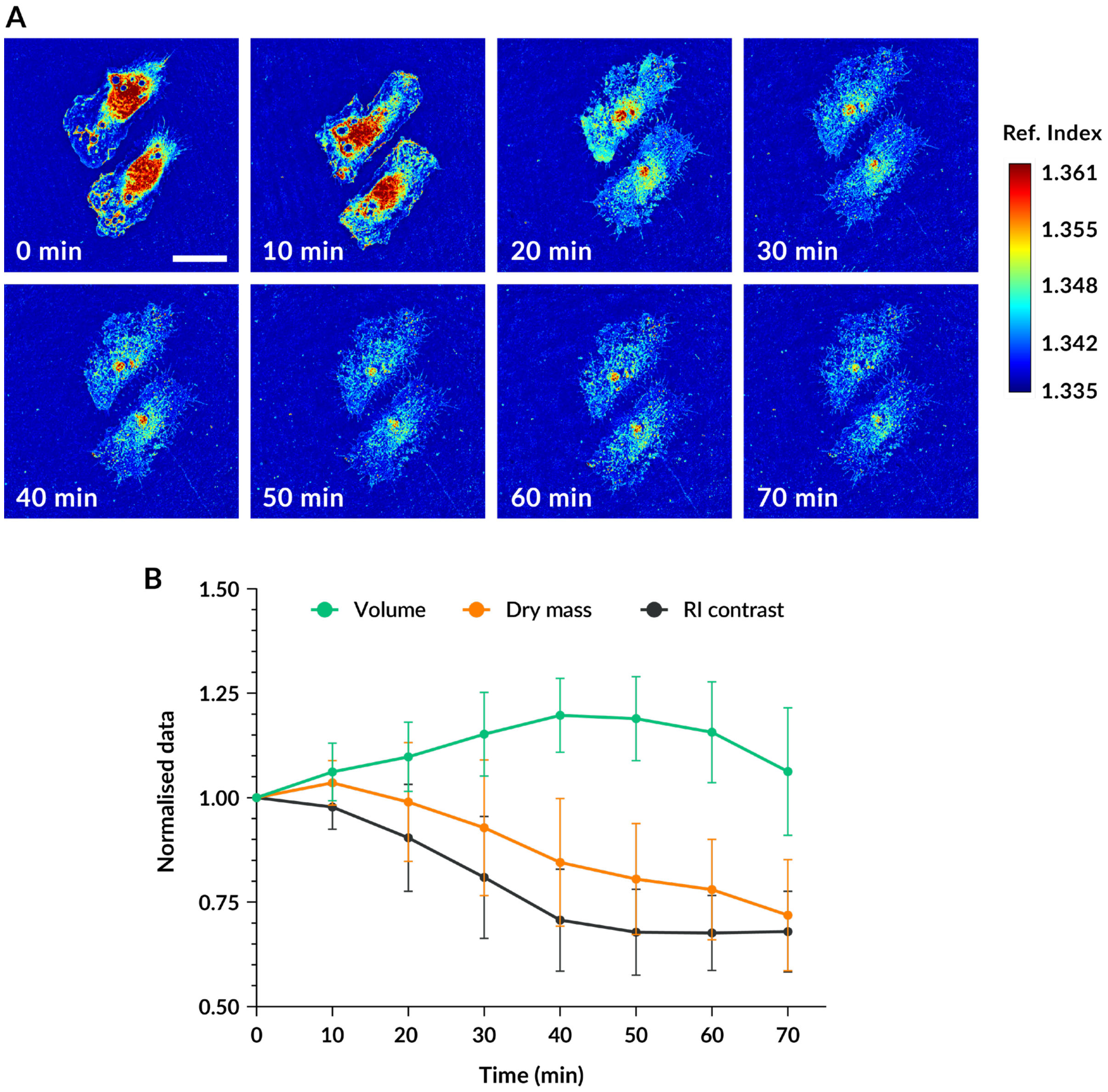

Fig. A.5 | Quantification of intra- and extracellular ASC specks upon macrophage stimulation on PAA hydrogels.

(A) Percentage of intra- and extracellular ASC specks relative to cell number. (B) Percentage of intra- and extracellular specks relative to the total speck number. Data corresponds to one of the independent experiments with 3 replicates per condition included in Fig. 3.14.

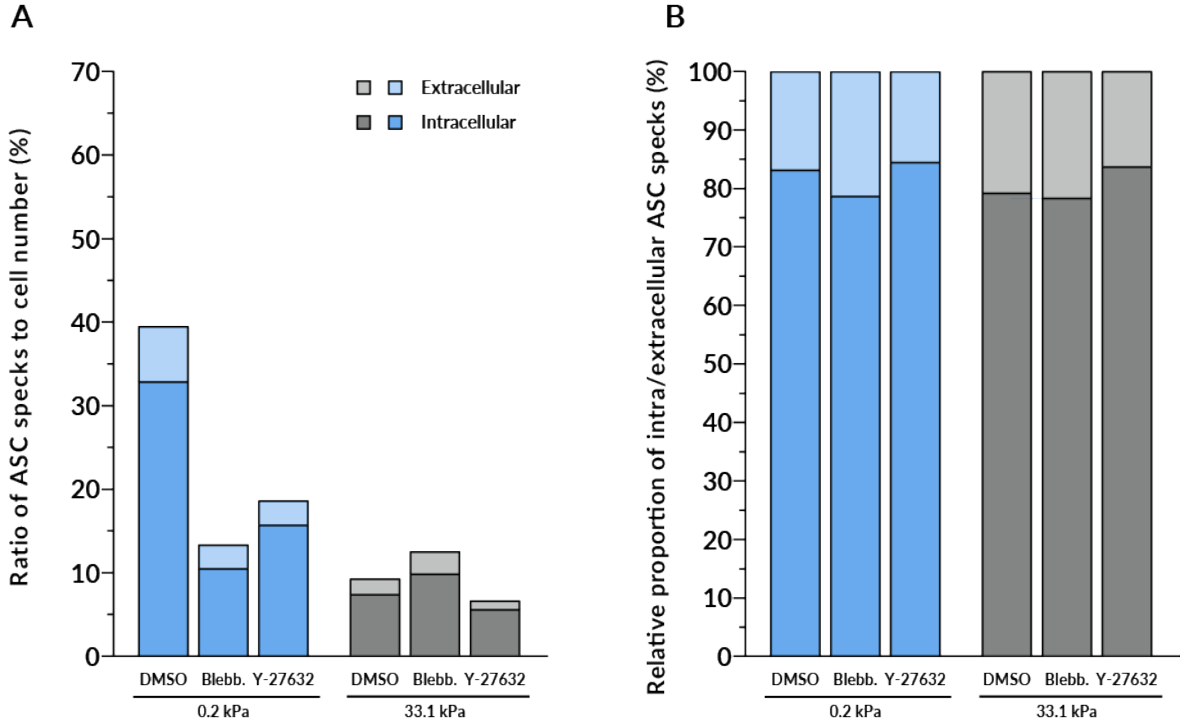

LIST OF ACRONYMS AND ABBREVIATIONS

AFM	Atomic force microscopy
AIM2	Absent-in-melanoma 2
APCs	Antigen-presenting cells
ASC	Apoptosis-associated speck-like protein containing a CARD
BCR	B cell receptor
BMDMs	Bone marrow-derived macrophages
CAPS	Cryopyrin-associated autoinflammatory diseases
CARD	Caspase activation and recruitment domain
CD14	Cluster of differentiation 14
CNS	Central nervous system
COVID-19	Coronavirus disease 2019
CTL	Cytotoxic T lymphocyte
CXCL	C-X-C motif 1 ligand
DAMPs	Damage-associated molecular patterns
DAPI	4′,6-diamidino-2-phenylindole
DCs	Dendritic cells
DMSO	Dimethyl sulfoxide
ECM	Extracellular matrix
ELISA	Enzyme-linked immunosorbent assay
EHD2	EH domain containing 2
F-actin	Actin filaments
FAK	Focal adhesion kinase
F-BAR	Fes/Cip4 homology Bin/amphiphysin/Rvs domain
FBR	Foreign Body Response
FBS	Fetal bovine serum
FITC	Fluorescein isothiocyanate
GSDMD	Gasdermin D
HDAC6	Histone deacetylase 6
HSCs	Hematopoietic stem cells
IL	Interleukin
IFN	Interferon

INM	Inner nuclear membrane
IRF3	Interferon regulatory factor 3
KASH	Klarsicht, ANC-1, Syne homology domain
LDH	Lactate dehydrogenase
LBP	LPS-binding protein
LIMK	LIM domain kinase
LINC	Linker of nucleoskeleton and cytoskeleton
LPS	Lipopolysaccharide
LRRs	Leucine-rich repeats
M0	Naïve macrophages
M1	Pro-inflammatory or classically-activated macrophages
M2	Anti-inflammatory or alternatively-activated macrophages
MD-2	Myeloid Differentiation factor 2
MHC	Major histocompatibility complex
MLC	Myosin light chain
MSC	Mechanosensitive ion channel
MSU	Monosodium urate crystals
MTOC	Microtubule-organising centre
MyDD88	Myeloid differentiation primary response 88
N	Newton
NACHT	Domain present in NAIP, CIITA, HET-E and TP1
NEK7	NIMA-related kinase 7
NF-κB	Nuclear factor kappa-light-chain-enhancer of activated B cells
NLR	NOD-like receptor
NLRC4	NLR family CARD domain containing 4
NLRP1	NLR family pyrin domain containing 1
NLRP3	NLR family pyrin domain containing 3
NEK7	NIMA Related Kinase 7
NOD	Nucleotide-binding oligomerisation domain
NOS2	Nitric oxide synthase 2
NPC	Nuclear pore complex
ONM	Outer nuclear membrane
P2X7R	Purinergic Receptor P2X 7

Pa	Pascal
PAA	Polyacrylamide
PAMPs	Pathogen-associated molecular patterns
PBS	Phosphate buffer saline
PEG-Hep	Poly(ethylene glycol)-Heparin
PFA	Paraformaldehyde
PDL	Poly-D-Lysine
PRRs	Pattern recognition receptors
PTMs	Post-translational modifications
PYD	Pyrin domain
RGD	Arginine-glycine-aspartate
ROCK	Rho-associated protein kinase
ROS	Reactive oxygen species
RT-DC	Real-time deformability cytometry
RT-PCR	Real-time polymerase chain reaction
SARS-CoV-2	Severe acute respiratory syndrome coronavirus 2
SRC	Proto-oncogene
SUN	Sad1p, UNC-84 protein
TAM	Tumour-associated macrophage
TAZ	Tafazzin
TCR	T cell receptor
TEAD	TEA domain transcription factor
TLR	Toll-like receptor
TNF-α	Tumour necrosis factor alfa
TRAAK	TWIK-related arachidonic acid activated K^+ channel
TREK	TWIK-related K^+ channel
TRIF	TIR-domain-containing adapter-inducing interferon-β
TRITC	Tetramethylrhodamine
TRP	Transient receptor potential channel
SD	Standard deviation
SEM	Standard error of the mean / Scanning electron microscopy
YAP	Yes-associated protein 1

LIST OF FIGURES

Figure 1.1 | Macrophage origin and self-renewal. 2

Figure 1.2 | Control of NLRP3 inflammasome formation. 7

Figure 1.3 | Forces in immune cell locomotion and CTL killing.................................... 11

Figure 1.4 | Forces involved during phagocytic target internalisation. 12

Figure 1.5 | Leukocyte rolling on blood and lymphatic vessels.................................... 13

Figure 1.6 | Force transmission along the ECM – integrin – adaptor protein – F-actin axis. 16

Figure 1.7 | Control of actomyosin activity by RhoA signalling. 18

Figure 1.8 | Podosome architecture.. 19

Figure 1.9 | YAP/TAZ mechanotransduction signalling... 20

Figure 1.10 | Nuclear components involved in nuclear mechanotransduction. 22

Figure 1.11 | Response of caveolae to membrane tension and compression. 24

Figure 3.1 | PAA gels are a suitable biomaterial to investigate macrophage mechanosensing. 31

Figure 3.2 | Macrophages are compatible with PAA gels. 32

Figure 3.3 | Macrophages on compliant substrates become smaller and rounder. 33

Figure 3.4 | PEG-Heparin hydrogels as an alternative hydrogel substrate. 34

Figure 3.5 | BMDMs on stiffer PEG-Hep hydrogels become more spread. 35

Figure 3.6 | Substrate stiffness induces changes in membrane morphology. 37

Figure 3.7 | Stiffness-induced morphological differences persist after macrophage lps priming.. 39

Figure 3.8 | Modifying substrate stiffness does not significantly influence macrophage pro-inflammatory gene expression. 40

Figure 3.9 | Macrophages secrete higher levels of the cytokines IL-6 and IL-1β on compliant substrates........ 41

Figure 3.10 | Nigericin-induced macrophage pyroptosis increases on compliant substrates........ 43

Figure 3.11 | NLRP3 inflammasome formation is enhanced on hydrogels of lower stiffness. 45

Figure 3.12 | Limiting cell spreading does not recapitulate the differences induced by stiffness on inflammasome formation........ 47

Figure 3.13 | Interfering with ROCK activity induces a decrease in macrophage spreading area. 49

Figure 3.14 | Inhibiting myosin diminishes the differences induced by stiffness on inflammasome formation. 50

Figure 5.1 | Production of bone marrow-derived macrophages. 69

Figure A.1 | Characterisation of macrophage purity after differentiation from murine bone marrow progenitors........ 79

Figure A.2 | Influence of PEG-Hep substrate stiffness on the mechanical properties of macrophages. 80

Figure A.3 | Relative gene expression levels of pro-inflammatory genes in non-treated macrophages and in primed cells........ 81

Figure A.4 | Refractive index changes during macrophage pyroptosis........ 82

Figure A.5 | Quantification of intra- and extracellular asc specks upon macrophage stimulation on PAA hydrogels. 83

BIBLIOGRAPHY

Adlerz, K. M., Aranda-Espinoza, H., and Hayenga, H. N. (2016). Substrate elasticity regulates the behavior of human monocyte-derived macrophages. Eur Biophys J, 301–309. doi:10.1007/s00249-015-1096-8.

Afonina, I. S., Müller, C., Martin, S. J., and Beyaert, R. (2015). Proteolytic Processing of Interleukin-1 Family Cytokines: Variations on a Common Theme. Immunity 42, 991–1004. doi:10.1016/j.immuni.2015.06.003.

Agostini, L., Martinon, F., Burns, K., McDermott, M. F., Hawkins, P. N., and Tschopp, J. (2004). NALP3 Forms an IL-1β-Processing Inflammasome with Increased Activity in Muckle-Wells Autoinflammatory Disorder. Immunity 20, 319–325. doi:10.1016/S1074-7613(04)00046-9.

Akira, S., and Takeda, K. (2004). Toll-like receptor signalling. Nat. Rev. Immunol. 4, 499–511. doi:10.1038/nri1391.

Alehashemi, S., and Goldbach-Mansky, R. (2020). Human Autoinflammatory Diseases Mediated by NLRP3-, Pyrin-, NLRP1-, and NLRC4-Inflammasome Dysregulation Updates on Diagnosis, Treatment, and the Respective Roles of IL-1 and IL-18. Front. Immunol. 11. doi:10.3389/fimmu.2020.01840.

Alert, R., Casademunt, J., Brugués, J., and Sens, P. (2015). Model for Probing Membrane-Cortex Adhesion by Micropipette Aspiration and Fluctuation Spectroscopy. Biophys. J. 108, 1878–1886. doi:10.1016/j.bpj.2015.02.027.

Alon, R., and Ley, K. (2008). Cells on the run: shear-regulated integrin activation in leukocyte rolling and arrest on endothelial cells. Curr. Opin. Cell Biol. 20, 525–532. doi:10.1016/j.ceb.2008.04.003.

Alonso-Nocelo, M., Raimondo, T. M., Vining, K. H., López-López, R., Fuente, M. de la, and Mooney, D. J. (2018). Matrix stiffness and tumor-associated macrophages modulate epithelial to mesenchymal transition of human adenocarcinoma cells. Biofabrication 10, 035004. doi:10.1088/1758-5090/aaafbc.

Alqahtani, M. S., Syed, R., and Alshehri, M. (2020). Size-Dependent Phagocytic Uptake and Immunogenicity of Gliadin Nanoparticles. Polymers 12, 2576. doi:10.3390/polym12112576.

Amano, M., Ito, M., Kimura, K., Fukata, Y., Chihara, K., Nakano, T., et al. (1996). Phosphorylation and Activation of Myosin by Rho-associated Kinase (Rho-kinase)*. J. Biol. Chem. 271, 20246–20249. doi:10.1074/jbc.271.34.20246.

Anand, P. K., Malireddi, R. K. S., and Kanneganti, T.-D. (2011). Role of the Nlrp3 Inflammasome in Microbial Infection. Front. Microbiol. 2. doi:10.3389/fmicb.2011.00012.

Anderson, J. M., Rodriguez, A., and Chang, D. T. (2008). Foreign body reaction to biomaterials. Semin. Immunol. 20, 86–100. doi:10.1016/j.smim.2007.11.004.

Anselmo, A. C., Zhang, M., Kumar, S., Vogus, D. R., Menegatti, S., Helgeson, M. E., et al. (2015). Elasticity of Nanoparticles Influences Their Blood Circulation, Phagocytosis, Endocytosis, and Targeting. ACS Nano 9, 3169–3177. doi:10.1021/acsnano.5b00147.

Arani, A., Murphy, M. C., Glaser, K. J., Manduca, A., Lake, D. S., Kruse, S. A., et al. (2015). Measuring the effects of aging and sex on regional brain stiffness with MR elastography in healthy older adults. NeuroImage 111, 59–64. doi:10.1016/j.neuroimage.2015.02.016.

Azizi, E., Carr, A. J., Plitas, G., Cornish, A. E., Konopacki, C., Prabhakaran, S., et al. (2018). Single-Cell Map of Diverse Immune Phenotypes in the Breast Tumor Microenvironment. Cell 174, 1293-1308.e36. doi:10.1016/j.cell.2018.05.060.

Barriga, E. H., Franze, K., Charras, G., and Mayor, R. (2018). Tissue stiffening coordinates morphogenesis by triggering collective cell migration in vivo. Nature 554, 523–527. doi:10.1038/nature25742.

Barton, G. M., and Medzhitov, R. (2003). Toll-Like Receptor Signaling Pathways. Science 300, 1524–1525. doi:10.1126/science.1085536.

Basu, R., Whitlock, B. M., Husson, J., Le Floc'h, A., Jin, W., Oyler-Yaniv, A., et al. (2016). Cytotoxic T Cells Use Mechanical Force to Potentiate Target Cell Killing. Cell 165, 100–110. doi:10.1016/j.cell.2016.01.021.

Bateman, G., Hill, B., Knight, R., and Boucher, D. (2021). Great balls of fire: activation and signalling of inflammatory caspases. Biochem. Soc. Trans. doi:10.1042/BST20200986.

Bauernfeind, F. G., Horvath, G., Stutz, A., Alnemri, E. S., MacDonald, K., Speert, D., et al. (2009). Cutting Edge: NF-κB Activating Pattern Recognition and Cytokine Receptors License NLRP3 Inflammasome Activation by Regulating NLRP3 Expression. J. Immunol. 183, 787–791. doi:10.4049/jimmunol.0901363.

Beilharz, M., De Nardo, D., Latz, E., and Franklin, B. S. (2016). "Measuring NLR Oligomerization II: Detection of ASC Speck Formation by Confocal Microscopy and Immunofluorescence," in NLR Proteins, eds. F. Di Virgilio and P. Pelegrín (New York, NY: Springer New York), 145–158. doi:10.1007/978-1-4939-3566-6_9.

Bellis, S. L. (2011). Advantages of RGD peptides for directing cell association with biomaterials. Biomaterials 32, 4205–4210. doi:10.1016/j.biomaterials.2011.02.029.

Beningo, K. A., and Wang, Y. (2002). Fc-receptor-mediated phagocytosis is regulated by mechanical properties of the target. J. Cell Sci. 115, 849–856.

Berg, S., Kutra, D., Kroeger, T., Straehle, C. N., Kausler, B. X., Haubold, C., et al. (2019). ilastik: interactive machine learning for (bio)image analysis. Nat. Methods 16, 1226–1232. doi:10.1038/s41592-019-0582-9.

Bhuwania, R., Cornfine, S., Fang, Z., Krüger, M., Luna, E. J., and Linder, S. (2012). Supervillin couples myosin-dependent contractility to podosomes and enables their turnover. J. Cell Sci. 125, 2300–2314. doi:10.1242/jcs.100032.

Blakney, A., Swartzlander, M., and Bryant, S. (2012). The effects of substrate stiffness on the in vitro activation of macrophages and in vivo host response to poly(ethylene glycol)-based hydrogels. J Biomed Mater Res A 100, 12. doi:10.1002/jbm.a.34104.

Bonnans, C., Chou, J., and Werb, Z. (2014). Remodelling the extracellular matrix in development and disease. Nat. Rev. Mol. Cell Biol. 15, 786–801. doi:10.1038/nrm3904.

Bonneh-Barkay, D., and Wiley, C. A. (2009). Brain Extracellular Matrix in Neurodegeneration. Brain Pathol. 19, 573–585. doi:10.1111/j.1750-3639.2008.00195.x.

Booth, A. J., Hadley, R., Cornett, A. M., Dreffs, A. A., Matthes, S. A., Tsui, J. L., et al. (2012). Acellular Normal and Fibrotic Human Lung Matrices as a Culture System for In Vitro Investigation. Am. J. Respir. Crit. Care Med. 186, 866–876. doi:10.1164/rccm.201204-0754OC.

Brodin, P. (2021). Immune determinants of COVID-19 disease presentation and severity. Nat. Med. 27, 6.

Burgdorf, S., Kautz, A., Bohnert, V., Knolle, P. A., and Kurts, C. (2007). Distinct Pathways of Antigen Uptake and Intracellular Routing in CD4 and CD8 T Cell Activation. Science 316, 612–616. doi:10.1126/science.1137971.

Burgdorf, S., and Kurts, C. (2008). Endocytosis mechanisms and the cell biology of antigen presentation. Curr. Opin. Immunol. 20, 89–95. doi:10.1016/j.coi.2007.12.002.

Burger, D., Fickentscher, C., de Moerloose, P., and Brandt, K. J. (2016). F-actin dampens NLRP3 inflammasome activity via Flightless-I and LRRFIP2. Sci. Rep. 6, 29834. doi:10.1038/srep29834.

Buxboim, A., Rajagopal, K., Brown, A. E. X., and Discher, D. E. (2010). How deeply cells feel: methods for thin gels. J. Phys. Condens. Matter 22, 194116. doi:10.1088/0953-8984/22/19/194116.

Cahalan, S. M., Lukacs, V., Ranade, S. S., Chien, S., Bandell, M., and Patapoutian, A. (2015). Piezo1 links mechanical forces to red blood cell volume. eLife 4, e07370. doi:10.7554/eLife.07370.

Caliari, S. R., and Burdick, J. A. (2016). A practical guide to hydrogels for cell culture. Nat. Methods 13, 405–414. doi:10.1038/nmeth.3839.

Cannon, G. J., and Swanson, J. A. (1992). The macrophage capacity for phagocytosis. J. Cell Sci. 101 (Pt 4), 907–913.

Capadona, J. R., Tyler, D. J., Zorman, C. A., Rowan, S. J., and Weder, C. (2012). Mechanically adaptive nanocomposites for neural interfacing. MRS Bull. 37, 581–589. doi:10.1557/mrs.2012.97.

Carnicer-Lombarte, A., Barone, D. G., Dimov, I. B., Hamilton, R. S., Prater, M., Zhao, X., et al. (2019). Mechanical matching of implant to host minimises foreign body reaction. bioRxiv, 829648. doi:10.1101/829648.

Carnicer-Lombarte, A., Chen, S.-T., Malliaras, G. G., and Barone, D. G. (2021). Foreign Body Reaction to Implanted Biomaterials and Its Impact in Nerve Neuroprosthetics. Front. Bioeng. Biotechnol. 9. doi:10.3389/fbioe.2021.622524.

Cezar, C. A., Roche, E. T., Vandenburgh, H. H., Duda, G. N., Walsh, C. J., and Mooney, D. J. (2016). Biologic-free mechanically induced muscle regeneration. Proc. Natl. Acad. Sci. 113, 1534–1539. doi:10.1073/pnas.1517517113.

Champion, J. A., and Mitragotri, S. (2006). Role of target geometry in phagocytosis. Proc. Natl. Acad. Sci. 103, 4930–4934. doi:10.1073/pnas.0600997103.

Chan, C. E., and Odde, D. J. (2008). Traction Dynamics of Filopodia on Compliant Substrates. Science 322, 1687–1691. doi:10.1126/science.1163595.

Chang, W., Worman, H. J., and Gundersen, G. G. (2015). Accessorizing and anchoring the LINC complex for multifunctionality. J. Cell Biol. 208, 11–22. doi:10.1083/jcb.201409047.

Changede, R., Xu, X., Margadant, F., and Sheetz, M. P. (2015). Nascent Integrin Adhesions Form on All Matrix Rigidities after Integrin Activation. Dev. Cell 35, 614–621. doi:10.1016/j.devcel.2015.11.001.

Chen, J., and Chen, Z. J. (2018). PtdIns4P on dispersed trans-Golgi network mediates NLRP3 inflammasome activation. Nature 564, 71–76. doi:10.1038/s41586-018-0761-3.

Chen, M., Zhang, Y., Zhou, P., Liu, X., Zhao, H., Zhou, X., et al. (2020). Substrate stiffness modulates bone marrow-derived macrophage polarization through NF-κB signaling pathway. Bioact. Mater. 5, 880–890. doi:10.1016/j.bioactmat.2020.05.004.

Chichili, G. R., and Rodgers, W. (2009). Cytoskeleton–membrane interactions in membrane raft structure. Cell. Mol. Life Sci. 66, 2319–2328. doi:10.1007/s00018-009-0022-6.

Christ, A. F., Franze, K., Gautier, H., Moshayedi, P., Fawcett, J., Franklin, R. J. M., et al. (2010). Mechanical difference between white and gray matter in the rat cerebellum measured by scanning force microscopy. J. Biomech. 43, 2986–2992. doi:10.1016/j.jbiomech.2010.07.002.

Comito, G., Segura, C. P., Taddei, M. L., Lanciotti, M., Serni, S., Morandi, A., et al. (2017). Zoledronic acid impairs stromal reactivity by inhibiting M2-macrophages polarization and prostate cancer-associated fibroblasts. Oncotarget 8, 118–132. doi:10.18632/oncotarget.9497.

Cox, C. D., Bae, C., Ziegler, L., Hartley, S., Nikolova-Krstevski, V., Rohde, P. R., et al. (2016). Removal of the mechanoprotective influence of the cytoskeleton reveals PIEZO1 is gated by bilayer tension. Nat. Commun. 7, 10366. doi:10.1038/ncomms10366.

Cuche, E., Marquet, P., and Depeursinge, C. (2000). Spatial filtering for zero-order and twin-image elimination in digital off-axis holography. Appl. Opt. 39, 4070–4075. doi:10.1364/AO.39.004070.

Dahl, K. N., Kahn, S. M., Wilson, K. L., and Discher, D. E. (2004). The nuclear envelope lamina network has elasticity and a compressibility limit suggestive of a molecular shock absorber. J. Cell Sci. 117, 4779–4786. doi:10.1242/jcs.01357.

Das, D. K., Feng, Y., Mallis, R. J., Li, X., Keskin, D. B., Hussey, R. E., et al. (2015). Force-dependent transition in the T-cell receptor β-subunit allosterically regulates peptide discrimination and pMHC bond lifetime. Proc. Natl. Acad. Sci. 112, 1517–1522.

Davis, B. K. (2013). "Isolation, Culture, and Functional Evaluation of Bone Marrow-Derived Macrophages," in Mouse Models of Innate Immunity, ed. I. C. Allen (Totowa, NJ: Humana Press), 27–35. doi:10.1007/978-1-62703-481-4_3.

de Leeuw, R., Gruenbaum, Y., and Medalia, O. (2018). Nuclear Lamins: Thin Filaments with Major Functions. Trends Cell Biol. 28, 34–45. doi:10.1016/j.tcb.2017.08.004.

de Vasconcelos, N. M., Van Opdenbosch, N., Van Gorp, H., Parthoens, E., and Lamkanfi, M. (2019). Single-cell analysis of pyroptosis dynamics reveals conserved GSDMD-mediated subcellular events that precede plasma membrane rupture. Cell Death Differ. 26, 146–161. doi:10.1038/s41418-018-0106-7.

Del Pozo, M. A., Lolo, F.-N., and Echarri, A. (2021). Caveolae: Mechanosensing and mechanotransduction devices linking membrane trafficking to mechanoadaptation. Curr. Opin. Cell Biol. 68, 113–123. doi:10.1016/j.ceb.2020.10.008.

dos Santos, G., Rogel, M. R., Baker, M. A., Troken, J. R., Urich, D., Morales-Nebreda, L., et al. (2015). Vimentin regulates activation of the NLRP3 inflammasome. Nat. Commun. 6, 6574. doi:10.1038/ncomms7574.

Dostert, C., Pétrilli, V., Bruggen, R. V., Steele, C., Mossman, B. T., and Tschopp, J. (2008). Innate Immune Activation Through Nalp3 Inflammasome Sensing of Asbestos and Silica. Science 320, 674–677. doi:10.1126/science.1156995.

Dumbauld, D. W., Shin, H., Gallant, N. D., Michael, K. E., Radhakrishna, H., and García, A. J. (2010). Contractility modulates cell adhesion strengthening through focal adhesion kinase and assembly of vinculin-containing focal adhesions. J. Cell. Physiol. 223, 746–756. doi:10.1002/jcp.22084.

Dupont, S., Morsut, L., Aragona, M., Enzo, E., Giulitti, S., Cordenonsi, M., et al. (2011). Role of YAP/TAZ in mechanotransduction. Nature 474, 179–183. doi:10.1038/nature10137.

Echarri, A., and Del Pozo, M. A. (2015). Caveolae – mechanosensitive membrane invaginations linked to actin filaments. J. Cell Sci. 128, 2747–2758. doi:10.1242/jcs.153940.

Ekpenyong, A. E., Toepfner, N., Fiddler, C., Herbig, M., Li, W., Cojoc, G., et al. (2017). Mechanical deformation induces depolarization of neutrophils. Sci. Adv. 3, e1602536. doi:10.1126/sciadv.1602536.

Elkin, B. S., Ilankovan, A., and Morrison, B. (2010). Age-Dependent Regional Mechanical Properties of the Rat Hippocampus and Cortex. J. Biomech. Eng. 132, 011010. doi:10.1115/1.4000164.

Elosegui-Artola, A., Andreu, I., Beedle, A. E. M., Lezamiz, A., Uroz, M., Kosmalska, A. J., et al. (2017). Force Triggers YAP Nuclear Entry by Regulating Transport across Nuclear Pores. Cell 171, 1397-1410.e14. doi:10.1016/j.cell.2017.10.008.

Elosegui-Artola, A., Oria, R., Chen, Y., Kosmalska, A., Pérez-González, C., Castro, N., et al. (2016). Mechanical regulation of a molecular clutch defines force transmission and transduction in response to matrix rigidity. Nat. Cell Biol. 18, 540–548. doi:10.1038/ncb3336.

Elosegui-Artola, A., Trepat, X., and Roca-Cusachs, P. (2018). Control of Mechanotransduction by Molecular Clutch Dynamics. Trends Cell Biol. 28, 356–367. doi:10.1016/j.tcb.2018.01.008.

Emon, B., Bauer, J., Jain, Y., Jung, B., and Saif, T. (2018). Biophysics of Tumor Microenvironment and Cancer Metastasis - A Mini Review. Comput. Struct. Biotechnol. J. 16, 279–287. doi:10.1016/j.csbj.2018.07.003.

Escolano, J.-C., Taubenberger, A. V., Abuhattum, S., Schweitzer, C., Farrukh, A., del Campo, A., et al. (2021). Compliant Substrates Enhance Macrophage Cytokine Release and NLRP3 Inflammasome Formation During Their Pro-Inflammatory Response. Front. Cell Dev. Biol. 9, 639815. doi:10.3389/fcell.2021.639815.

Esser, N., L'homme, L., De Roover, A., Kohnen, L., Scheen, A. J., Moutschen, M., et al. (2013). Obesity phenotype is related to NLRP3 inflammasome activity and immunological profile of visceral adipose tissue. Diabetologia 56, 2487–2497. doi:10.1007/s00125-013-3023-9.

Evavold, C. L., Ruan, J., Tan, Y., Xia, S., Wu, H., and Kagan, J. C. (2018). The Pore-Forming Protein Gasdermin D Regulates Interleukin-1 Secretion from Living Macrophages. Immunity 48, 35-44.e6. doi:10.1016/j.immuni.2017.11.013.

Fang, X.-Z., Zhou, T., Xu, J.-Q., Wang, Y.-X., Sun, M.-M., He, Y.-J., et al. (2021). Structure, kinetic properties and biological function of mechanosensitive Piezo channels. Cell Biosci. 11, 13. doi:10.1186/s13578-020-00522-z.

Farrukh, A., Paez, J. I., Salierno, M., and del Campo, A. (2016). Bioconjugating Thiols to Poly(acrylamide) Gels for Cell Culture Using Methylsulfonyl Co-monomers. Angew. Chem. Int. Ed. 55, 2092–2096. doi:10.1002/anie.201509986.

Finger, E. B., Purl, K. D., Alon, R., Lawrence, M. B., von Andrian, U. H., and Springer, T. A. (1996). Adhesion through L-selectin requires a threshold hydrodynamic shear. Nature 379, 266–269. doi:10.1038/379266a0.

Franchi, L., Eigenbrod, T., and Núñez, G. (2009). Cutting Edge: TNF-α Mediates Sensitization to ATP and Silica via the NLRP3 Inflammasome in the Absence of Microbial Stimulation. J. Immunol. 183, 792–796. doi:10.4049/jimmunol.0900173.

Franchi, L., Kanneganti, T.-D., Dubyak, G. R., and Núñez, G. (2007). Differential Requirement of P2X7 Receptor and Intracellular K+ for Caspase-1 Activation Induced by Intracellular and Extracellular Bacteria*. J. Biol. Chem. 282, 18810–18818. doi:10.1074/jbc.M610762200.

Franklin, B. S., Bossaller, L., De Nardo, D., Ratter, J. M., Stutz, A., Engels, G., et al. (2014). The adaptor ASC has extracellular and "prionoid" activities that propagate inflammation. Nat. Immunol. 15, 727–737. doi:10.1038/ni.2913.

Franz, S., Rammelt, S., Scharnweber, D., and Simon, J. C. (2011). Immune responses to implants – A review of the implications for the design of immunomodulatory biomaterials. Biomaterials 32, 6692–6709. doi:10.1016/j.biomaterials.2011.05.078.

Franze, K., Janmey, P. A., and Guck, J. (2013). Mechanics in Neuronal Development and Repair. Annu. Rev. Biomed. Eng. 15, 227–251. doi:10.1146/annurev-bioeng-071811-150045.

Freeman, S. A., and Grinstein, S. (2014). Phagocytosis: receptors, signal integration, and the cytoskeleton. Immunol. Rev. 262, 193–215. doi:10.1111/imr.12212.

Freudenberg, U., Hermann, A., Welzel, P. B., Stirl, K., Schwarz, S. C., Grimmer, M., et al. (2009). A star-PEG–heparin hydrogel platform to aid cell replacement therapies for neurodegenerative diseases. Biomaterials 30, 5049–5060. doi:10.1016/j.biomaterials.2009.06.002.

Friedemann, M., Kalbitzer, L., Franz, S., Moeller, S., Schnabelrauch, M., Simon, J.-C., et al. (2017). Instructing Human Macrophage Polarization by Stiffness and Glycosaminoglycan Functionalization in 3D Collagen Networks. Adv. Healthc. Mater. 6, 1600967. doi:10.1002/adhm.201600967.

Fritzsche, M. (2021). What Is the Right Mechanical Readout for Understanding the Mechanobiology of the Immune Response? Front. Cell Dev. Biol. 9. doi:10.3389/fcell.2021.612539.

Galbraith, C. G., Yamada, K. M., and Sheetz, M. P. (2002). The relationship between force and focal complex development. J. Cell Biol. 159, 695–705. doi:10.1083/jcb.200204153.

Gaudino, S. J., and Kumar, P. (2019). Cross-Talk Between Antigen Presenting Cells and T Cells Impacts Intestinal Homeostasis, Bacterial Infections, and Tumorigenesis. Front. Immunol. 10, 360. doi:10.3389/fimmu.2019.00360.

Gautier, E. L., Shay, T., Miller, J., Greter, M., Jakubzick, C., Ivanov, S., et al. (2012). Gene-expression profiles and transcriptional regulatory pathways that underlie the identity and diversity of mouse tissue macrophages. Nat. Immunol. 13, 1118–1128. doi:10.1038/ni.2419.

Gawden-Bone, C., Zhou, Z., King, E., Prescott, A., Watts, C., and Lucocq, J. (2010). Dendritic cell podosomes are protrusive and invade the extracellular matrix using metalloproteinase MMP-14. J. Cell Sci. 123, 1427–1437. doi:10.1242/jcs.056515.

Ge, J., Li, W., Zhao, Q., Li, N., Chen, M., Zhi, P., et al. (2015). Architecture of the mammalian mechanosensitive Piezo1 channel. Nature 527, 64–69. doi:10.1038/nature15247.

Geiger, B., and Yamada, K. M. (2011). Molecular Architecture and Function of Matrix Adhesions. Cold Spring Harb. Perspect. Biol. 3, a005033. doi:10.1101/cshperspect.a005033.

Gervásio, O. L., Phillips, W. D., Cole, L., and Allen, D. G. (2011). Caveolae respond to cell stretch and contribute to stretch-induced signaling. J. Cell Sci. 124, 3581–3590. doi:10.1242/jcs.084376.

Ginhoux, F., Greter, M., Leboeuf, M., Nandi, S., See, P., Gokhan, S., et al. (2010). Fate Mapping Analysis Reveals That Adult Microglia Derive from Primitive Macrophages. Science 330, 841–845. doi:10.1126/science.1194637.

Ginhoux, F., and Jung, S. (2014). Monocytes and macrophages: developmental pathways and tissue homeostasis. Nat. Rev. Immunol. 14, 392–404. doi:10.1038/nri3671.

Gnant, M., Mlineritsch, B., Stoeger, H., Luschin-Ebengreuth, G., Heck, D., Menzel, C., et al. (2011). Adjuvant endocrine therapy plus zoledronic acid in premenopausal women with early-stage breast cancer: 62-month follow-up from the ABCSG-12 randomised trial. Lancet Oncol. 12, 631–641. doi:10.1016/S1470-2045(11)70122-X.

Golani, G., Ariotti, N., Parton, R. G., and Kozlov, M. M. (2019). Membrane Curvature and Tension Control the Formation and Collapse of Caveolar Superstructures. Dev. Cell 48, 523-538.e4. doi:10.1016/j.devcel.2018.12.005.

Gordon, S. (2016). Phagocytosis: An Immunobiologic Process. Immunity 44, 463–475. doi:10.1016/j.immuni.2016.02.026.

Gordon, S., and Martinez-Pomares, L. (2017). Physiological roles of macrophages. Pflüg. Arch. - Eur. J. Physiol. 469, 365–374. doi:10.1007/s00424-017-1945-7.

Gordon, S., Plüddemann, A., and Martinez Estrada, F. (2014). Macrophage heterogeneity in tissues: phenotypic diversity and functions. Immunol. Rev. 262, 36–55. doi:10.1111/imr.12223.

Green, J. P., Yu, S., Martín-Sánchez, F., Pelegrin, P., Lopez-Castejon, G., Lawrence, C. B., et al. (2018). Chloride regulates dynamic NLRP3-dependent ASC oligomerization and inflammasome priming. Proc. Natl. Acad. Sci. 115, E9371–E9380.

Gruber, E., Heyward, C., Cameron, J., and Leifer, C. (2018). Toll-like receptor signaling in macrophages is regulated by extracellular substrate stiffness and Rho-associated coiled-coil kinase (ROCK1/2). Int. Immunol. 30, 267–278. doi:10.1093/intimm/dxy027.

Guimarães, C. F., Gasperini, L., Marques, A. P., and Reis, R. L. (2020). The stiffness of living tissues and its implications for tissue engineering. Nat. Rev. Mater. doi:10.1038/s41578-019-0169-1.

Hamilton, C., and Anand, P. K. (2019). Right place, right time: localisation and assembly of the NLRP3 inflammasome. F1000Research 8, 676. doi:10.12688/f1000research.18557.1.

Handorf, A. M., Zhou, Y., Halanski, M. A., and Li, W.-J. (2015). Tissue Stiffness Dictates Development, Homeostasis, and Disease Progression. Organogenesis 11, 1–15. doi:10.1080/15476278.2015.1019687.

Harr, J. C., Luperchio, T. R., Wong, X., Cohen, E., Wheelan, S. J., and Reddy, K. L. (2015). Directed targeting of chromatin to the nuclear lamina is mediated by chromatin state and A-type lamins. J. Cell Biol. 208, 33–52. doi:10.1083/jcb.201405110.

Harris, J. P., Capadona, J. R., Miller, R. H., Healy, B. C., Shanmuganathan, K., Rowan, S. J., et al. (2011). Mechanically adaptive intracortical implants improve the proximity of neuronal cell bodies. J. Neural Eng. 8, 066011. doi:10.1088/1741-2560/8/6/066011.

Hashimoto, D., Chow, A., Noizat, C., Teo, P., Beasley, M. B., Leboeuf, M., et al. (2013). Tissue-Resident Macrophages Self-Maintain Locally throughout Adult Life with Minimal Contribution from Circulating Monocytes. Immunity 38, 792–804. doi:10.1016/j.immuni.2013.04.004.

Hayakawa, K., Tatsumi, H., and Sokabe, M. (2011). Actin filaments function as a tension sensor by tension-dependent binding of cofilin to the filament. J. Cell Biol. 195, 721–727. doi:10.1083/jcb.201102039.

He, L., Si, G., Huang, J., Samuel, A. D. T., and Perrimon, N. (2018). Mechanical regulation of stem-cell differentiation by the stretch-activated Piezo channel. Nature 555, 103–106. doi:10.1038/nature25744.

He, W., Wan, H., Hu, L., Chen, P., Wang, X., Huang, Z., et al. (2015). Gasdermin D is an executor of pyroptosis and required for interleukin-1β secretion. Cell Res. 25, 1285–1298. doi:10.1038/cr.2015.139.

Heap, R. E., Marín-Rubio, J. L., Peltier, J., Heunis, T., Dannoura, A., Moore, A., et al. (2021). Proteomics characterisation of the L929 cell supernatant and its role in BMDM differentiation. Life Sci. Alliance 4. doi:10.26508/lsa.202000957.

Heneka, M. T., Kummer, M. P., Stutz, A., Delekate, A., Schwartz, S., Vieira-Saecker, A., et al. (2013). NLRP3 is activated in Alzheimer's disease and contributes to pathology in APP/PS1 mice. Nature 493, 674–678. doi:10.1038/nature11729.

Heng, B. C., Zhang, X., Aubel, D., Bai, Y., Li, X., Wei, Y., et al. (2021). An overview of signaling pathways regulating YAP/TAZ activity. Cell. Mol. Life Sci. 78, 497–512. doi:10.1007/s00018-020-03579-8.

Herant, M., Heinrich, V., and Dembo, M. (2006). Mechanics of neutrophil phagocytosis: experiments and quantitative models. J. Cell Sci. 119, 1903–1913. doi:10.1242/jcs.02876.

Herant, M., Lee, C.-Y., Dembo, M., and Heinrich, V. (2011). Protrusive Push versus Enveloping Embrace: Computational Model of Phagocytosis Predicts Key Regulatory Role of Cytoskeletal Membrane Anchors. PLOS Comput. Biol. 7, e1001068. doi:10.1371/journal.pcbi.1001068.

Hess, A. E., Capadona, J. R., Shanmuganathan, K., Hsu, L., Rowan, S. J., Weder, C., et al. (2011). Development of a stimuli-responsive polymer nanocomposite toward biologically optimized, MEMS-based neural probes. J. Micromechanics Microengineering 21, 054009. doi:10.1088/0960-1317/21/5/054009.

Hind, L. E., Dembo, M., and Hammer, D. A. (2015). Macrophage motility is driven by frontal-towing with a force magnitude dependent on substrate stiffness. Integr. Biol. 7, 447–453. doi:10.1039/c4ib00260a.

Hind, L. E., Lurier, E. B., Dembo, M., Spiller, K. L., and Hammer, D. A. (2016). Effect of M1–M2 Polarization on the Motility and Traction Stresses of Primary Human Macrophages. Cell. Mol. Bioeng. 9, 455–465. doi:10.1007/s12195-016-0435-x.

Hinz, B. (2016). The role of myofibroblasts in wound healing. Curr. Res. Transl. Med. 64, 171–177. doi:10.1016/j.retram.2016.09.003.

Hirata, H., Tatsumi, H., Lim, C. T., and Sokabe, M. (2014). Force-dependent vinculin binding to talin in live cells: a crucial step in anchoring the actin cytoskeleton to focal adhesions. Am. J. Physiol.-Cell Physiol. 306, C607–C620. doi:10.1152/ajpcell.00122.2013.

Hodge, R. G., and Ridley, A. J. (2016). Regulating Rho GTPases and their regulators. Nat. Rev. Mol. Cell Biol. 17, 496–510. doi:10.1038/nrm.2016.67.

Honda, K., Takaoka, A., and Taniguchi, T. (2006). Type I Inteferon Gene Induction by the Interferon Regulatory Factor Family of Transcription Factors. Immunity 25, 349–360. doi:10.1016/j.immuni.2006.08.009.

Hornung, V., Bauernfeind, F., Halle, A., Samstad, E. O., Kono, H., Rock, K. L., et al. (2008). Silica crystals and aluminum salts activate the NALP3 inflammasome through phagosomal destabilization. Nat. Immunol. 9, 847–856. doi:10.1038/ni.1631.

Horton, E. R., Astudillo, P., Humphries, M. J., and Humphries, J. D. (2016a). Mechanosensitivity of integrin adhesion complexes: role of the consensus adhesome. Exp. Cell Res. 343, 7–13. doi:10.1016/j.yexcr.2015.10.025.

Horton, E. R., Byron, A., Askari, J. A., Ng, D. H. J., Millon-Frémillon, A., Robertson, J., et al. (2015). Definition of a consensus integrin adhesome and its dynamics during adhesion complex assembly and disassembly. Nat. Cell Biol. 17, 1577–1587. doi:10.1038/ncb3257.

Horton, E. R., Humphries, J. D., James, J., Jones, M. C., Askari, J. A., and Humphries, M. J. (2016b). The integrin adhesome network at a glance. J. Cell Sci. 129, 4159–4163. doi:10.1242/jcs.192054.

Horváth, Á. I., Gyimesi, M., Várkuti, B. H., Képiró, M., Szegvári, G., Lőrincz, I., et al. (2020). Effect of allosteric inhibition of non-muscle myosin 2 on its intracellular diffusion. Sci. Rep. 10, 13341. doi:10.1038/s41598-020-69853-8.

Hsieh, J. Y., Keating, M. T., Smith, T. D., Meli, V. S., Botvinick, E. L., and Liu, W. F. (2019). Matrix crosslinking enhances macrophage adhesion, migration, and inflammatory activation. APL Bioeng. 3, 016103. doi:10.1063/1.5067301.

Huang, C., Wang, Y., Li, X., Ren, L., Zhao, J., Hu, Y., et al. (2020). Clinical features of patients infected with 2019 novel coronavirus in Wuhan, China. The Lancet 395, 497–506. doi:10.1016/S0140-6736(20)30183-5.

Hui, Y., Yi, X., Wibowo, D., Yang, G., Middelberg, A. P. J., Gao, H., et al. (2020). Nanoparticle elasticity regulates phagocytosis and cancer cell uptake. Sci. Adv. 6, eaaz4316. doi:10.1126/sciadv.aaz4316.

Humphries, J. D., Byron, A., and Humphries, M. J. (2006). Integrin ligands at a glance. J. Cell Sci. 119, 3901–3903. doi:10.1242/jcs.03098.

Humphries, J. D., Chastney, M. R., Askari, J. A., and Humphries, M. J. (2019). Signal transduction via integrin adhesion complexes. Curr. Opin. Cell Biol. 56, 14–21. doi:10.1016/j.ceb.2018.08.004.

Huse, M. (2017). Mechanical forces in the immune system. Nat. Rev. Immunol. 17, 679–690. doi:10.1038/nri.2017.74.

Ip, W. K. E., and Medzhitov, R. (2015). Macrophages monitor tissue osmolarity and induce inflammatory response through NLRP3 and NLRC4 inflammasome activation. Nat. Commun. 6, 6931. doi:10.1038/ncomms7931.

Iskratsch, T., Wolfenson, H., and Sheetz, M. P. (2014). Appreciating force and shape — the rise of mechanotransduction in cell biology. Nat. Rev. Mol. Cell Biol. 15, 825–833. doi:10.1038/nrm3903.

Ivanovska, I. L., Swift, J., Spinler, K., Dingal, D., Cho, S., and Discher, D. E. (2017). Cross-linked matrix rigidity and soluble retinoids synergize in nuclear lamina regulation of stem cell differentiation. Mol. Biol. Cell 28, 2010–2022. doi:10.1091/mbc.e17-01-0010.

Jahed, Z., Soheilypour, M., Peyro, M., and Mofrad, M. R. K. (2016). The LINC and NPC relationship – it's complicated! J. Cell Sci. 129, 3219–3229. doi:10.1242/jcs.184184.

Jain, N., and Vogel, V. (2018). Spatial confinement downsizes the inflammatory response of macrophages. Nat. Mater. 17, 1134–1144. doi:10.1038/s41563-018-0190-6.

Jakubzick, C., Gautier, E. L., Gibbings, S. L., Sojka, D. K., Schlitzer, A., Johnson, T. E., et al. (2013). Minimal Differentiation of Classical Monocytes as They Survey Steady-State Tissues and Transport Antigen to Lymph Nodes. Immunity 39, 599–610. doi:10.1016/j.immuni.2013.08.007.

Janmey, P. A., Fletcher, D. A., and Reinhart-King, C. A. (2020). Stiffness Sensing by Cells. Physiol. Rev. 100, 695–724. doi:10.1152/physrev.00013.2019.

Jansen, K. A., Atherton, P., and Ballestrem, C. (2017). Mechanotransduction at the cell-matrix interface. Semin. Cell Dev. Biol. 71, 75–83. doi:10.1016/j.semcdb.2017.07.027.

Jaumouillé, V., Cartagena-Rivera, A. X., and Waterman, C. M. (2019). Coupling of β 2 integrins to actin by a mechanosensitive molecular clutch drives complement receptor-mediated phagocytosis. Nat. Cell Biol. 21, 1357–1369. doi:10.1038/s41556-019-0414-2.

Jaumouillé, V., and Waterman, C. M. (2020). Physical Constraints and Forces Involved in Phagocytosis. Front. Immunol. 11. doi:10.3389/fimmu.2020.01097.

Jiang, S., Lyu, C., Zhao, P., Li, W., Kong, W., Huang, C., et al. (2019). Cryoprotectant enables structural control of porous scaffolds for exploration of cellular mechano-responsiveness in 3D. Nat. Commun. 10, 3491. doi:10.1038/s41467-019-11397-1.

Jin, P., Jan, L. Y., and Jan, Y.-N. (2020). Mechanosensitive Ion Channels: Structural Features Relevant to Mechanotransduction Mechanisms. Annu. Rev. Neurosci. 43, 207–229. doi:10.1146/annurev-neuro-070918-050509.

Jo, J., Abdi Nansa, S., and Kim, D.-H. (2020). Molecular Regulators of Cellular Mechanoadaptation at Cell–Material Interfaces. Front. Bioeng. Biotechnol. 0. doi:10.3389/fbioe.2020.608569.

Jung, K. Y., Cho, S. W., Kim, Y. A., Kim, D., Oh, B.-C., Park, D. J., et al. (2015). Cancers with Higher Density of Tumor-Associated Macrophages Were Associated with Poor Survival Rates. J. Pathol. Transl. Med. 49, 318–324. doi:10.4132/jptm.2015.06.01.

Katsnelson, M. A., Rucker, L. G., Russo, H. M., and Dubyak, G. R. (2015). K+ Efflux Agonists Induce NLRP3 Inflammasome Activation Independently of Ca2+ Signaling. J. Immunol. 194, 3937–3952. doi:10.4049/jimmunol.1402658.

Kaufmann, S. H. E. (2008). Immunology's foundation: the 100-year anniversary of the Nobel Prize to Paul Ehrlich and Elie Metchnikoff. Nat. Immunol. 9, 705–712. doi:10.1038/ni0708-705.

Kawai, T., and Akira, S. (2010). The role of pattern-recognition receptors in innate immunity: update on Toll-like receptors. Nat. Immunol. 11, 373–384. doi:10.1038/ni.1863.

Kechagia, J. Z., Ivaska, J., and Roca-Cusachs, P. (2019). Integrins as biomechanical sensors of the microenvironment. Nat. Rev. Mol. Cell Biol. 20, 457–473. doi:10.1038/s41580-019-0134-2.

Kessels, M. M., and Qualmann, B. (2020). The role of membrane-shaping BAR domain proteins in caveolar invagination: from mechanistic insights to pathophysiological consequences. Biochem. Soc. Trans. 48, 137–146. doi:10.1042/BST20190377.

Kim, K., and Guck, J. (2020). The Relative Densities of Cytoplasm and Nuclear Compartments Are Robust against Strong Perturbation. Biophys. J. 119, 1946–1957. doi:10.1016/j.bpj.2020.08.044.

Kim, K., Yoon, H., Diez-Silva, M., Dao, M., Dasari, R. R., and Park, Y. (2013). High-resolution three-dimensional imaging of red blood cells parasitized by Plasmodium falciparum and in situ hemozoin crystals using optical diffraction tomography. J. Biomed. Opt. 19, 1. doi:10.1117/1.JBO.19.1.011005.

Kim, N.-G., and Gumbiner, B. M. (2015). Adhesion to fibronectin regulates Hippo signaling via the FAK–Src–PI3K pathway. J. Cell Biol. 210, 503–515. doi:10.1083/jcb.201501025.

Kim, W., and Jho, E. (2018). The history and regulatory mechanism of the Hippo pathway. BMB Rep. 51, 106–118. doi:10.5483/BMBRep.2018.51.3.022.

Kimura, K., Ito, M., Amano, M., Chihara, K., Fukata, Y., Nakafuku, M., et al. (1996). Regulation of Myosin Phosphatase by Rho and Rho-Associated Kinase (Rho-Kinase). Science 273, 245–248. doi:10.1126/science.273.5272.245.

Kirby, T. J., and Lammerding, J. (2018). Emerging views of the nucleus as a cellular mechanosensor. Nat. Cell Biol. 20, 373–381. doi:10.1038/s41556-018-0038-y.

Klaas, M., Kangur, T., Viil, J., Mäemets-Allas, K., Minajeva, A., Vadi, K., et al. (2016). The alterations in the extracellular matrix composition guide the repair of damaged liver tissue. Sci. Rep. 6, 27398. doi:10.1038/srep27398.

Klopfleisch, R. (2016). Macrophage reaction against biomaterials in the mouse model – Phenotypes, functions and markers. Acta Biomater. 43, 3–13. doi:10.1016/j.actbio.2016.07.003.

Knockenhauer, K. E., and Schwartz, T. U. (2016). The Nuclear Pore Complex as a Flexible and Dynamic Gate. Cell 164, 1162–1171. doi:10.1016/j.cell.2016.01.034.

Kolarcik, C. L., Luebben, S. D., Sapp, S. A., Hanner, J., Snyder, N., Kozai, T. D. Y., et al. (2015). Elastomeric and soft conducting microwires for implantable neural interfaces. Soft Matter 11, 4847–4861. doi:10.1039/C5SM00174A.

Kong, F., García, A. J., Mould, A. P., Humphries, M. J., and Zhu, C. (2009). Demonstration of catch bonds between an integrin and its ligand. J. Cell Biol. 185, 1275–1284. doi:10.1083/jcb.200810002.

Koser, D. E., Thompson, A. J., Foster, S. K., Dwivedy, A., Pillai, E. K., Sheridan, G. K., et al. (2016). Mechanosensing is critical for axon growth in the developing brain. Nat. Neurosci. 19, 1592–1598. doi:10.1038/nn.4394.

Kovtun, O., Tillu, V. A., Ariotti, N., Parton, R. G., and Collins, B. M. (2015). Cavin family proteins and the assembly of caveolae. J. Cell Sci. 128, 1269–1278. doi:10.1242/jcs.167866.

Krendel, M., Zenke, F. T., and Bokoch, G. M. (2002). Nucleotide exchange factor GEF-H1 mediates cross-talk between microtubules and the actin cytoskeleton. Nat. Cell Biol. 4, 294–301. doi:10.1038/ncb773.

Kumar, A., Ouyang, M., Van den Dries, K., McGhee, E. J., Tanaka, K., Anderson, M. D., et al. (2016). Talin tension sensor reveals novel features of focal adhesion force transmission and mechanosensitivity. J. Cell Biol. 213, 371–383. doi:10.1083/jcb.201510012.

Kuzmich, N. N., Sivak, K. V., Chubarev, V. N., Porozov, Y. B., Savateeva-Lyubimova, T. N., and Peri, F. (2017). TLR4 Signaling Pathway Modulators as Potential Therapeutics in Inflammation and Sepsis. Vaccines 5, 34. doi:10.3390/vaccines5040034.

Labernadie, A., Bouissou, A., Delobelle, P., Balor, S., Voituriez, R., Proag, A., et al. (2014). Protrusion force microscopy reveals oscillatory force generation and mechanosensing activity of human macrophage podosomes. Nat. Commun. 5, 5343. doi:10.1038/ncomms6343.

Lacour, S. P., Courtine, G., and Guck, J. (2016). Materials and technologies for soft implantable neuroprostheses. Nat. Rev. Mater. 1, 1–14. doi:10.1038/natrevmats.2016.63.

Lammerding, J., Fong, L. G., Ji, J. Y., Reue, K., Stewart, C. L., Young, S. G., et al. (2006). Lamins A and C but Not Lamin B1 Regulate Nuclear Mechanics *. J. Biol. Chem. 281, 25768–25780. doi:10.1074/jbc.M513511200.

Lavin, Y., Winter, D., Blecher-Gonen, R., David, E., Keren-Shaul, H., Merad, M., et al. (2014). Tissue-Resident Macrophage Enhancer Landscapes Are Shaped by the Local Microenvironment. Cell 159, 1312–1326. doi:10.1016/j.cell.2014.11.018.

Le Roux, A.-L., Quiroga, X., Walani, N., Arroyo, M., and Roca-Cusachs, P. (2019). The plasma membrane as a mechanochemical transducer. Philos. Trans. R. Soc. B Biol. Sci. 374, 20180221. doi:10.1098/rstb.2018.0221.

Leclerc, L., Rima, W., Boudard, D., Pourchez, J., Forest, V., Bin, V., et al. (2012). Size of submicrometric and nanometric particles affect cellular uptake and biological activity of macrophages in vitro. Inhal. Toxicol. 24, 580–588. doi:10.3109/08958378.2012.699984.

Lee, A.-J., Cho, K.-J., and Kim, J.-H. (2015). MyD88–BLT2-dependent cascade contributes to LPS-induced interleukin-6 production in mouse macrophage. Exp. Mol. Med. 47, e156–e156. doi:10.1038/emm.2015.8.

Lee, G.-S., Subramanian, N., Kim, A. I., Aksentijevich, I., Goldbach-Mansky, R., Sacks, D. B., et al. (2012). The calcium-sensing receptor regulates the NLRP3 inflammasome through Ca2+ and cAMP. Nature 492, 123–127. doi:10.1038/nature11588.

Lee, H.-M., Kim, J.-J., Kim, H. J., Shong, M., Ku, B. J., and Jo, E.-K. (2013). Upregulated NLRP3 Inflammasome Activation in Patients With Type 2 Diabetes. Diabetes 62, 194–204. doi:10.2337/db12-0420.

Lessey, E. C., Guilluy, C., and Burridge, K. (2012). From Mechanical Force to RhoA Activation. Biochemistry 51, 7420–7432. doi:10.1021/bi300758e.

Levin, R., Grinstein, S., and Canton, J. (2016). The life cycle of phagosomes: formation, maturation, and resolution. Immunol. Rev. 273, 156–179. doi:10.1111/imr.12439.

Li, R., Serrano, J. C., Xing, H., Lee, T. A., Azizgolshani, H., Zaman, M., et al. (2018). Interstitial flow promotes macrophage polarization toward an M2 phenotype. Mol. Biol. Cell 29, 1927–1940. doi:10.1091/mbc.E18-03-0164.

Lieber, A. D., Yehudai-Resheff, S., Barnhart, E. L., Theriot, J. A., and Keren, K. (2013). Membrane Tension in Rapidly Moving Cells Is Determined by Cytoskeletal Forces. Curr. Biol. 23, 1409–1417. doi:10.1016/j.cub.2013.05.063.

Lin, K. C., Park, H. W., and Guan, K.-L. (2017). Regulation of the Hippo Pathway Transcription Factor TEAD. Trends Biochem. Sci. 42, 862–872. doi:10.1016/j.tibs.2017.09.003.

Lin, Y., Xu, J., and Lan, H. (2019). Tumor-associated macrophages in tumor metastasis: biological roles and clinical therapeutic applications. J. Hematol. Oncol.J Hematol Oncol 12, 76. doi:10.1186/s13045-019-0760-3.

Linder, S., and Cervero, P. (2020). The podosome cap: past, present, perspective. Eur. J. Cell Biol. 99, 151087. doi:10.1016/j.ejcb.2020.151087.

Linder, S., Higgs, H., Hüfner, K., Schwarz, K., Pannicke, U., and Aepfelbacher, M. (2000). The Polarization Defect of Wiskott-Aldrich Syndrome Macrophages Is Linked to Dislocalization of the Arp2/3 Complex. J. Immunol. 165, 221–225. doi:10.4049/jimmunol.165.1.221.

Linder, S., and Wiesner, C. (2015). Tools of the trade: podosomes as multipurpose organelles of monocytic cells. Cell. Mol. Life Sci. 72, 121–135. doi:10.1007/s00018-014-1731-z.

Linder, S., and Wiesner, C. (2016). Feel the force: Podosomes in mechanosensing. Exp. Cell Res. 343, 67–72. doi:10.1016/j.yexcr.2015.11.026.

Liu, B., Chen, W., Evavold, B. D., and Zhu, C. (2014). Accumulation of Dynamic Catch Bonds between TCR and Agonist Peptide-MHC Triggers T Cell Signaling. Cell 157, 357–368. doi:10.1016/j.cell.2014.02.053.

Liu, X., Zhang, Z., Ruan, J., Pan, Y., Magupalli, V. G., Wu, H., et al. (2016). Inflammasome-activated gasdermin D causes pyroptosis by forming membrane pores. Nature 535, 153–158. doi:10.1038/nature18629.

Lo, H. P., Nixon, S. J., Hall, T. E., Cowling, B. S., Ferguson, C., Morgan, G. P., et al. (2015). The caveolin–cavin system plays a conserved and critical role in mechanoprotection of skeletal muscle. J. Cell Biol. 210, 833–849. doi:10.1083/jcb.201501046.

Lombardi, M. L., Jaalouk, D. E., Shanahan, C. M., Burke, B., Roux, K. J., and Lammerding, J. (2011). The Interaction between Nesprins and Sun Proteins at the Nuclear Envelope Is Critical for Force Transmission between the Nucleus and Cytoskeleton*. J. Biol. Chem. 286, 26743–26753. doi:10.1074/jbc.M111.233700.

López, M. P., Huber, F., Grigoriev, I., Steinmetz, M. O., Akhmanova, A., Koenderink, G. H., et al. (2014). Actin–microtubule coordination at growing microtubule ends. Nat. Commun. 5, 4778. doi:10.1038/ncomms5778.

Lucas, C., Wong, P., Klein, J., Castro, T. B. R., Silva, J., Sundaram, M., et al. (2020). Longitudinal analyses reveal immunological misfiring in severe COVID-19. Nature 584, 463–469. doi:10.1038/s41586-020-2588-y.

Luxenburg, C., Geblinger, D., Klein, E., Anderson, K., Hanein, D., Geiger, B., et al. (2007). The Architecture of the Adhesive Apparatus of Cultured Osteoclasts: From Podosome Formation to Sealing Zone Assembly. PLOS ONE 2, e179. doi:10.1371/journal.pone.0000179.

Luxenburg, C., Winograd-Katz, S., Addadi, L., and Geiger, B. (2012). Involvement of actin polymerization in podosome dynamics. J. Cell Sci. 125, 1666–1672. doi:10.1242/jcs.075903.

Maekawa, M., Ishizaki, T., Boku, S., Watanabe, N., Fujita, A., Iwamatsu, A., et al. (1999). Signaling from Rho to the actin cytoskeleton through protein kinases ROCK and LIM-kinase. Science 285, 895–898. doi:10.1126/science.285.5429.895.

Magupalli, V. G., Negro, R., Tian, Y., Hauenstein, A. V., Caprio, G. D., Skillern, W., et al. (2020). HDAC6 mediates an aggresome-like mechanism for NLRP3 and pyrin inflammasome activation. Science 369. doi:10.1126/science.aas8995.

Majedi, F. S., Hasani-Sadrabadi, M. M., Thauland, T. J., Li, S., Bouchard, L.-S., and Butte, M. J. (2020). T-cell activation is modulated by the 3D mechanical microenvironment. Biomaterials 252, 120058. doi:10.1016/j.biomaterials.2020.120058.

Man, S. M., Ekpenyong, A., Tourlomousis, P., Achouri, S., Cammarota, E., Hughes, K., et al. (2014). Actin polymerization as a key innate immune effector mechanism to control Salmonella infection. Proc. Natl. Acad. Sci. 111, 17588–17593. doi:10.1073/pnas.1419925111.

Mangan, M. S. J., Olhava, E. J., Roush, W. R., Seidel, H. M., Glick, G. D., and Latz, E. (2018). Targeting the NLRP3 inflammasome in inflammatory diseases. Nat. Rev. Drug Discov. 17, 588–606. doi:10.1038/nrd.2018.97.

Mantovani, A., Sozzani, S., Locati, M., Allavena, P., and Sica, A. (2002). Macrophage polarization: tumor-associated macrophages as a paradigm for polarized M2 mononuclear phagocytes. Trends Immunol. 23, 549–555. doi:10.1016/S1471-4906(02)02302-5.

Manzanero, S. (2012). “Generation of Mouse Bone Marrow-Derived Macrophages,” in Leucocytes, ed. R. B. Ashman (Totowa, NJ: Humana Press), 177–181. doi:10.1007/978-1-61779-527-5_12.

Martinon, F., Burns, K., and Tschopp, J. (2002). The Inflammasome: A Molecular Platform Triggering Activation of Inflammatory Caspases and Processing of proIL-β. Mol. Cell 10, 417–426. doi:10.1016/S1097-2765(02)00599-3.

Martinon, F., Pétrilli, V., Mayor, A., Tardivel, A., and Tschopp, J. (2006). Gout-associated uric acid crystals activate the NALP3 inflammasome. Nature 440, 237–241. doi:10.1038/nature04516.

Maruyama, K., Sakisaka, Y., Suto, M., Tada, H., Nakamura, T., Yamada, S., et al. (2018). Cyclic Stretch Negatively Regulates IL-1β Secretion Through the Inhibition of NLRP3 Inflammasome Activation by Attenuating the AMP Kinase Pathway. Front. Physiol. 9, 802. doi:10.3389/fphys.2018.00802.

Masters, T. A., Pontes, B., Viasnoff, V., Li, Y., and Gauthier, N. C. (2013). Plasma membrane tension orchestrates membrane trafficking, cytoskeletal remodeling, and biochemical signaling during phagocytosis. Proc. Natl. Acad. Sci. 110, 11875–11880.

Maurer, M., and Lammerding, J. (2019). The Driving Force: Nuclear Mechanotransduction in Cellular Function, Fate, and Disease. Annu. Rev. Biomed. Eng. 21, 443–468. doi:10.1146/annurev-bioeng-060418-052139.

McKee, C. M., and Coll, R. C. (2020). NLRP3 inflammasome priming: A riddle wrapped in a mystery inside an enigma. J. Leukoc. Biol. 108, 937–952. doi:10.1002/JLB.3MR0720-513R.

McWhorter, F. Y., Wang, T., Nguyen, P., Chung, T., and Liu, W. F. (2013). Modulation of macrophage phenotype by cell shape. Proc. Natl. Acad. Sci. 110, 17253–17258. doi:10.1073/pnas.1308887110.

Meli, V. S., Atcha, H., Veerasubramanian, P. K., Nagalla, R. R., Luu, T. U., Chen, E. Y., et al. (2020). YAP-mediated mechanotransduction tunes the macrophage inflammatory response. Sci. Adv. 6, eabb8471. doi:10.1126/sciadv.abb8471.

Meng, K. P., Majedi, F. S., Thauland, T. J., and Butte, M. J. (2020). Mechanosensing through YAP controls T cell activation and metabolism. J. Exp. Med. 217, e20200053. doi:10.1084/jem.20200053.

Mennens, S. F. B., Bolomini-Vittori, M., Weiden, J., Joosten, B., Cambi, A., and van den Dries, K. (2017). Substrate stiffness influences phenotype and function of human antigen-presenting dendritic cells. Sci. Rep. 7, 17511. doi:10.1038/s41598-017-17787-z.

Metschnikoff, É. (1878). Über die Verdauungsorgane einiger Süsswasserturbellarien. Zool Anz 1, 387–390.

Metschnikoff, É. (1883). Untersuchungen über die mesodermalen Phagocyten einiger Wirbeltiere. Biol Zentralbl 3, 560–5.

Metschnikoff, É. (1884a). Eine neue Entzündungstheorie. Allg Wien. Med Ztg 29, 307.

Metschnikoff, É. (1884b). Memoirs: researches on the intracellular digestion of invertebrates. J. Cell Sci. 2, 89–111.

Metschnikoff, É. (1884c). Ueber die beziehung der phagocyten zu milzbrandbacillen. Arch. Für Pathol. Anat. Physiol. Für Klin. Med. 97, 502–526.

Metschnikoff, É. (1884d). Untersuchungen uber die intracellulare Verdauung bei wirbellosen Thieren. Arb Zool Inst Univ Wien U Zool Stat Triest 5, 141.

Metschnikoff, É. (1887). "VIII. Ueber den Kampf der Zellen gegen Erysipelkokken. Ein Beitrag zur Phagocytenlehre," in Band 107 (De Gruyter), 209–249.

Metschnikoff, É. (1888). Über die phagozytäre. Rolle der Tuberkelbazillen-Riesenzellen. Virchows Arch. 113, 63–63.

Mih, J. D., Marinkovic, A., Liu, F., Sharif, A. S., and Tschumperlin, D. J. (2012). Matrix stiffness reverses the effect of actomyosin tension on cell proliferation. J. Cell Sci. 125, 5974–5983. doi:10.1242/jcs.108886.

Milovanovic, P., Potocnik, J., Djonic, D., Nikolic, S., Zivkovic, V., Djuric, M., et al. (2012). Age-related deterioration in trabecular bone mechanical properties at material level: Nanoindentation study of the femoral neck in women by using AFM. Exp. Gerontol. 47, 154–159. doi:10.1016/j.exger.2011.11.011.

Miroshnikova, Y. A., Mouw, J. K., Barnes, J. M., Pickup, M. W., Lakins, J. N., Kim, Y., et al. (2016). Tissue mechanics promote IDH1-dependent HIF1α–tenascin C feedback to regulate glioblastoma aggression. Nat. Cell Biol. 18, 1336–1345. doi:10.1038/ncb3429.

Mirzaali, M. J., Schwiedrzik, J. J., Thaiwichai, S., Best, J. P., Michler, J., Zysset, P. K., et al. (2016). Mechanical properties of cortical bone and their relationships with age, gender, composition and microindentation properties in the elderly. Bone 93, 196–211. doi:10.1016/j.bone.2015.11.018.

Mitra, S. K., Hanson, D. A., and Schlaepfer, D. D. (2005). Focal adhesion kinase: in command and control of cell motility. Nat. Rev. Mol. Cell Biol. 6, 56–68. doi:10.1038/nrm1549.

Möller, J., Luehmann, T., Hall, H., and Vogel, V. (2012). The Race to the Pole: How High-Aspect Ratio Shape and Heterogeneous Environments Limit Phagocytosis of Filamentous Escherichia coli Bacteria by Macrophages. Nano Lett. 12, 2901–2905. doi:10.1021/nl3004896.

Möllmert, S., Kharlamova, M. A., Hoche, T., Taubenberger, A. V., Abuhattum, S., Kuscha, V., et al. (2020). Zebrafish Spinal Cord Repair Is Accompanied by Transient Tissue Stiffening. Biophys. J. 118, 448–463. doi:10.1016/j.bpj.2019.10.044.

Monteleone, M., Stanley, A. C., Chen, K. W., Brown, D. L., Bezbradica, J. S., von Pein, J. B., et al. (2018). Interleukin-1β Maturation Triggers Its Relocation to the Plasma Membrane for Gasdermin-D-Dependent and -Independent Secretion. Cell Rep. 24, 1425–1433. doi:10.1016/j.celrep.2018.07.027.

Morén, B., Shah, C., Howes, M. T., Schieber, N. L., McMahon, H. T., Parton, R. G., et al. (2012). EHD2 regulates caveolar dynamics via ATP-driven targeting and oligomerization. Mol. Biol. Cell 23, 1316–1329. doi:10.1091/mbc.e11-09-0787.

Moreno-Vicente, R., Pavón, D. M., Martín-Padura, I., Català-Montoro, M., Díez-Sánchez, A., Quílez-Álvarez, A., et al. (2018). Caveolin-1 Modulates Mechanotransduction Responses to Substrate Stiffness through Actin-Dependent Control of YAP. Cell Rep. 25, 1622-1635.e6. doi:10.1016/j.celrep.2018.10.024.

Moretti, J., and Blander, J. M. (2021). Increasing complexity of NLRP3 inflammasome regulation. J. Leukoc. Biol. 109, 561–571. doi:10.1002/JLB.3MR0520-104RR.

Morris, C. E., and Homann, U. (2001). Cell Surface Area Regulation and Membrane Tension. J. Membr. Biol. 179, 79–102. doi:10.1007/s002320010040.

Moshayedi, P., Ng, G., Kwok, J. C. F., Yeo, G. S. H., Bryant, C. E., Fawcett, J. W., et al. (2014). The relationship between glial cell mechanosensitivity and foreign body reactions in the central nervous system. Biomaterials 35, 3919–3925. doi:10.1016/j.biomaterials.2014.01.038.

Mosser, D. M., and Edwards, J. P. (2008). Exploring the full spectrum of macrophage activation. Nat. Rev. Immunol. 8, 958–969. doi:10.1038/nri2448.

Muñoz-Planillo, R., Kuffa, P., Martínez-Colón, G., Smith, B. L., Rajendiran, T. M., and Núñez, G. (2013). K+ Efflux Is the Common Trigger of NLRP3 Inflammasome Activation by Bacterial Toxins and Particulate Matter. Immunity 38, 1142–1153. doi:10.1016/j.immuni.2013.05.016.

Murakami, T., Ockinger, J., Yu, J., Byles, V., McColl, A., Hofer, A. M., et al. (2012). Critical role for calcium mobilization in activation of the NLRP3 inflammasome. Proc. Natl. Acad. Sci. 109, 11282–11287. doi:10.1073/pnas.1117765109.

Murray, P. J., Allen, J. E., Biswas, S. K., Fisher, E. A., Gilroy, D. W., Goerdt, S., et al. (2014). Macrophage Activation and Polarization: Nomenclature and Experimental Guidelines. Immunity 41, 14–20. doi:10.1016/j.immuni.2014.06.008.

Murray, P. J., and Wynn, T. A. (2011). Protective and pathogenic functions of macrophage subsets. Nat. Rev. Immunol. 11, 723–737. doi:10.1038/nri3073.

Nardone, G., Oliver-De La Cruz, J., Vrbsky, J., Martini, C., Pribyl, J., Skládal, P., et al. (2017). YAP regulates cell mechanics by controlling focal adhesion assembly. Nat. Commun. 8, 15321. doi:10.1038/ncomms15321.

Nassoy, P., and Lamaze, C. (2012). Stressing caveolae new role in cell mechanics. Trends Cell Biol. 22, 381–389. doi:10.1016/j.tcb.2012.04.007.

Naumanen, P., Lappalainen, P., and Hotulainen, P. (2008). Mechanisms of actin stress fibre assembly. J. Microsc. 231, 446–454. doi:10.1111/j.1365-2818.2008.02057.x.

Netea, M. G., Simon, A., Veerdonk, F. van de, Kullberg, B.-J., Meer, J. W. M. V. der, and Joosten, L. A. B. (2010). IL-1β Processing in Host Defense: Beyond the Inflammasomes. PLOS Pathog. 6, e1000661. doi:10.1371/journal.ppat.1000661.

Newton, K., and Dixit, V. M. (2012). Signaling in Innate Immunity and Inflammation. Cold Spring Harb. Perspect. Biol. 4, a006049. doi:10.1101/cshperspect.a006049.

Nguyen, J. K., Park, D. J., Skousen, J. L., Hess-Dunning, A. E., Tyler, D. J., Rowan, S. J., et al. (2014). Mechanically-compliant intracortical implants reduce the neuroinflammatory response. J. Neural Eng. 11, 056014. doi:10.1088/1741-2560/11/5/056014.

Nia, H. T., Munn, L. L., and Jain, R. K. (2020). Physical traits of cancer. Science 370. doi:10.1126/science.aaz0868.

Okamoto, T., Takagi, Y., Kawamoto, E., Park, E. J., Usuda, H., Wada, K., et al. (2018). Reduced substrate stiffness promotes M2-like macrophage activation and enhances peroxisome proliferator-activated receptor γ expression. Exp. Cell Res. 367, 264–273. doi:10.1016/j.yexcr.2018.04.005.

Orlowski, G. M., Colbert, J. D., Sharma, S., Bogyo, M., Robertson, S. A., and Rock, K. L. (2015). Multiple Cathepsins Promote Pro–IL-1β Synthesis and NLRP3-Mediated IL-1β Activation. J. Immunol. 195, 1685–1697. doi:10.4049/jimmunol.1500509.

Otsu, N. (1979). A Threshold Selection Method from Gray-Level Histograms. IEEE Trans. Syst. Man Cybern. 9, 62–66. doi:10.1109/TSMC.1979.4310076.

Paik, S., Kim, J. K., Silwal, P., Sasakawa, C., and Jo, E.-K. (2021). An update on the regulatory mechanisms of NLRP3 inflammasome activation. Cell. Mol. Immunol. 18, 1141–1160. doi:10.1038/s41423-021-00670-3.

Park, B. S., Song, D. H., Kim, H. M., Choi, B.-S., Lee, H., and Lee, J.-O. (2009). The structural basis of lipopolysaccharide recognition by the TLR4–MD-2 complex. Nature 458, 1191–1195. doi:10.1038/nature07830.

Parpaite, T., and Coste, B. (2017). Piezo channels. Curr. Biol. 27, R250–R252. doi:10.1016/j.cub.2017.01.048.

Paszek, M. J., Zahir, N., Johnson, K. R., Lakins, J. N., Rozenberg, G. I., Gefen, A., et al. (2005). Tensional homeostasis and the malignant phenotype. Cancer Cell, 14.

Patel, N. R., Bole, M., Chen, C., Hardin, C. C., Kho, A. T., Mih, J., et al. (2012). Cell Elasticity Determines Macrophage Function. PLoS ONE 7, e41024. doi:10.1371/journal.pone.0041024.

Pathak, M. M., Nourse, J. L., Tran, T., Hwe, J., Arulmoli, J., Le, D. T. T., et al. (2014). Stretch-activated ion channel Piezo1 directs lineage choice in human neural stem cells. Proc. Natl. Acad. Sci. 111, 16148–16153. doi:10.1073/pnas.1409802111.

Pennacchio, F. A., Nastały, P., Poli, A., and Maiuri, P. (2021). Tailoring Cellular Function: The Contribution of the Nucleus in Mechanotransduction. Front. Bioeng. Biotechnol. 0. doi:10.3389/fbioe.2020.596746.

Pétrilli, V., Papin, S., Dostert, C., Mayor, A., Martinon, F., and Tschopp, J. (2007). Activation of the NALP3 inflammasome is triggered by low intracellular potassium concentration. Cell Death Differ. 14, 1583–1589. doi:10.1038/sj.cdd.4402195.

Petty, H. R., Hafeman, D. G., and McConnell, H. M. (1981). Disappearance of macrophage surface folds after antibody-dependent phagocytosis. J. Cell Biol. 89, 223–229. doi:10.1083/jcb.89.2.223.

Pfannenstill, V., Barbotin, A., Colin-York, H., and Fritzsche, M. (2021). Quantitative Methodologies to Dissect Immune Cell Mechanobiology. Cells 10, 851. doi:10.3390/cells10040851.

Piccini, A., Carta, S., Tassi, S., Lasiglié, D., Fossati, G., and Rubartelli, A. (2008). ATP is released by monocytes stimulated with pathogen-sensing receptor ligands and induces IL-1β and IL-18 secretion in an autocrine way. Proc. Natl. Acad. Sci. 105, 8067–8072. doi:10.1073/pnas.0709684105.

Previtera, M. L., and Sengupta, A. (2015). Substrate Stiffness Regulates Proinflammatory Mediator Production through TLR4 Activity in Macrophages. PLOS ONE 10, e0145813. doi:10.1371/journal.pone.0145813.

Qin, R., Schmid, H., Münzberg, C., Maass, U., Krndija, D., Adler, G., et al. (2015). Phosphorylation and turnover of paxillin in focal contacts is controlled by force and defines the dynamic state of the adhesion site. Cytoskeleton 72, 101–112. doi:10.1002/cm.21209.

R Core Team (2020). R: A language and environment for statistical computing. Vienna, Austria.: R Foundation for Statistical Computing Available at: http://www.R-project.org/.

Raab, M., and Discher, D. E. (2017). Matrix rigidity regulates microtubule network polarization in migration: Matrix Rigidity Regulates Cell Polarization. Cytoskeleton 74, 114–124. doi:10.1002/cm.21349.

Rabinovitch, M. (1995). Professional and non-professional phagocytes: an introduction. Trends Cell Biol. 5, 85–87. doi:10.1016/S0962-8924(00)88955-2.

Rafiq, N. B. M., Nishimura, Y., Plotnikov, S. V., Thiagarajan, V., Zhang, Z., Shi, S., et al. (2019). A mechano-signalling network linking microtubules, myosin IIA filaments and integrin-based adhesions. Nat. Mater. 18, 638–649. doi:10.1038/s41563-019-0371-y.

Ranade, S. S., Syeda, R., and Patapoutian, A. (2015). Mechanically Activated Ion Channels. Neuron 87, 1162–1179. doi:10.1016/j.neuron.2015.08.032.

Renkawitz, J., Schumann, K., Weber, M., Lämmermann, T., Pflicke, H., Piel, M., et al. (2009). Adaptive force transmission in amoeboid cell migration. Nat. Cell Biol. 11, 1438–1443. doi:10.1038/ncb1992.

Renkawitz, J., and Sixt, M. (2010). Mechanisms of force generation and force transmission during interstitial leukocyte migration. EMBO Rep. 11, 744–750. doi:10.1038/embor.2010.147.

Ricart, B. G., Yang, M. T., Hunter, C. A., Chen, C. S., and Hammer, D. A. (2011). Measuring Traction Forces of Motile Dendritic Cells on Micropost Arrays. Biophys. J. 101, 2620–2628. doi:10.1016/j.bpj.2011.09.022.

Ridone, P., Vassalli, M., and Martinac, B. (2019). Piezo1 mechanosensitive channels: what are they and why are they important. Biophys. Rev. 11, 795–805. doi:10.1007/s12551-019-00584-5.

Rio, A. del, Perez-Jimenez, R., Liu, R., Roca-Cusachs, P., Fernandez, J. M., and Sheetz, M. P. (2009). Stretching Single Talin Rod Molecules Activates Vinculin Binding. Science 323, 638–641. doi:10.1126/science.1162912.

Roca-Cusachs, P., Rio, A. del, Puklin-Faucher, E., Gauthier, N. C., Biais, N., and Sheetz, M. P. (2013). Integrin-dependent force transmission to the extracellular matrix by α-actinin triggers adhesion maturation. Proc. Natl. Acad. Sci. 110, E1361–E1370. doi:10.1073/pnas.1220723110.

Rodrigues, T. S., de Sá, K. S. G., Ishimoto, A. Y., Becerra, A., Oliveira, S., Almeida, L., et al. (2020). Inflammasomes are activated in response to SARS-CoV-2 infection and are associated with COVID-19 severity in patients. J. Exp. Med. 218. doi:10.1084/jem.20201707.

Rong, Y., Yang, W., Hao, H., Wang, W., Lin, S., Shi, P., et al. (2021). The Golgi microtubules regulate single cell durotaxis. EMBO Rep. 22. doi:10.15252/embr.202051094.

Rothberg, K. G., Heuser, J. E., Donzell, W. C., Ying, Y.-S., Glenney, J. R., and Anderson, R. G. W. (1992). Caveolin, a protein component of caveolae membrane coats. Cell 68, 673–682. doi:10.1016/0092-8674(92)90143-Z.

Ruytinx, P., Proost, P., Van Damme, J., and Struyf, S. (2018). Chemokine-Induced Macrophage Polarization in Inflammatory Conditions. Front. Immunol. 9, 1930. doi:10.3389/fimmu.2018.01930.

Ryu, J.-K., Kim, S. J., Rah, S.-H., Kang, J. I., Jung, H. E., Lee, D., et al. (2017). Reconstruction of LPS Transfer Cascade Reveals Structural Determinants within LBP, CD14, and TLR4-MD2 for Efficient LPS Recognition and Transfer. Immunity 46, 38–50. doi:10.1016/j.immuni.2016.11.007.

Sack, I., Beierbach, B., Hamhaber, U., Klatt, D., and Braun, J. (2008). Non-invasive measurement of brain viscoelasticity using magnetic resonance elastography. NMR Biomed. 21, 265–271. doi:10.1002/nbm.1189.

Saitakis, M., Dogniaux, S., Goudot, C., Bufi, N., Asnacios, S., Maurin, M., et al. (2017). Different TCR-induced T lymphocyte responses are potentiated by stiffness with variable sensitivity. eLife 6, e23190. doi:10.7554/eLife.23190.

Sánchez-Madrid, F., and Serrador, J. M. (2009). Bringing up the rear: defining the roles of the uropod. Nat. Rev. Mol. Cell Biol. 10, 353–359. doi:10.1038/nrm2680.

Saotome, K., Murthy, S. E., Kefauver, J. M., Whitwam, T., Patapoutian, A., and Ward, A. B. (2018). Structure of the mechanically activated ion channel Piezo1. Nature 554, 481–486. doi:10.1038/nature25453.

Sathe, A. R., Shivashankar, G. V., and Sheetz, M. P. (2016). Nuclear transport of paxillin depends on focal adhesion dynamics and FAT domains. J. Cell Sci. 129, 1981–1988. doi:10.1242/jcs.172643.

Scheraga, R. G., Abraham, S., Niese, K. A., Southern, B. D., Grove, L. M., Hite, R. D., et al. (2016). TRPV4 Mechanosensitive Ion Channel Regulates Lipopolysaccharide-Stimulated Macrophage Phagocytosis. J. Immunol. 196, 428–436. doi:10.4049/jimmunol.1501688.

Schindelin, J., Arganda-Carreras, I., Frise, E., Kaynig, V., Longair, M., Pietzsch, T., et al. (2012). Fiji: an open-source platform for biological-image analysis. Nat. Methods 9, 676–682. doi:10.1038/nmeth.2019.

Schneider, C. A., Rasband, W. S., and Eliceiri, K. W. (2012). NIH Image to ImageJ: 25 years of image analysis. Nat. Methods 9, 671–675. doi:10.1038/nmeth.2089.

Serrano, I., McDonald, P. C., Lock, F., Muller, W. J., and Dedhar, S. (2013). Inactivation of the Hippo tumour suppressor pathway by integrin-linked kinase. Nat. Commun. 4, 2976. doi:10.1038/ncomms3976.

Sharif, H., Wang, L., Wang, W. L., Magupalli, V. G., Andreeva, L., Qiao, Q., et al. (2019). Structural mechanism for NEK7-licensed activation of NLRP3 inflammasome. Nature 570, 338–343. doi:10.1038/s41586-019-1295-z.

Sharma, G., Valenta, D. T., Altman, Y., Harvey, S., Xie, H., Mitragotri, S., et al. (2010). Polymer particle shape independently influences binding and internalization by macrophages. J. Controlled Release 147, 408–412. doi:10.1016/j.jconrel.2010.07.116.

Shi, J., Zhao, Y., Wang, K., Shi, X., Wang, Y., Huang, H., et al. (2015). Cleavage of GSDMD by inflammatory caspases determines pyroptotic cell death. Nature 526, 660–665. doi:10.1038/nature15514.

Shrivastava, G., León-Juárez, M., García-Cordero, J., Meza-Sánchez, D. E., and Cedillo-Barrón, L. (2016). Inflammasomes and its importance in viral infections. Immunol. Res. 64, 1101–1117. doi:10.1007/s12026-016-8873-z.

Shvets, E., Bitsikas, V., Howard, G., Hansen, C. G., and Nichols, B. J. (2015). Dynamic caveolae exclude bulk membrane proteins and are required for sorting of excess glycosphingolipids. Nat. Commun. 6, 6867. doi:10.1038/ncomms7867.

Sica, A., and Mantovani, A. (2012). Macrophage plasticity and polarization: in vivo veritas. J. Clin. Invest. 122, 787–795. doi:10.1172/JCI59643.

Sieweke, M. H., and Allen, J. E. (2013). Beyond Stem Cells: Self-Renewal of Differentiated Macrophages. Science 342, 1242974–1242974. doi:10.1126/science.1242974.

Sinha, B., Köster, D., Ruez, R., Gonnord, P., Bastiani, M., Abankwa, D., et al. (2011). Cells Respond to Mechanical Stress by Rapid Disassembly of Caveolae. Cell 144, 402–413. doi:10.1016/j.cell.2010.12.031.

Sitarska, E., and Diz-Muñoz, A. (2020). Pay attention to membrane tension: Mechanobiology of the cell surface. Curr. Opin. Cell Biol. 66, 11–18. doi:10.1016/j.ceb.2020.04.001.

Smith, L. A., Aranda-Espinoza, H., Haun, J. B., Dembo, M., and Hammer, D. A. (2007). Neutrophil Traction Stresses are Concentrated in the Uropod during Migration. Biophys. J. 92, L58–L60. doi:10.1529/biophysj.106.102822.

Solis, A. G., Bielecki, P., Steach, H. R., Sharma, L., Harman, C. C. D., Yun, S., et al. (2019). Mechanosensation of cyclical force by PIEZO1 is essential for innate immunity. Nature 573, 69–74. doi:10.1038/s41586-019-1485-8.

Solovei, I., Wang, A. S., Thanisch, K., Schmidt, C. S., Krebs, S., Zwerger, M., et al. (2013). LBR and Lamin A/C Sequentially Tether Peripheral Heterochromatin and Inversely Regulate Differentiation. Cell 152, 584–598. doi:10.1016/j.cell.2013.01.009.

Song, Y., Li, D., Farrelly, O., Miles, L., Li, F., Kim, S. E., et al. (2019). The Mechanosensitive Ion Channel Piezo Inhibits Axon Regeneration. Neuron 102, 373-389.e6. doi:10.1016/j.neuron.2019.01.050.

Sridharan, R., Cameron, A. R., Kelly, D. J., Kearney, C. J., and O'Brien, F. J. (2015). Biomaterial based modulation of macrophage polarization: a review and suggested design principles. Mater. Today 18, 313–325. doi:10.1016/j.mattod.2015.01.019.

Sridharan, R., Cavanagh, B., Cameron, A. R., Kelly, D. J., and O'Brien, F. J. (2019a). Material stiffness influences the polarization state, function and migration mode of macrophages. Acta Biomater. 89, 47–59. doi:10.1016/j.actbio.2019.02.048.

Sridharan, R., Ryan, E. J., Kearney, C. J., Kelly, D. J., and O'Brien, F. J. (2019b). Macrophage Polarization in Response to Collagen Scaffold Stiffness Is Dependent on Cross-Linking Agent Used To Modulate the Stiffness. ACS Biomater. Sci. Eng. 5, 544–552. doi:10.1021/acsbiomaterials.8b00910.

Stanley, P., Smith, A., McDowall, A., Nicol, A., Zicha, D., and Hogg, N. (2008). Intermediate-affinity LFA-1 binds α-actinin-1 to control migration at the leading edge of the T cell. EMBO J. 27, 62–75. doi:10.1038/sj.emboj.7601959.

Stinchcombe, J. C., and Griffiths, G. M. (2007). Secretory Mechanisms in Cell-Mediated Cytotoxicity. Annu. Rev. Cell Dev. Biol. 23, 495–517. doi:10.1146/annurev.cellbio.23.090506.123521.

Strohmeyer, N., Bharadwaj, M., Costell, M., Fässler, R., and Müller, D. J. (2017). Fibronectin-bound α5β1 integrins sense load and signal to reinforce adhesion in less than a second. Nat. Mater. 16, 1262–1270. doi:10.1038/nmat5023.

Stutz, A., Horvath, G. L., Monks, B. G., and Latz, E. (2013). "ASC Speck Formation as a Readout for Inflammasome Activation," in The Inflammasome, eds. C. M. De Nardo and E. Latz (Totowa, NJ: Humana Press), 91–101. doi:10.1007/978-1-62703-523-1_8.

Sugimoto, A., Miyazaki, A., Kawarabayashi, K., Shono, M., Akazawa, Y., Hasegawa, T., et al. (2017). Piezo type mechanosensitive ion channel component 1 functions as a regulator of the cell fate determination of mesenchymal stem cells. Sci. Rep. 7, 17696. doi:10.1038/s41598-017-18089-0.

Sun, Z., Guo, S. S., and Fässler, R. (2016). Integrin-mediated mechanotransduction. J. Cell Biol. 215, 445–456. doi:10.1083/jcb.201609037.

Sung, Y., Choi, W., Fang-Yen, C., Badizadegan, K., Dasari, R. R., and Feld, M. S. (2009). Optical diffraction tomography for high resolution live cell imaging. 17, 266–277. doi:10.1364/oe.17.000266.

Suzaki, E., Kobayashi, H., Kodama, Y., Masujima, T., and Terakawa, S. (1997). Video-rate dynamics of exocytotic events associated with phagocytosis in neutrophils. Cell Motil. Cytoskeleton 38, 215–228. doi:10.1002/(SICI)1097-0169(1997)38:3<215::AID-CM1>3.0.CO;2-4.

Swanson, K. V., Deng, M., and Ting, J. P.-Y. (2019). The NLRP3 inflammasome: molecular activation and regulation to therapeutics. Nat. Rev. Immunol. 19, 477–489. doi:10.1038/s41577-019-0165-0.

Tabata, Y., and Ikada, Y. (1988). Effect of the size and surface charge of polymer microspheres on their phagocytosis by macrophage. Biomaterials 9, 356–362. doi:10.1016/0142-9612(88)90033-6.

Takagi, J., Petre, B. M., Walz, T., and Springer, T. A. (2002). Global Conformational Rearrangements in Integrin Extracellular Domains in Outside-In and Inside-Out Signaling. Cell 110, 599–611. doi:10.1016/S0092-8674(02)00935-2.

Tang, T., Lang, X., Xu, C., Wang, X., Gong, T., Yang, Y., et al. (2017). CLICs-dependent chloride efflux is an essential and proximal upstream event for NLRP3 inflammasome activation. Nat. Commun. 8, 202. doi:10.1038/s41467-017-00227-x.

Thomas, W. E., Vogel, V., and Sokurenko, E. (2008). Biophysics of Catch Bonds. Annu. Rev. Biophys. 37, 399–416. doi:10.1146/annurev.biophys.37.032807.125804.

Toldo, S., Bussani, R., Nuzzi, V., Bonaventura, A., Mauro, A. G., Cannatà, A., et al. (2021). Inflammasome formation in the lungs of patients with fatal COVID-19. Inflamm. Res. 70, 7–10. doi:10.1007/s00011-020-01413-2.

Torrino, S., Shen, W.-W., Blouin, C. M., Mani, S. K., Viaris de Lesegno, C., Bost, P., et al. (2018). EHD2 is a mechanotransducer connecting caveolae dynamics with gene transcription. J. Cell Biol. 217, 4092–4105. doi:10.1083/jcb.201801122.

Totaro, A., Panciera, T., and Piccolo, S. (2018). YAP/TAZ upstream signals and downstream responses. Nat. Cell Biol. 20, 888–899. doi:10.1038/s41556-018-0142-z.

Trouplin, V., Boucherit, N., Gorvel, L., Conti, F., Mottola, G., and Ghigo, E. (2013). Bone Marrow-derived Macrophage Production. J. Vis. Exp., 50966. doi:10.3791/50966.

Uhler, C., and Shivashankar, G. V. (2017). Regulation of genome organization and gene expression by nuclear mechanotransduction. Nat. Rev. Mol. Cell Biol. 18, 717–727. doi:10.1038/nrm.2017.101.

Ungricht, R., and Kutay, U. (2017). Mechanisms and functions of nuclear envelope remodelling. Nat. Rev. Mol. Cell Biol. 18, 229–245. doi:10.1038/nrm.2016.153.

Uribe-Querol, E., and Rosales, C. (2020). Phagocytosis: Our Current Understanding of a Universal Biological Process. Front. Immunol. 11, 1066. doi:10.3389/fimmu.2020.01066.

van den Dries, K., Linder, S., Maridonneau-Parini, I., and Poincloux, R. (2019). Probing the mechanical landscape – new insights into podosome architecture and mechanics. J. Cell Sci. 132, jcs236828. doi:10.1242/jcs.236828.

van den Dries, K., Schwartz, S. L., Byars, J., Meddens, M. b. m., Bolomini-Vittori, M., Lidke, D. S., et al. (2013). Dual-color superresolution microscopy reveals nanoscale organization of mechanosensory podosomes. Mol. Biol. Cell 24, 2112–2123. doi:10.1091/mbc.e12-12-0856.

van Furth, R., Cohn, Z. A., Hirsch, J. G., Humphrey, J. H., Spector, W. G., and Langevoort, H. L. (1972). The mononuclear phagocyte system: a new classification of macrophages, monocytes, and their precursor cells. Bull. World Health Organ. 46, 845–852.

Vandanmagsar, B., Youm, Y.-H., Ravussin, A., Galgani, J. E., Stadler, K., Mynatt, R. L., et al. (2011). The NLRP3 inflammasome instigates obesity-induced inflammation and insulin resistance. Nat. Med. 17, 179–188. doi:10.1038/nm.2279.

Vicente-Manzanares, M., Choi, C. K., and Horwitz, A. R. (2009). Integrins in cell migration – the actin connection. J. Cell Sci. 122, 199–206. doi:10.1242/jcs.018564.

Vladimer, G. I., Marty-Roix, R., Ghosh, S., Weng, D., and Lien, E. (2013). Inflammasomes and host defenses against bacterial infections. Curr. Opin. Microbiol. 16, 23–31. doi:10.1016/j.mib.2012.11.008.

Vorselen, D., Barger, S. R., Wang, Y., Cai, W., Theriot, J. A., Gauthier, N. C., et al. (2021). Phagocytic "teeth" and myosin-II "jaw" power target constriction during phagocytosis. Cell Biology doi:10.1101/2021.03.14.435346.

Vorselen, D., Wang, Y., de Jesus, M. M., Shah, P. K., Footer, M. J., Huse, M., et al. (2020). Microparticle traction force microscopy reveals subcellular force exertion patterns in immune cell–target interactions. Nat. Commun. 11, 20. doi:10.1038/s41467-019-13804-z.

Wan, Z., Chen, X., Chen, H., Ji, Q., Chen, Y., Wang, J., et al. (2015). The activation of IgM- or isotype-switched IgG- and IgE-BCR exhibits distinct mechanical force sensitivity and threshold. eLife 4, e06925. doi:10.7554/eLife.06925.

Wang, L., Luo, J.-Y., Li, B., Tian, X. Y., Chen, L.-J., Huang, Y., et al. (2016). Integrin-YAP/TAZ-JNK cascade mediates atheroprotective effect of unidirectional shear flow. Nature 540, 579–582. doi:10.1038/nature20602.

Wang, L., Yan, F., Yang, Y., Xiang, X., and Qiu, L. (2017). Quantitative Assessment of Skin Stiffness in Localized Scleroderma Using Ultrasound Shear-Wave Elastography. Ultrasound Med. Biol. 43, 1339–1347. doi:10.1016/j.ultrasmedbio.2017.02.009.

Wang, L., Zhou, H., Zhang, M., Liu, W., Deng, T., Zhao, Q., et al. (2019a). Structure and mechanogating of the mammalian tactile channel PIEZO2. Nature 573, 225–229. doi:10.1038/s41586-019-1505-8.

Wang, W. Y., Davidson, C. D., Lin, D., and Baker, B. M. (2019b). Actomyosin contractility-dependent matrix stretch and recoil induces rapid cell migration. Nat. Commun. 10, 1186. doi:10.1038/s41467-019-09121-0.

Wani, K., AlHarthi, H., Alghamdi, A., Sabico, S., and Al-Daghri, N. M. (2021). Role of NLRP3 Inflammasome Activation in Obesity-Mediated Metabolic Disorders. Int. J. Environ. Res. Public. Health 18, 511. doi:10.3390/ijerph18020511.

Ware, T., Simon, D., Arreaga-Salas, D. E., Reeder, J., Rennaker, R., Keefer, E. W., et al. (2012). Fabrication of Responsive, Softening Neural Interfaces. Adv. Funct. Mater. 22, 3470–3479. doi:10.1002/adfm.201200200.

Welzel, P. B., Prokoph, S., Zieris, A., Grimmer, M., Zschoche, S., Freudenberg, U., et al. (2011). Modulating Biofunctional starPEG Heparin Hydrogels by Varying Size and Ratio of the Constituents. Polymers 3, 602–620. doi:10.3390/polym3010602.

Wilson, C. J., Clegg, R. E., Leavesley, D. I., and Pearcy, M. J. (2005). Mediation of Biomaterial–Cell Interactions by Adsorbed Proteins: A Review. Tissue Eng. 11, 1–18. doi:10.1089/ten.2005.11.1.

Witherel, C. E., Abebayehu, D., Barker, T. H., and Spiller, K. L. (2019). Macrophage and Fibroblast Interactions in Biomaterial-Mediated Fibrosis. Adv. Healthc. Mater., 1801451. doi:10.1002/adhm.201801451.

Wolf, E. (1969). Three-dimensional structure determination of semi-transparent objects from holographic data. Opt. Commun. 1, 153–156. doi:10.1016/0030-4018(69)90052-2.

Wolf, J., Rose-John, S., and Garbers, C. (2014). Interleukin-6 and its receptors: A highly regulated and dynamic system. Cytokine 70, 11–20. doi:10.1016/j.cyto.2014.05.024.

Wong, S. W., Lenzini, S., Cooper, M. H., Mooney, D. J., and Shin, J.-W. (2020). Soft extracellular matrix enhances inflammatory activation of mesenchymal stromal cells to induce monocyte production and trafficking. Sci. Adv. 6, eaaw0158. doi:10.1126/sciadv.aaw0158.

Woo, S.-H., Lukacs, V., de Nooij, J. C., Zaytseva, D., Criddle, C. R., Francisco, A., et al. (2015). Piezo2 is the principal mechanotransduction channel for proprioception. Nat. Neurosci. 18, 1756–1762. doi:10.1038/nn.4162.

Woo, S.-H., Ranade, S., Weyer, A. D., Dubin, A. E., Baba, Y., Qiu, Z., et al. (2014). Piezo2 is required for Merkel-cell mechanotransduction. Nature 509, 622–626. doi:10.1038/nature13251.

Xiang, X., Wang, J., Lu, D., and Xu, X. (2021). Targeting tumor-associated macrophages to synergize tumor immunotherapy. Signal Transduct. Target. Ther. 6, 75. doi:10.1038/s41392-021-00484-9.

Xing, X., Wang, Y., Zhang, X., Gao, X., Li, M., Wu, S., et al. (2020). Matrix stiffness-mediated effects on macrophages polarization and their LOXL2 expression. FEBS J., febs.15566. doi:10.1111/febs.15566.

Yabal, M., Calleja, D. J., Simpson, D. S., and Lawlor, K. E. (2019). Stressing out the mitochondria: Mechanistic insights into NLRP3 inflammasome activation. J. Leukoc. Biol. 105, 377–399. doi:10.1002/JLB.MR0318-124R.

Yago, T., Wu, J., Wey, C. D., Klopocki, A. G., Zhu, C., and McEver, R. P. (2004). Catch bonds govern adhesion through L-selectin at threshold shear. J. Cell Biol. 166, 913–923. doi:10.1083/jcb.200403144.

Yeung, O. W. H., Lo, C.-M., Ling, C.-C., Qi, X., Geng, W., Li, C.-X., et al. (2015). Alternatively activated (M2) macrophages promote tumour growth and invasiveness in hepatocellular carcinoma. J. Hepatol. 62, 607–616. doi:10.1016/j.jhep.2014.10.029.

Yona, S., and Gordon, S. (2015). From the Reticuloendothelial to Mononuclear Phagocyte System – The Unaccounted Years. Front. Immunol. 6. doi:10.3389/fimmu.2015.00328.

Yona, S., Kim, K.-W., Wolf, Y., Mildner, A., Varol, D., Breker, M., et al. (2013). Fate Mapping Reveals Origins and Dynamics of Monocytes and Tissue Macrophages under Homeostasis. Immunity 38, 79–91. doi:10.1016/j.immuni.2012.12.001.

Zamyatina, A., and Heine, H. (2020). Lipopolysaccharide Recognition in the Crossroads of TLR4 and Caspase-4/11 Mediated Inflammatory Pathways. Front. Immunol. 11. doi:10.3389/fimmu.2020.585146.

Zangle, T. A., and Teitell, M. A. (2014). Live-cell mass profiling: an emerging approach in quantitative biophysics. Nat. Methods 11, 1221–1228. doi:10.1038/nmeth.3175.

Zeng, Y., Yi, J., Wan, Z., Liu, K., Song, P., Chau, A., et al. (2015). Substrate stiffness regulates B-cell activation, proliferation, class switch, and T-cell-independent antibody responses in vivo. Eur. J. Immunol. 45, 1621–1634. doi:10.1002/eji.201444777.

Zhao, C., and Zhao, W. (2020). NLRP3 Inflammasome—A Key Player in Antiviral Responses. Front. Immunol. 11. doi:10.3389/fimmu.2020.00211.

Zhao, H., Brown, P. H., and Schuck, P. (2011). On the Distribution of Protein Refractive Index Increments. Biophys. J. 100, 2309–2317. doi:10.1016/j.bpj.2011.03.004.

Zhao, N., Li, C., Di, B., and Xu, L. (2020). Recent advances in the NEK7-licensed NLRP3 inflammasome activation: Mechanisms, role in diseases and related inhibitors. J. Autoimmun. 113, 102515. doi:10.1016/j.jaut.2020.102515.

Zhao, Q., Zhou, H., Chi, S., Wang, Y., Wang, J., Geng, J., et al. (2018). Structure and mechanogating mechanism of the Piezo1 channel. Nature 554, 487–492. doi:10.1038/nature25743.

Zhou, D. W., Lee, T. T., Weng, S., Fu, J., and García, A. J. (2017). Effects of substrate stiffness and actomyosin contractility on coupling between force transmission and vinculin–paxillin recruitment at single focal adhesions. Mol. Biol. Cell 28, 1901–1911. doi:10.1091/mbc.e17-02-0116.

Zhou, R., Yazdi, A. S., Menu, P., and Tschopp, J. (2011). A role for mitochondria in NLRP3 inflammasome activation. Nature 469, 221–225. doi:10.1038/nature09663.

Zhou, Z., Peng, Y., Wu, X., Meng, S., Yu, W., Zhao, J., et al. (2019). CCL18 secreted from M2 macrophages promotes migration and invasion via the PI3K/Akt pathway in gallbladder cancer. Cell. Oncol. 42, 81–92. doi:10.1007/s13402-018-0410-8.

Zigmond, S. H. (2004). Formin-induced nucleation of actin filaments. Curr. Opin. Cell Biol. 16, 99–105. doi:10.1016/j.ceb.2003.10.019.

Zullo, J. M., Demarco, I. A., Piqué-Regi, R., Gaffney, D. J., Epstein, C. B., Spooner, C. J., et al. (2012). DNA Sequence-Dependent Compartmentalization and Silencing of Chromatin at the Nuclear Lamina. Cell 149, 1474–1487. doi:10.1016/j.cell.2012.04.035.

ACKNOWLEDGEMENTS

As Isaac Newton said, *"If I have seen further it is by standing on the shoulders of Giants"*. In my case, they were not giants but a bunch of fantastic human beings with whom I had the chance of sharing this journey. To all the people cited here and the ones I may be missing, a big THANK YOU.

First, I would like to show my gratitude to my *Doktorvater*, Jochen Guck. Thank you for daring to take the risk of bringing me to the lab. You sparked my interest in biophysics, a field that I discovered and learned to enjoy by your side. You provided me with an excellent environment where I became a scientist and grew as a person. Thanks for providing guidance, criticism and support whenever were needed. This was not an easy endeavour, and I am thankful for your patience and for letting me stand up after science slapped me in the face again and again.

Second, to Anna Taubenberger. For being a role model on how to think, experiment, and do science. I think I have never learned as much from a single person. I am extremely grateful for your generosity and unlimited feedback and insight. The tremendous positivity you irradiate even managed to counterbalance my innate negativity. You have been a lighthouse in the middle of the darkness and I will never be able to thank you enough.

I would like to thank Michael Schlierf for agreeing to review this thesis. I am also very grateful to my second thesis reviewer and paper co-author, Clare Bryant. The first time I talked with you was such a breath of fresh air! I deeply appreciate our discussions and the way your feedback, ideas and your attention to detail shaped and improved this work.

I would like to acknowledge my thesis advisory committee, Michael Schlierf and Angela Rösen-Wolff, and also Christophe Lamaze and Michael Sieweke, for the discussions during the first years of my journey. I would also like to express my gratitude to all the people working in the CMCB infrastructures that provided support to this work, especially the ones from the light and electron microscopy, flow cytometry and animal facilities.

I am deeply grateful to the myriad of colleagues and friends from the Guck Lab. Beginning with the 306 crew. Shada, you are such an incredible human being. You gave me the chance to discover not only all your colours but also the flavours of your culture. I felt we have evolved a lot together and I hope we never stop growing. Stephanie, thanks for providing your support in all sorts of topics and circumstances, and for being the official abstract translator. I will always admire your hard work, language precision and attention to detail. I believe you were made in Glashütte instead of in Spremberg! Mirjam, I am glad that at the beginning I could learn from the efficiency

personified. You and Stephanie were my first German cultural shock, which now makes for a fun story to tell everybody. Raimund, thanks for coping with my constant mood changes and keeping the plants and the zen in the office in their optimal state. Geo, *mulțumesc* for engaging with me from the very beginning. Your doses of humour and mentoring saved me for a long time. And Kyoo, despite our hometowns are 9679 km away I am very happy we established such a fantastic friendship. Your future looks as bright as a jar of *Makgeolli*, of which I hope to have a glass with you soon!

I am enormously grateful to Katrin, the first person I met once I arrived to Dresden and the one who made sure my landing in Germany was as smooth as possible. Thanks for all the little pieces of advice you shared with me in and outside the lab. The same goes to Elke, for welcoming me so well and for your support during the sour moments. Definitively the best cook in town, undisputable. I owe you both a proper dinner and Spanish tortilla masterclass!

To Angela, for taking care of me and my health during my critical weeks in 2020. You saved the whole lab from having to cope with my drama for too long. Marta, *dziękuję* for your support during all the long and writing road. I am sure great things are waiting for you in the near future. When you hit the ball with your forehand, you are unstoppable!

To Saeed, thanks for welcoming me into the first social network I had in Dresden. You and the rest made of my first months in the city a fantastic time. Gonzalo, Gonzalito! So glad you brought some more latin flavour to the lab! I am very thankful for all the feedback and encouragement you gave me during this time. It really helped to keep pushing during these last years and bring this project to an end. To Chrissi, for your invaluable and continued technical help, you have the best pair of hands in the whole country. And Martin, thanks for taking care of Chrissi!

To Nicole Träber, for your positive attitude, help with the AFM and for letting me discover how the life in your charming Stolpen is. To Dominic, for all the discussions and help at the beginning when I barely knew how to write my name. To Isabel, for your assistance ordering consumables, sending parcels and keeping the lab operational. And for always being at the forefront of lab retreat organisation! To Markéta, for organising such fantastic weekends in the Czech Republic. Salvatore, *grazie* for making me look at the lab problems from a different perspective and for hosting me in Erlangen, your kitchen is my number 1 hostel in Bavaria.

To Till, Heike, Ruth, Gee and all the others who provided all the assistance needed to successfully navigate the German bureaucracy. To Katarzyna Plak and Maria Winzi, for all their insight and inspiration during the first years of my PhD. To Felix, for bringing me to the Dynamo stadium. And together with him, to my Deutsche fellas Timon, Lucas, Oliver, Paul and Maik. I hope during these years I absorbed a bit from your always-positive always-calm attitude. To Ahsan, for sharing with me during the uncertainties upon our arrival to Dresden. To "Joe" Chan. We overlapped for a short time, but you tried to pass all the knowledge you could on how to make it through this. It is great to see how you grew and became a group leader! To Daniel and Jona, for your energy and feedback. And to the rest of the lab. Philipp, Nicole Töpfner, Daniel, Conny, Yan, Conrad, Benedikt, Claudia… and all the core members and students I came across during these years. You all contributed to make our lab a great environment to work in, and if there is something I will always state is that I was extremely lucky to come across such a fantastic group of colleagues.

I also enjoyed a lot spending time with the colleagues I shared the 3rd floor with. Thanks to the Grillers, who showed us how all the hours spent at the kicker translated into excellent science. To the new rising star, Vaibhav, for bringing a lot of fresh air and tons of sweets. And Antje, for all her generosity and for being my last minute guardian angel. To Kamran, for being of invaluable help during the writing times. To Johannes, for trying hard the impossible mission of teaching us some German. And to Mirco, Valentin and all the others for keeping ours the best floor in all the building.

I am also very grateful to Miguel Ángel del Pozo and all his group for welcoming me into their lab during those two months in late 2017 where I learned both science and diplomacy. I am very thankful to Fidel for his help and supervision during the stressful weeks. And to Víctor, Antonio, Giulio and all the *madrileños*, thank you for showing the Catalan guy how to have a proper *café con leche en la Plaza Mayor*.

To all my ITN fellows, for bringing a flair of fresh air to the journey in every meeting. A special mention goes to my loved ones Henry and Larisa, whom I would really like to see succeeding in their academic journey. And I am also thankful to Ilaria and Lluc for being my great Swiss hosts.

I very much appreciate the time I spent with all the friends I made in Dresden, you will forever be the characters of my German tales. If you read this, I hope it means I am no longer a boring human being and became your annoyingly fun friend again. Special thanks go to Romina, for sharing those great pieces of advice and even greater chunks of Catalan imported food. And for reminding me to write these acknowledgement lines and avoiding a diplomatic crisis with half the globe. To Sílvia, for being an essential piece from beginning to end. When I met you in the narrow streets of Terrassa I was still hesitant about what to expect from Dresden. But your words always helped me cope with the daily problems at the bench and made the time outside the lab become as enjoyable as one of your cakes. To Lokesh, for being one of the most generous and cheerful people I will ever know. I will always be in debt with you for sharing so much no matter when and where. An invitation to come eat in the delicious South is always on the table for you.

To Gabriel, for being a fantastic partner in crime all these years. The time spent with you passed as fast as an evening of couch & Netflix. Thanks for your encouragement and your gazpacho recipe. I will always feel honoured to have met such a wise old man trapped in the body of a young boy. And to Isabel, who embraced the difficult challenge of teaching Gaby some English. Since you arrived you have not stopped growing and now it is your time to shine. To the Italian mafia, what a cocktail! Riccardo, thanks for keeping me fit and fed. You were the first person I met in Dresden and back then I thought I would not see you again. I am glad I was wrong! And Daniel, thanks for letting me break the engine but not the electronics. I am still trying to learn from your mental clarity and mixing skills. I hope that even bigger parties are waiting for us in the near future! To Adrián, for being an infinite source of energy and amusement, *fuah*! To Leila, for letting us discover our lifesaver abilities. To Simon, for his bright notes of dark humour. To Iván, for always keeping everyone's mood up. To Frank, for la libertad! To Sylvia, for one of the best chocolate birthday cakes I ever had. And to Chiara, Jelena, Alice, Michael, Gloria, Marta and Teresa for sweetening so many summer evenings.

Thanks to Paul, John, Ringo and George for providing the main soundtrack of this work. To past JC: you claimed that the PhD was an exciting challenge you wanted to embark on. Did you enjoy, *capgròs*? Jokes aside, thanks for making it through the desert and for surviving, from the first day to the last one. To future JC: if you read this in 10 or 20 years time (fingers crossed) and you come across any PhD students, please be kind to them, do not be greedy and pay them a drink. And remember that you made it through the desert, so… why stopping now? Keep pushing and always, always, enjoy the ride.

And to my family, without whom I would not have made it this far and without whom I would not be who I am today. Gràcies per haver-me ensenyat a aixecar-me ben d'hora, ben d'hora i a treballar de valent. Tot el que aconsegueixi és en gran mesura gràcies a l'esforç que vosaltres heu abocat abans. I sobretot, gràcies per transmetre'm l'humor que també forma part del meu caràcter i que ha sigut l'eina més útil durant aquests anys. Així que alegria, que als pròxims dinars convido jo!

Author's declaration

Most of the data and parts of the text published in this thesis have been taken or adapted from my published work:

Compliant substrates enhance macrophage cytokine release and NLRP3 inflammasome formation during their pro-inflammatory response.

Escolano JC, Taubenberger AV, Abuhattum S, Schweitzer C, Farrukh A, del Campo A, Bryant CE and Guck J (2021). Front. Cell Dev. Biol. 9 : 639815.
DOI: 10.3389/ fcell.2021.639815.

Frontiers articles are distributed under the terms of a CC-BY Creative Commons attribution license that enables the authors to retain copyright and permits unrestricted use and redistribution provided that the original author and source are credited.

Erklärung entsprechend §5.5 der Promotionsordnung

Hiermit versichere ich, dass ich die vorliegende Arbeit ohne unzulässige Hilfe Dritter und ohne Benutzung anderer als der angegebenen Hilfsmittel angefertigt habe; die aus fremden Quellen direkt oder indirekt übernommenen Gedanken sind als solche kenntlich gemacht. Die Arbeit wurde bisher weder im Inland noch im Ausland in gleicher oder ähnlicher Form einer anderen Prüfungsbehörde vorgelegt. Die vorliegende Arbeit wurde am Biotechnologischen Zentrum der TU Dresden (BIOTEC) unter Betreuung und in der Arbeitsgruppe von Prof. Dr. Jochen Guck angefertigt.

Meine Person betreffend erkläre ich hiermit, dass keine früheren erfolglosen Promotionsverfahren stattgefunden haben.

Ich erkenne die Promotionsordnung der Fakultät Mathematik und Naturwissenschaften das Technischen Universität Dresden an.

Dresden, August 2021 Joan Carles Escolano Caselles